FACULTY OF SCIENCES

THE POTENTIAL FOR AQUIFER THERMAL ENERGY STORAGE IN LOW-PERMEABLE SEDIMENTS

A FEASIBILITY STUDY ON CAMPUS STERRE, GHENT UNIVERSITY, BELGIUM

Luka Tas
Student number: 01708456

Promotor: Prof. dr. Thomas Hermans
Copromotor: Prof. dr. David Simpson

Jury: Prof. dr. Kristine Walraevens, Dr. Tanguy Robert

Master's dissertation submitted in partial fulfilment of the requirements for the degree of master in geology

Academic year: 2021-2022

GHENT UNIVERSITY

KU LEUVEN

Preface – Acknowledgements

First, I would like to express my sincere thanks and appreciation to my supervisors professor Thomas Hermans of Ghent University and David Simpson of the AGT company for freeing up time to help out with the field tests and giving me a deeper insight into the principles behind ATES systems. Furthermore, I am very grateful for their overall support and motivation.

Special thanks also go to Marieke Paepen and Robin Thibaut of the hydrogeology department. Marieke for always being ready to give a hand in carrying out the field tests. Robin for playing a part in running the simulations, even though they took a lot of time and almost all of his computer memory.

I also wish to thank my fellow students for the great cooperation over the past few years.

Finally, yet importantly, I wish to thank my family and my dear boyfriend Jeroen to undergo and take part in the endless conversations about geology-related topics. I'd also like to extend my gratitude to Jeroen for guiding me with his knowledge and for always keeping calm.

TABLE OF CONTENTS

LIST OF FIGURES

LIST OF TABLES

1. Introduction

The Member States of the European Union pledged to reduce greenhouse gas (GHG) emissions by 80-95% by 2050. Innovation is indispensable to achieve this goal. Nowadays, the building sector is the largest energy consumer in Europe. It is responsible for 40% of energy consumption and 36% of CO_2 emissions (European Commission, 2012, 2019; Ramos-Escudero et al., 2021). Within the building sector, heating and hot water account for 79% of total energy use. In contrast, cooling currently represents a small share of the total final energy use, however, an increasing demand is observed (European Commission, 2012, 2019; Bloemendal et al., 2015; Ramos-Escudero et al., 2021). This can be explained by the increasing air temperature linked to climate change and the stricter regulations concerning insulation in new modern buildings which, especially in summer, heat up quickly. In this light, the housing sector is considered to be key in reducing global GHG emissions with a strong saving potential of up to 90% by 2050 (Ramos-Escudero et al., 2021). To reach this goal, geothermal energy, i.e. the energy present due to heat transfer from the Earth's core to the outer areas of the crust, might play a meaningful role (Parsons, 1970; Muela Maya et al., 2018).

Namely, the use of shallow geothermal systems has proven to be a locally available, green, and renewable alternative to fossil fuels both for cooling in summer and heating in winter (Perego et al., 2020). In contrast to deep geothermal systems (> 500 m), they do not extract net energy from the earth but use it as a medium for seasonal storage of heat and cold. The main advantage of such systems over the use of oil and propane is not only their minimal CO_2 output but also their cost-effectiveness. Based on a study in the Netherlands, open-loop geothermal systems can save on average about 0.5 kg of CO_2 per m^3 of pumped water (Fleuchaus et al., 2018). In short, the shallow ground (< 200 m) is considered to be a large energy reservoir. Shallow geothermal systems make use of the thermal properties of the subsurface. To extract and use this energy, ground-source or groundwater heat pumps (GSHP and GWHP respectively) are needed to transfer heat from a low-temperature source to a high-temperature sink. To circulate the groundwater, the pump performs work. Next, a compressor is used in the heat pump to match the fluid temperature that is needed to heat a building to on average 20-21 °C. In new buildings with good insulation and a low-temperature heating system, the required fluid temperature is about 30-45 °C (Glassley, 2014). These works can be translated to electricity consumption. The heat pump is required because the average groundwater temperature usually is roughly the annual average temperature of the region plus 1 °C or 2 °C, which would be around 10-12°C in Belgium. This temperature remains stable starting from a depth of approximately 15 m, where the ground dampens the thermal oscillations (diurnal and seasonal) occurring at the surface (Parsons, 1970; Muela Maya et al., 2018). Climatization, on the other hand, does not always require the use of a heat pump (Glassley, 2014).

Two main groups of shallow geothermal systems can be distinguished (Figure 1) (Perego et al., 2020).

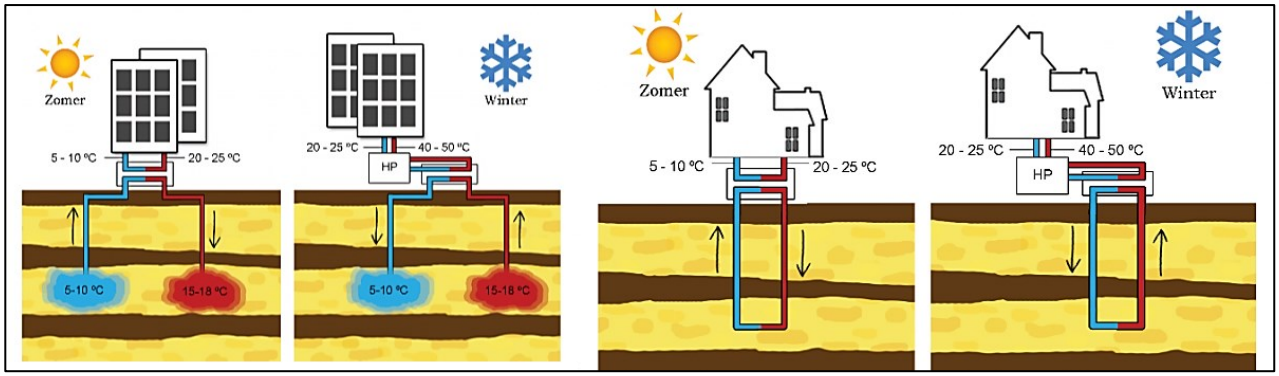

Figure 1: Graphical representation of an open-loop (left) and closed-loop (right) shallow geothermal system in summer and winter. Notice that open-loop systems make direct use of the (ground)water while there is no direct interaction with (sub)surface water with closed-loop systems (Bloemendal, 2018).

First, the closed-loop systems, also referred to as GSHP systems, use ground heat exchangers installed in the subsurface. The ground heat exchangers can be described as loops through which water, together with an antifreeze, circulates. Multiple types of heat exchangers exist such as horizontal and vertical borehole heat exchangers (BHE). Second, the open-loop systems, also referred to as GWHP systems, extract groundwater from an aquifer through a pumping well. Pump and Dump systems inject the extracted water into a nearby sewage system or river, which is not allowed in Belgium or the Netherlands. This is in contrast with aquifer thermal energy storage systems (ATES) which consist of one (or more) well doublet(s) of one warm well and one cold well. Depending on the heating or cooling demand, one of these wells becomes the injection well and the other one the pumping well. As such, in winter, heat will be subtracted by the building and, in summer, heat will be subtracted from the building. Respectively, this cold and heat will be stored in the subsurface increasing the efficiency for the upcoming seasons. To clarify, the warm well area, which will be the pumping area if heating is needed, will become warmer and the cold well area, which will be the pumping area when climatization is needed, will become cooler. This concept of storing thermal energy can also be applied to closed-loop systems such as borehole thermal energy storage (BTES). However, in comparison with BTES systems, ATES systems can produce more energy. Nevertheless, BTES systems are more commonly used (Lund and Boyd, 2016; Rivera et al., 2017; Perego et al., 2020). This could be attributed to the fact that the efficiency of BTES systems relies on the thermal conductivity of the subsurface (i.e. how easily a material can transfer heat), while the efficiency of ATES systems relies on the hydraulic conductivity which governs the pumping rate (i.e. how easily water can flow). The former condition is more often fulfilled considering that ATES systems generally are not cost-efficient (i.e. the pay-back time is longer) if the pumping rate cannot reach 10 m^3/h (Bloemendal et al., 2015; Hermans et al., 2018).

Besides, when storing thermal energy in the subsurface, attention must be paid to many other aspects within different fields of study. As such, a natural groundwater gradient might cause the stored thermal energy to move away together with the groundwater flow. Moreover, the thermal interference between different wells as well as clogging might reduce the efficiency of the system. And finally, a temperature change might induce a change in groundwater chemistry which may or may not be acceptable (Bloemendal et al., 2015; Hermans et al., 2018).

Bearing this in mind, this project focuses on carrying out a feasibility study for an ATES project at the Ghent University campus of the Faculty of Sciences in Belgium (Figure 2), where conditions for ATES are less ideal.

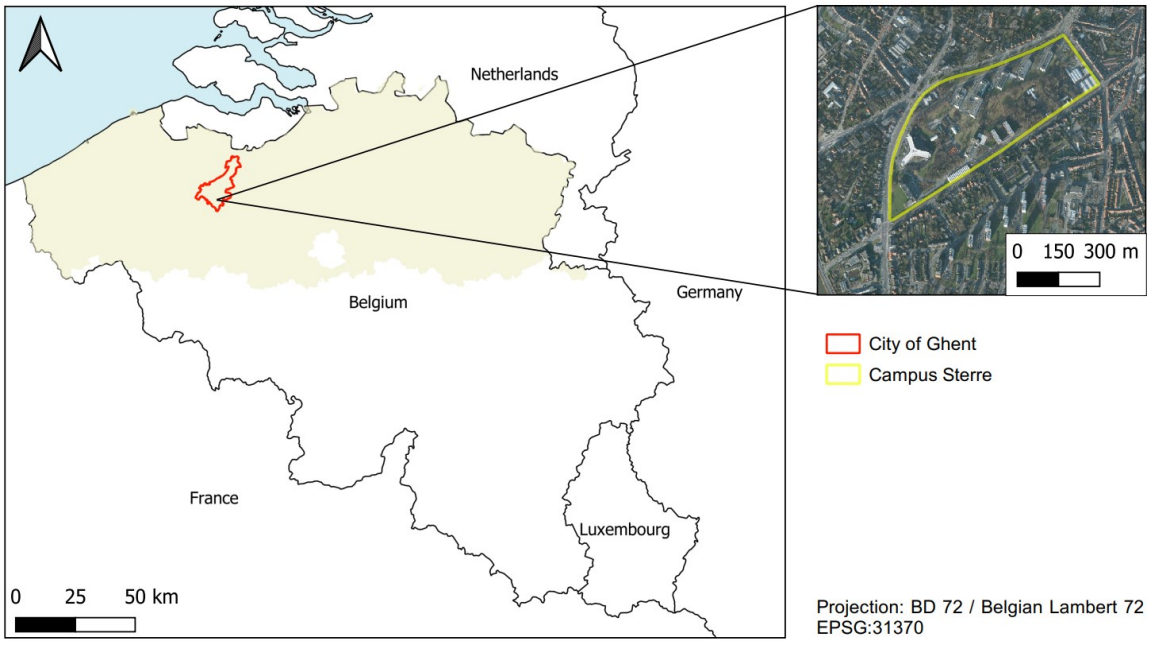

Figure 2: Localization of the study area Campus Sterre.

The goal of Ghent University is to become CO_2 neutral in this area by 2050. Reaching this scope is a challenge and different sustainable, green, and innovative technologies should be studied and evaluated. An audit of the energy demand and possible solutions has been conducted by SWECO (Hermans, personal communication). This report has shown that the most sustainable alternative to cover the heating demand was to combine the residual heat from the cooling system of the servers with a shallow geothermal system. The geothermal system would store the residual heat of the servers during the summer period when heating is not needed, so it can be released in winter as an addition to the directly used residual heat from the servers. It has been estimated that the power of the geothermal system should be at least 0.63 MW. For such power requirements, usually, ATES systems are considered to be more cost-effective in comparison to BTES systems. However, a quick evaluation of the study area showed that, because of the absence of a thick productive aquifer on campus, the transmissivity of the available aquifers might not be sufficient to reach the cut-off criteria of the pumping rate of 10 m^3/h. On the other hand, the power delivered by a BTES system is directly proportional to the length of the drilled borehole and the power requirement. In the study area, there is a need for a minimum of 175 boreholes of each 100 m deep resulting in an investment cost of approximately € 3 500 000. For such high investment costs, it is nevertheless interesting to further explore the possibility for the development of an ATES system since those systems can usually produce more energy per pumping well resulting in fewer, and in this case less deep, drillings. However, the cost per well is higher for ATES and the system is more complex and therefore more prone to failure. This master thesis focuses on determining the feasibility of an ATES system on Campus Sterre and on addressing and investigating the issues that might arise when implementing it. To do this, the following objectives were set:

1. Estimate the maximum yield of the aquifer. The lower the maximum yield, the more wells that would be required.
2. Carry out a brief chemical analysis. The implementation of an ATES system induces a temperature change in the aquifer. Also, groundwater of different pervious layers might be mixed. It must thus be ensured that the effect on the ecology and the risk for chemical clogging is negligible.
3. Estimate the risk of clogging and the capacity for long-term injection. The fine sediment which causes the low hydraulic conductivity in the study area might also increase the risk of well clogging and in turn limit the injection capacity. Additionally, it must be able to maintain a low enough pressure in the injection wells to avoid damaging the confining clay layer.
4. Estimate and model the hydraulic and thermal radius. While for BTES, generally, a borehole every 5 m is assumed, for ATES enough space in between wells is required to avoid the risk of thermal interference. However, the low-permeable sediments in the study area might be an advantage by reducing the thermal radius of influence of the wells (Kim et al., 2010; Yapparova et al., 2014).
5. Propose a design for the ATES system in a way that the storage efficiency and usage of space are optimal.
6. Analyse the related costs. The ATES project must be worthwhile from an economic perspective in comparison to BTES despite the uncertainties related to the thermal and hydrogeological properties of the aquifer.

2. Research description

To assess the feasibility of an ATES project in the study area, this chapter will start with a thorough description of the lithostratigraphy and the hydrogeology of the study area. Next, the methods used to evaluate the sustainability of the project will be discussed. Sustainability applies to the way the resource is used. One must be able to provide for the current need without compromising on the ability to provide for the future's needs. It is strongly connected with renewability which refers to the natural state (initial groundwater quality, quantity, and ecology) of the resource (Hänlein et al., 2013). For this purpose, first, pumping tests were executed to estimate the maximum pumping and injection rate and to validate the model that will predict the behaviour of the system. Next, the risk that chemical reactions, induced by the mixing of groundwater and temperature changes, will influence the ecology and the efficiency of the system will be assessed. Additionally, a chapter will be devoted to the risk of clogging the wells. Furthermore, the use and implementation of a groundwater model in light of this feasibility study will be described in detail. Finally, a brief economic analysis will be carried out. One could also argue that the water balance must be investigated when using an open-loop system to avoid the risk of subsidence, however, this risk is not considered because the pressure in the aquifer will be maintained in equilibrium (extraction = injection at all times).

2.1. Lithostratigraphic and hydrogeological setting of the study area

As mentioned earlier, the study area encompasses Campus Sterre occupied by the Faculty of Sciences of Ghent University. It is located approximately 3 km south of the city centre of Ghent (Figure 2). Describing and understanding the lithology and hydrogeology of the study area is the first essential step in determining the suitability of the site for aquifer thermal energy storage. The sediment type affects the permeability which is of major importance for an open-loop geothermal system.

Near the surface of the study area, Holocene and Pleistocene deposits can be found. According to the geological map of Flanders, this Quaternary layer has an average thickness of 9.5 m (DOV, Databank Ondergrond Vlaanderen, n.d.). It has a heterogeneous composition consisting of clays, silt, sand and gravel. The Quaternary in the study area can be subdivided into the Formation of Gent on top and the Formation of Rozebeke, Kruishoutem, Meulbeke, Adegem, Oostwinkel, Eeklo, Oostende and Herzele at the bottom (Figure 3).

Below, deposits of the Eocene are present (the Tertiary) (DOV). The Tertiary in Belgium is characterized by the recurrence of transgressions and regressions which resulted in a dominant sub-horizontal stratification. The sea flooded the continent from a North-Northeastern direction. As a result, the deposits dip slightly towards the NNE and the oldest Tertiary layers are exposed in the SSW while the youngest are exposed in the Northeast. When the turbidity was high, i.e. dominantly during a regression, the deposits were mostly sandy. When the turbidity was low, i.e. dominantly during a transgression, the deposits were more clayey. This clarifies the presence of alternately pervious and semi-pervious layers in a great part of Flanders. In the study area, the Formation (Fm) of Gentbrugge is the youngest Eocene deposit. It has an irregular extension and a limited, varying thickness in the campus area. It is composed of two members: the Merelbeke Member (Mb) below and on top of it the Pittem Mb. The Merelbeke Mb consists of silty clay or clayey very fine silt with intercalations of sand lenses in which organic material and small pyritic concretions can occur. The Pittem Mb on the other hand is more sandy: it can be described as clayey silty glauconiferous very fine sand alternating with layers of clayey sandy coarse silt. The Gentbugge Fm thickens towards the Northeast and might be absent in the Southwest of the study area. Below, at the top of the main groundwater reservoir in the study area, the Formation of Hyon and Gentbrugge is present. This deposit of clayey fine sand has a uniform thickness of approximately 20 m. It covers the Formation of Tielt and Hyon which has a similar thickness and composition. The latter is bounded below, from -37 mTAW on, by the more clayey Formation of Kortrijk. The Kortrijk Fm has a thickness of up to 95 m. This is the oldest Eocene deposit in the study area.

On top, the Holocene and Pleistocene deposits hydrogeologically correspond to the Quaternary Aquifer systems (classified as HCOV 0100 under the Hydrogeological coding of the underground of Flanders, 'HCOV') (DOV). Hydrostratigraphically, the Gentbrugge Fm, on the one hand, corresponds to the Paniselian Aquitard system (HCOV 0700). However, on the other hand, towards the Northwest, the latter will be overlain by the Ledo Paniselian Brusselian Aquifer system (HCOV 0600 which belongs to the CVS_0600_GWL_1). The Hyon and Gentbrugge Fm and the Tielt and Hyon Fm correspond hydrostratigraphically to the Ypresian Aquifer system (HCOV 0800 belonging to CVS_0800_GWL_2). This is the groundwater reservoir that will be used for further analysis. Finally, the Kortrijk Fm can be described as an aquitard (i.e. the Ypresian Aquitard system (HCOV 0900)).

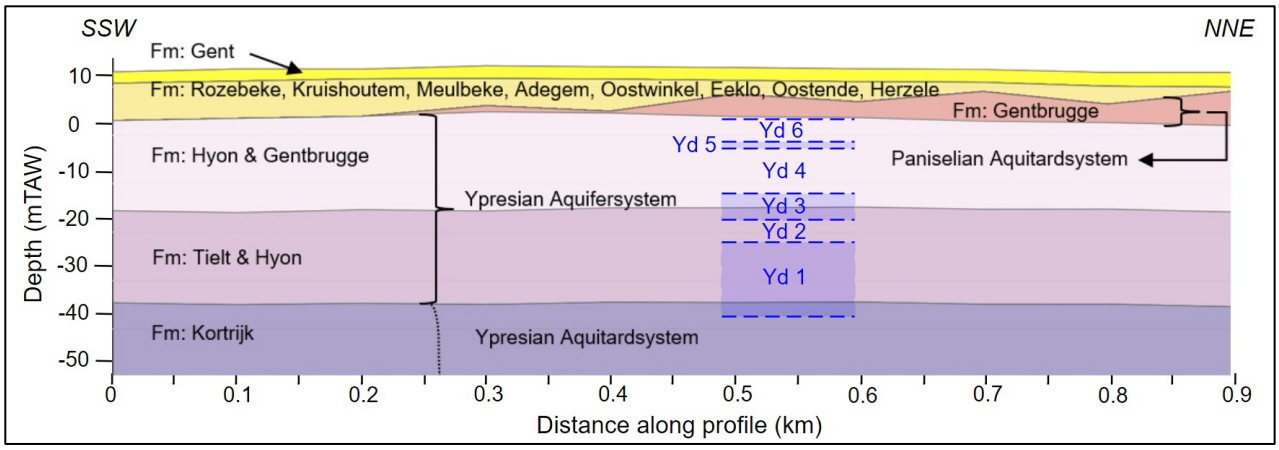

Figure 3: Graphical representation of the lithostratigraphy and hydrogeology across Campus Sterre. The more accurate hydrostratigraphy of the Ypresian Aquifersystem according to Lebbe, Mahauden & De Breuck (1992) is indicated in blue). (created after DOV).

A more accurate description and subdivision of the lithostratigraphy and hydrogeology near the Geological Institute of the University of Ghent was made by Lebbe et al. (1992) (Figure 3). This was accomplished using information gathered by the analysis of samples collected during drilling and by geophysical well logging methods. Especially, the single point resistance log characterized the layering of the groundwater reservoir of interest very well. On top of the layered aquifer, the Formation of Gentbrugge (and the Quaternary) are considered semi-pervious. Noteworthy is that the Merelbeke Mb could be clearly observed in the single point resistance log. This is in contrast to the sediment on top which was identified as the Pittem Mb by Lebbe et al. (1992). The latter might be questioned as the Quaternary also consists of clay, silt and fine sand. Nevertheless, the Ypresian Aquifersystem is the main aquifer at a moderately shallow depth in the study area. The base of which was observed at a depth of -40 mTAW according to Lebbe et al. (1992). Based on the pervious or semi-pervious character of the Ypresian Aquifersystem, it was subdivided into 6 units: Yd 1, Yd 3 and Yd 5 are semi-pervious while Yd 2, Yd 4 and Yd 6 are pervious. Taking the accurate well-logging results into consideration, it was decided to use this detailed lithostratigraphy of the Ypresian Aquifer system for further analysis.

From bottom to top, unit Yd 1 corresponds to the Kortemark Mb which is a sandy and silty clay with intercalations of thin clayey fine sand beds. Above, units Yd 2 to Yd 6 correspond to the Egem Mb which is not uniform. Yd 2 consists of clayey glauconitic fine sand while Yd 3 is more sandy clay to clay. Unit Yd 4 is again sandier like Yd 2, however, it also contains small shell fragments. It can be described as slightly clayey glauconitic fine sand. Yd 6 has the same lithology. Yd 5 on the other hand is very sandy clay.

2.2. Material and methods

2.2.1. Literature review of a triple pumping test on Campus Sterre

A previous work of Lebbe et al. (1992) has been of significant importance for the accomplishment of this thesis. It consisted of a triple pumping test on Campus Sterre to determine the hydraulic parameters of the different layers more accurately (Figure 4). The latter is required to ensure a good quantitative and qualitative management of groundwater resources. The similar study area indicates that the results of their paper were particularly relevant for this research.

Figure 4: Localization of the well area used for pumping tests on Campus Sterre.

For their study, pumping wells and piezometers were drilled in the pervious layers Yd 2, Yd 4 and Yd 6 (Figure 5). They are named PP 2, PP 4 and PP 6 accordingly. Each pumping well was accompanied by three observation wells which are named PB x.y (x referring to the layer in which the filter was placed, y referring to the distance to the pumping well in the concerned pumped layer (1 for 6.3m, 2 for 12.5m and 3 for 25m)) (Figure 5). The diameter of the pumping wells (screen and riser pipe) is 125/116 mm, and the drilling diameter is 250 mm. The observation wells are smaller and have a diameter of 63/57 mm and a drilling diameter of 110 mm. It is worth noting that, during well completion, the annular space between the riser pipe and the semi-pervious layers was sealed with neat cement. Nevertheless, leakages through these semi-pervious layers due to improper sealing turned out to be responsible for a high amount of perturbations in the results.

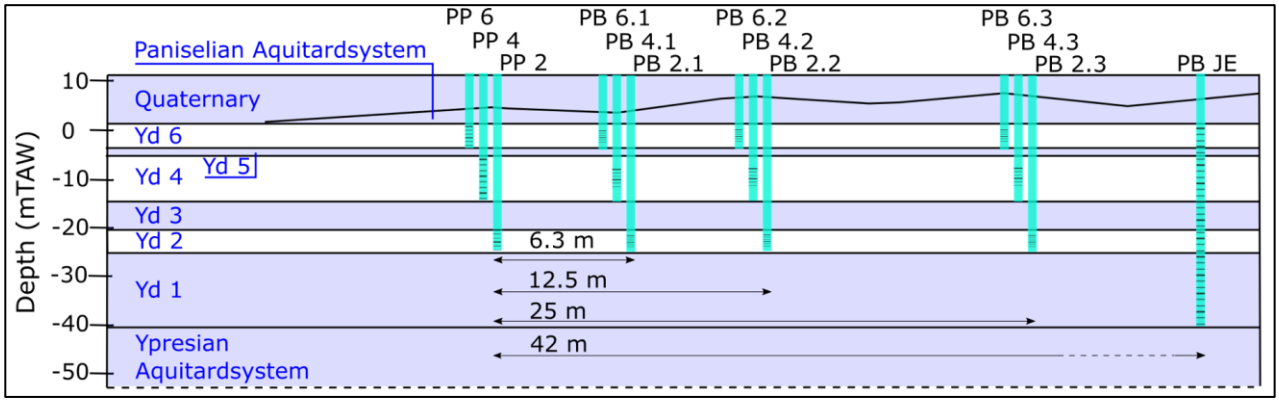

Figure 5: 2D image of the filter placement of the wells used for pumping tests on Campus Sterre. (For the horizontal distribution of the wells the reader is referred to Figure 4.)

The first of three pumping tests started at 15h00 on October 10, 1989, and was performed on well PP6. The flow rate was 18 m^3/d (or 0.75 m^3/h). Drawdowns in the observation wells were measured by means of electronic pressure transducers connected to a data logger. Important to mention is that the observations were done in the directly pumped layer as well as in the indirectly pumped layers at the same time. As such, more observations can contribute to determining the set of parameters. The test was stopped at 11h00 on October 13, 1989, but the transducers were kept in place to measure the recovery. Residual drawdowns were measured until 13h00, October 14. The second pumping test, on PP2, started at 16h00 on October 18 and stopped at 16h00, October 20. The measured pumping rate was 39.9 m^3/d (or 1.66 m^3/h). The residual drawdowns were measured in the observation wells until 22h00, October 22. The final pumping test, on PP4, started at 14h00 on October 24 and stopped at 14h00, October 26. The pumping rate was 74.2 m^3/d (or 3.09 m^3/h). The residual drawdowns were measured until 8h00 October 27.

The hydraulic parameters of the subsurface were determined using a numerical model by fitting the observed drawdowns to the simulated ones (Figure 6). The numerical model used by Lebbe et al. (1992) is two-dimensional and axisymmetric consisting of 9 homogeneous layers which are numbered from bottom to top. Layer 1 is bound below by an impervious layer (Formation of Kortrijk) and the top of the model is bound by the water table. This schematization was done based on the lithostratigraphic and geophysical data collected during the execution of the boreholes (Figure 3). For accuracy reasons, the upper unit of the model was subdivided into 3 layers. It is noteworthy to mention that the Gentbrugge Fm (Merelbeke Mb, Paniselian Aquitard) was not considered one of the layers of the model. This can probably be explained by the fact that it is only very thinly present in the study area and even absent in some parts. However, a high hydraulic resistance was assigned between layers 6 and 7 accounting for the semi-pervious character of this formation. Hence, this semi-pervious layer is just considered as the horizon between layers 6 and 7.

To initialize the calibration of the model, initial values of the horizontal hydraulic conductivity (Kx), the Specific storage (Ss) and the specific yield (Sy, storage coefficient near the water table) had to be chosen. By means of these values, a sensitivity analysis was performed. In short, the calibration started with the ordinary least squares method and only the most sensitive parameters were modified to restrict the number of iterations of the inverse model. SSE can be defined as:

$$\boldsymbol{SSE} = \sum_{\boldsymbol{i=1}}^{\boldsymbol{n}} (\boldsymbol{y_i} - \boldsymbol{f}(\boldsymbol{x_i}))^2 \qquad \{\mathbf{1}\}$$

Where:

SSE	: sum of squared errors [-]
n	: number of observations [-]
y_i	: observed drawdown [m]
$f(x_i)$	: simulated drawdown [m]

Every time the minimum SSE is reached, the next most sensitive parameters were introduced.
A solution is approximated when all parameters are introduced and a minimum SSE is reached (Table 1). The accuracy with which the set of parameters can be derived can be estimated by means of the marginal and conditional standard deviation which is deduced from the covariance matrix. The latter was in turn deduced from the sensitivity (or Jacobian) matrix. Because of the presence of many outliers, related to the leakage of seals in the semi-pervious layers, this method was followed by the biweighted least-squares method in order to reduce their effect on the estimates. Using this biweighted least-squares method a kind of standardized residual was calculated as:

$$\boldsymbol{u = \frac{r}{3} \times IQR} \qquad \{2\}$$

Where:

u : standardized residual [-]
r : residual (defined as the difference between the logarithmic values of the observed and calculated drawdowns) [-]
IQR : interquartile range [-]

Gathering data using this kind of set-up of a triple pumping test showed that the accuracies reached for the vertical hydraulic conductivities (Kz) of the semi-pervious layers were comparable to the accuracies with which the horizontal hydraulic conductivities of the pumped layers could be estimated. Hence, the advantage of a triple pumping test over a simple one was evident, especially when dealing with a layered groundwater reservoir where leakage through seals in semi-pervious layers might be present.

Table 1: Final hydraulic parameters deduced with the inverse model from all observations of the triple pumping test analysed by Lebbe et al. (1992). Note that the Merelbeke Mb (Gentrbugge Fm) is only accounted for in the hydraulic resistance (c6).

Layer	Kx (m/d)	Ss (1/m)	Sy (m^3/m^3)	Hydraulic resistance	
9	0,25	0,000055	0,009843	**c8** (8--9)	6,257
8	0,25	0,000055	0,009843	**c7** (7--8)	39
7	0,25	0,000055	0,009843	**c6** (6--7)	3922
6 (Yd 6)	0,859	0,000055	0,009843	**c5** (5--6)	40,32
5 (Yd 5)	0,02	0,000055	0,009843	**c4** (4--5)	40,32
4 (Yd 4)	1,106	0,000036	0,009843	**c3** (3--4)	4037
3 (Yd 3)	0,002	0,000036	0,009843	**c2** (2--3)	6055
2 (Yd 2)	1,261	0,000038	0,009843	**c1** (1--2)	236,9
1 (Yd 1)	0,04	0,000012	0,009843		

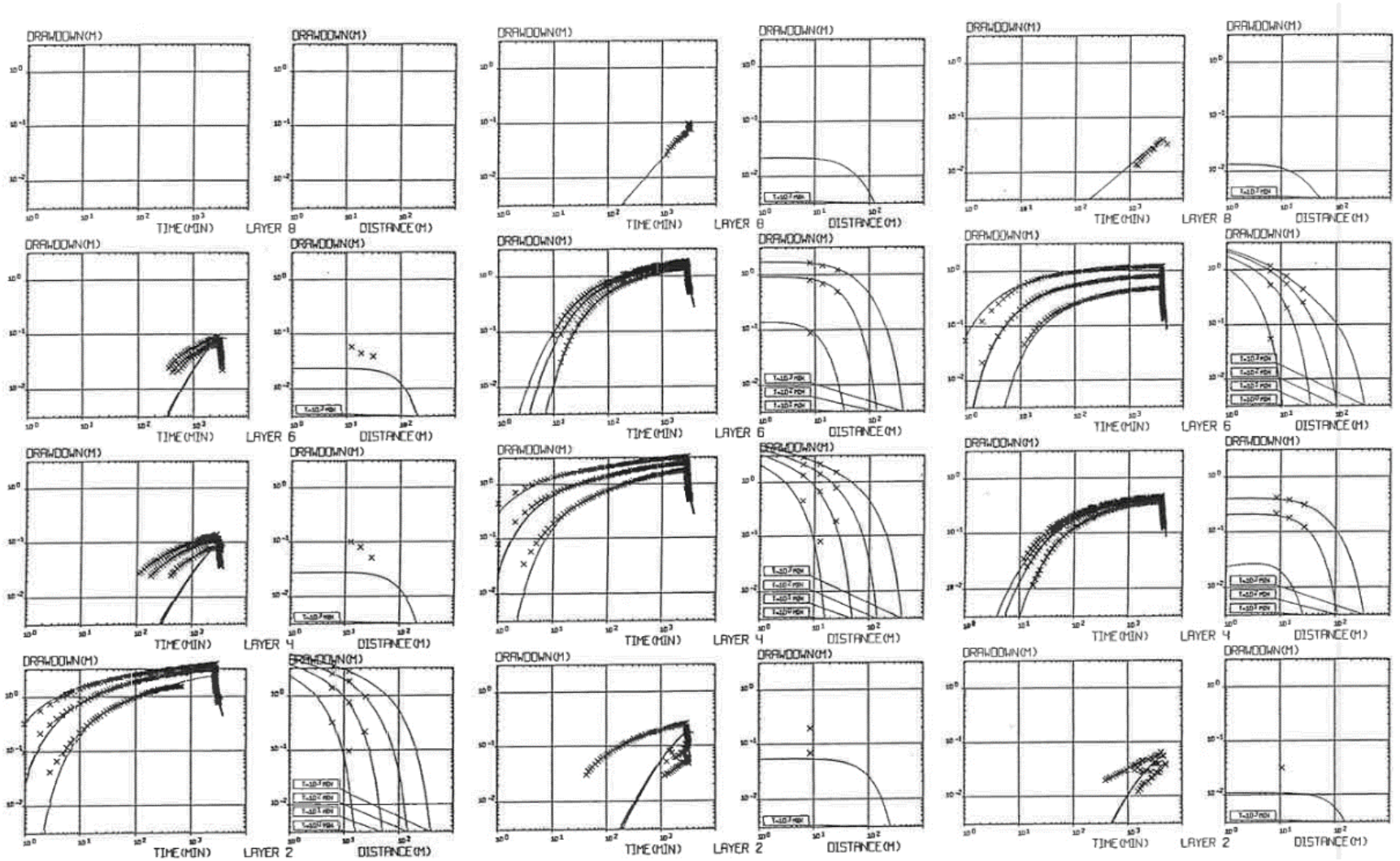

Figure 6: Measured (x-signs) and calculated (solid curves) in time- and distance-drawdown graphs for the three pumping tests (left two columns for the pumping test in layer Yd 2, middle two columns for the pumping test in layer Yd 4, and right two columns for the pumping test in layer Yd 6 (Lebbe et al., 1992).

2.2.2. Pumping and reinjection tests

While Lebbe et al. (1992) carried out a triple pumping test to accurately derive the hydraulic parameters of the Ypresian aquifer system, this research focused on using pumping and reinjection tests to reach the following objectives:

1. Estimate the maximum pumping rate in the entire Ypresian aquifer system. In absence of a fully filtered pumping well, the maximum pumping rate was estimated in each pervious layer separately. The total maximum pumping rate in the entire Ypresian aquifer system could be estimated using the superposition principle. This however assumes that all pervious layers are fully confined.

2. Estimate the maximum injection rate. For the injection test, a fully filtered well (PB JE) is present in the Ypresian aquifer system (Figure 5). However, this well was constructed as a piezometer and not as a pumping well with a larger diameter. As such the well efficiency is not optimal limiting the capacity for injection. Bearing this in mind, the injection might also cause water pressures which might extend above the ground level. When excessive, this might cause flooding and/or instability of the clay layer (Gentbrugge Fm) between Yd 6 and the top layer. (These issues will also be discussed later on.)

3. Simulate the stability of a well pair consisting of one injection and one pumping well.

4. Generate data sets for validation of the groundwater model.

In practice, the pumping and reinjection tests took place on the same site that was used by Lebbe et al. (1992) where the filters of the observation and pumping wells were placed in three pervious layers of the Ypresian sands (Figure 4, Figure 5). Unfortunately, the three observation wells that accompanied pumping well PP4 (PB 4.1, 4.2 and 4.3) were destroyed during construction activities on Campus Sterre. In August 2021 the wells were checked and the maximum pumping rate in each pumping well was estimated. The maximum pumping rate indicates the critical flow rate above which the aquifer will not reach a new equilibrium. This means that, when the pumping rate becomes too high, an unsaturated zone is likely to be established and the drawdown will not be stable. An injection test in each piezometer was also carried out. However, not all wells stood the test of time. As such, the condition of some wells was not ideal anymore. Well PB JE, which was used as the injection well, has silted up over the years. This well was not used for the triple pumping test of Lebbe et al. (1992). It has a similar diameter as the observation wells in the study area (63/57 mm) and it is filtered over the entire depth of the Ypresian Aquifersystem (Figure 4, Figure 5). Consequently, well PB JE was cleaned.

To simulate the stability of a well pair, PP4 was selected as the pumping well and PB JE as the injection well. Divers were installed in PP2, PB 2.1, PP4, PP6, PB 6.1, PB 6.2 and PB JE. Regular TD divers which monitor the temperature and pressure were installed in the observation wells. CTD divers, which also measure the electrical conductivity of the water, were installed in wells where a significant change in this property could be expected (i.e. in the pumping well). Additionally, another diver, not installed in one of the wells, was programmed to monitor the atmospheric pressure (the barodiver). This was necessary because the divers measure the combined pressure of the water column and the atmosphere.

Knowing the density of water, the atmospheric pressure, and making a manual reference measurement of the water level from the top of each casing when the divers start measuring, the height of the water column above the pressure sensor in the diver could be established. The latter could afterwards be converted to mTAW which is the water level relative to the sea level. This intermediate step of data processing is illustrated by the formulas below (Van Essen Instruments, 2016):

$$\boldsymbol{WC = 9806.65\ \frac{P_{Diver} - P_{Baro}}{\rho \times g}} \qquad \{3\}$$

$$\boldsymbol{WL = TOC - CL + WC} \quad \boldsymbol{with\ CL = MM + WC} \qquad \{4\}$$

Where:

WC	: height of the water column above the diver [cm]
P_{Diver}	: pressure measured by the divers in the well [cmH_2O]
P_{Baro}	: pressure measured by the barodiver [cmH_2O]
ρ	: density of the water [1000 kg/m^3]
g	: acceleration due to gravity [9.81 m/s^2]
WL	: water level in relation to the vertical reference datum [cm]
TOC	: top of the casing measured in relation to the vertical reference datum [cm]
CL	: cable length [cm]
MM	: manual reference measurement of the water level from the top of the casing [cm]

The actual pumping started at 15h14, October 25 2021, with a maximum estimated pumping and reinjection rate of 3.8 m^3/h (see 'Pumping tests') in PP4. After roughly half an hour the injection in PB JE was initiated. From 11h45 to 13h00, October 28, the pumping and injection were disturbed due to the execution of an MFI-test (see later). Also on November 5, the test was disturbed because the divers had to be programmed again when their memory was full. More specifically, the barodiver and the divers in PP2 and PB JE started measuring every 20 seconds from 10h00, October 22. Because of memory limitations, the CTD divers in PP4 and PP6 started measuring every 20 seconds from 10h00, October 24. Finally, the divers in PB 6.1, 6.2 and 2.1 started measuring every minute from 12h00, October 25. All divers stopped on the 5th of November. Only the barodiver and the divers in PB JE and PP4 were programmed again to monitor the pressure every minute from November 5 to December 8 (December 20 for the diver in PB JE and the barodiver). The pumping and injection test stopped on December 20. To have an idea of the seasonal variations of the water level, the divers in PB JE and PP4 were programmed to monitor the pressure every 3 minutes from December 20 (2021) until May 2 (2022).

2.2.3. Chemical analysis

When implementing an ATES system, the impacts on the groundwater quality (and ecology) should be negligible. For instance, if iron or calcite would precipitate due to a change in chemical equilibria, this might result in a reduction of permeability due to chemical clogging.

Usage of the shallow subsurface results in local temperature anomalies. In Flanders and the Netherlands, the natural groundwater temperature typically increases from 9-12 °C to 15-20 °C for the warm well area and it decreases to 5-10 °C in the cold well area. This induced temperature difference in the subsurface can influence chemical equilibria and/or biological activity (Bonte et al., 2011; Hänlein et al., 2013; Meng et al., 2019; Perego et al., 2020; Todorov et al., 2020). However, not only the temperature difference might result in a change in the groundwater chemistry. In water table aquifers, a vertical groundwater quality gradient with oxidized, nitrate-rich, shallow groundwater and reduced, iron-rich, deeper groundwater is present. These are zones in which the redox potential is determined by a dominant redox couple. Their existence is due to the depletion of O_2 (mainly) in the saturated zone. Otherwise, the oxidation of organic matter (strongest reductant) for example would always be accompanied by O_2 reduction (with O_2 being the strongest oxidant). But when O_2 has been depleted, the second strongest oxidant (NO_3^-) will take over and the redox potential will drop. Subsequently, the reduction of for instance iron oxides will take over and the redox potential will be lowered again (Edmunds and Shand, 2008). Due to the implementation of an ATES system, mixing of different types of groundwater (aerobic/anoxic) might occur, homogenising the natural vertical quality gradient. Also, groundwater contaminants present in many urban areas might be mobilized. Most research focuses on the significant impact of temperature changes > 30°C such as changes in mineral solubility, reaction kinetics, and organic matter oxidation. Nevertheless, it was also shown that redox reactions are sensitive to smaller temperature changes as well (5-15°C) (Bonte et al., 2011). The possible negative effects of ATES implementation and their probability are listed in Figure 7. Hence, not only the hydrology and temperature difference due to the ATES operation must be paid attention to but also the chemical (and microbiological) impacts in the affected areas should be carefully evaluated (Bonte et al., 2011; Todorov et al., 2020).

To estimate the risk for a significant adverse impact on the groundwater quality in the study area, a multi-parameter probe in a flow-through cell was used on-site to measure the pH, the oxidation-reduction potential (ORP), the temperature (which is also measured by all the installed divers), the electrical conductivity (also measured by the CTD divers), dissolved O_2, the salinity and the total dissolved solids (TDS). This was measured for each pervious layer separately (Yd 2, Yd 4 and Yd 6). Additionally, groundwater samples were taken from the same pervious layers. These were analysed in the Laboratory for Applied Geology and Hydrogeology of the geological department of Ghent University. Also, a TA-TAC titration, where HCl (0.01 molarity) was added to a sample of 10 ml, was carried out to determine the bicarbonate/carbonate content. In the end, using these results, the groundwater was classified according to the Stuyfzand classification and the quality was compared to the standards drawn up in Vlarem II, 2019 (Stuyfzand, 1986; Vlaamse Milieumaatschappij, 1995).

Negative effect of underground thermal energy storage	Probability[†]	Consequence[‡]	Risk[§]
Hydrological impacts			
Changing water levels and fluxes	++	Desiccation, water logging, settlements	±
Changing other well's capture zone	++	Increasing vulnerability, pollution	++
Poorly sealed boreholes	+	Cross-aquifer flow	++
Thermal impacts			
Changing water temperature	++	Temperature, reaction kinetics	+
Chemical impacts			
Mixing processes and chemical reactions	++	Salinity, IMIPO, OMIPO	++
Reactivation of otherwise stable groundwater pollution plumes	±	IMIPO, OMIPO	++
Oxidation of organic matter	±	Nutrients, DOC, color	+
Oxidation of iron sulfides	±	Fe, SO_4, As, Ni, Co, Zn	+
Dissolution/precipitation of carbonates	-	Ca, HCO_3, Sr	±
Dissolution/precipitation of silicates	-	SiO_2	±
Leaching from installation materials	±	Cd, Cu, Cr, Ni, Pb, VC	+
Leaking anti-freeze fluids or additives	±	Glycol, biocides, corrosion inhibitors	++
Microbiological impacts			
Introduction or mobilization of pathogens	-	Pathogens	±
Increasing biodegradation rate	±	Nutrients, IMIPO, OMIPO	- or +
Changing microbiological population	+	Unknown	?

[†]Probability of occurrence is small (-), moderate (±), high (+), or almost always (++).
[‡]IMIPO = inorganic micro-pollutants, OMIPO = organic micro-pollutants, DOC = dissolved organic carbon, VC = vinyl chloride.
[§]Probability of risk is negative, resulting in opportunity (-); none (±); low (+), high (++).

Figure 7: Qualitative overview of risks of low temperature (< 30°C) underground thermal energy storage on groundwater systems (Bonte et al., 2011; Todorov et al., 2020). Beware that leaking is only of importance when implementing a BTES system.

2.2.4. Membrane Filtering Index test

The pumped water contains some sediment particles which may damage the installation and clog the (injection) wells. As a result, it might increase the injection pressure over time and therefore decrease the specific capacity. For ATES systems, the wells are alternately injection or pumping wells according to the season. As such, if the capacity of the wells would decrease over time due to clogging, this would be detrimental to the overall efficiency and capacity of the ATES system. Also, the pressure at the injection well cannot become too high as it will increase the risk of wetting the ground surface. Research has shown that backflushing can restore well performance after clogging from silt- and sand-sized sediment particles. Clogging due to clay-sized particles, on the other hand, is less easily restored (Jenne et al., 1992; De Zwart, 2007). However, neither way of clogging is desirable. As such, a Membrane Filtering Index (MFI) test must be carried out on-site to determine the clogging risk. The latter is of particular importance in the study area since the groundwater reservoir consists of a considerable amount of silt- and clay-sized particles. This index is a measure of the rate at which a filter paper (0.45 µm) becomes clogged under constant water pressure (2 bar), in this case, 3.1 m^3/h (Figure 8) (Schippers & Verdouw, 1979, 1980; Olsthoorn, 1982).

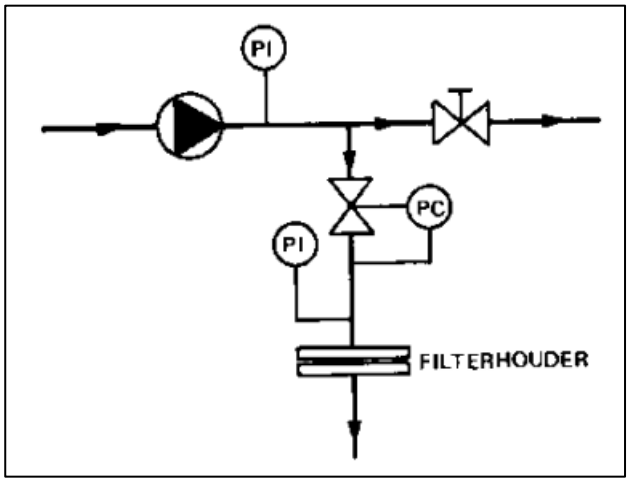

Figure 8: Schematization of the setup for the Membrane Filtering Index test including two valves to regulate the water pressure and a holder for the filter paper (Schippers & Verdouw, 1979).

In practice, every time 100 ml of water passed through the filter, the total filtered volume and time are monitored. As such, the index can be derived by plotting the ratio of the filtration time and the filtered sample volume (t/V) as a function of the total filtered volume (V) in the MFI test. If the filter paper becomes clogged by the filtrate (the filtered sediment), the time to filter 100 ml of water will increase as the filtrate becomes compressed. In the graph, this will be expressed as a steeper slope. When the slope of the graph is <10, the water purity is considered acceptable for reinjection purposes for ATES systems. When the slope of the graph is <3, the water purity is excellent for reinjection (Schippers & Verdouw, 1980; Olsthoorn, 1982). An MFI test does not include further analysis of the amount of filtrate (filtered sediment). The actual MFI test for this study was carried out twice from 11h45 to 13h00 on October 28, 2021, after the sand content (> 70 µm) of the pumped water was visually analysed. For the latter, the pumping rate on PP4 was 3.8 m^3/h for 20 minutes. It is important to develop the pumping well before the execution of the tests as the wells are not often used and sediment content typically diminishes when the well is better developed (Aalten & Witteveen, 2015). The long-term pumping and reinjection test described earlier (October 25 - December 20) also served to verify whether there was a decrease in injection capacity with time.

Notice that clogging, besides being caused by mechanical-physical processes, can also be of a microbiological or geochemical origin or due to corrosion and gas (Jenne et al., 1992; De Zwart, 2007). These processes will not be discussed or investigated because clogging by sediment particles is expected to be the dominant source of clogging in the study area.

2.2.5. Groundwater model

When implementing an ATES system, changes in the local groundwater levels and flow are inevitable. A cone of depression will be established around a pumping well and the inverse will happen around an injection well. The system must be carefully designed to avoid interaction between the wells and to ensure that the desired pumping/injection rate can be reached in each well. Also, the storage efficiency of the geothermal energy in the aquifer, which is strongly related to the well placement, must be optimal. Creating a numerical model is therefore a viable and indispensable tool to assess the feasibility of the project. It not only helps in understanding and predicting the behaviour of complex systems but it also helps to optimize the desired project implementation (Yapparova et al., 2014). The different aspects that must be considered when creating the groundwater model as well as its use for this study are discussed below.

2.2.5.1. Conceptual model

The (hydro)geology of the study area must be translated into a numerical model. This schematization of the complex reality is called the conceptual model. In order to do this, some simplifying hypotheses were made. Additionally, boundary conditions must be specified to solve the mathematical equations linked to the model.

2.2.5.1.1. Geological and Hydrogeological context

Based on the previously elaborated 'Lithostratigraphic and hydrogeological setting of the study area' and Figure 5, a 3D model of 5 x 5 km around Campus Sterre was made. This size was chosen to limit the influence of the boundary conditions on the estimates in the study area (see also later). The model consists of 8 horizontal and homogeneous layers (Table 2). Only the Gentbrugge Fm. (Paniselian Aquitard) ceases to exist towards the Southwest, as was also described earlier. The boundary for its occurrence was set using the catalogue of Geopunt Vlaanderen. To implement this in the model, its thickness was set to almost 0 in the Southwest. Its thickness in the model increases towards the Northeast to 4 m which is less than it would be at that location in reality. However, it is far away from the actual study area and will not have an influence on the results as it is not a permeable layer and no observation wells are present in the Quaternary unit. Also, it can be explained by the fact that no dipping of the layers towards the Northeast was implemented in the model, thus limiting the possibility to increase the thickness of the layers in this direction. Varying the thickness of the Gentbrugge Fm. was done using an interpolation method. All layers, except for the Quaternary, were set to be confined in the model. This means that they are expected to remain fully saturated at all times. The Quaternary was set as unconfined implying that the saturated thickness of this layer varies together with the water table.

Slight differences can be observed between this conceptual model and the one created by Lebbe et al., 1992 (Table 1, Table 2). For instance, the model is bounded above by the top of the Quaternary and not by the water table. Additionally, the Gentbrugge Fm. was modelled as a separate layer and the upper layer was not subdivided into three units.

Table 2: The layers that were used for the conceptual model (after Lebbe et al., 1992).

Layer	Top and bottom (mTAW)	Thickness (m)
Quaternary	+10.4 to +2.4 (varying)	8 (varying)
Gentbrugge Fm.	+2.4 (varying) to +1.4	1 (varying)
Yd 6	+1.4 to -3.6	5
Yd 5	-3.6 to -5.1	1.5
Yd 4	-5.1 to -14.6	9.5
Yd 3	-14.6 to -20.6	6
Yd 2	-20.6 to -24.6	4
Yd 1	-24.6 to -40.6	16

2.2.5.1.2. Flow and transport boundary conditions

By default, the bottom and sides of the model are set as zero-flux boundaries which means there will be no flow through these surfaces. This boundary condition was not changed for the bottom boundary because, below Yd 1, the aquitard corresponding to the Kortrijk Fm is present. The Northern, Eastern, Southern and Western boundaries were set as constant head boundaries, a Dirichlet condition. This means that a hydraulic head was imposed which remains constant during the entire simulated period. A value of 10 mTAW was selected for all four boundaries. This value will not influence the results of the simulation (performed in transient state conditions) in the study area because the boundaries are chosen far away i.e. 5 x 5 km around the study area. This choice can also be justified considering that an ATES system does not have any net abstraction. Using such boundary conditions, no hydraulic gradient was imposed for the initial simulations. However, for the long-term simulation, the gradient might have an influence so this will change later on (see: 'Modelling scenario'). At the start of each simulation, an initial head of 6.97 mTAW was chosen. This is the hydraulic head that was measured in PP 4 before the installation of the diver in October 2021.

Transport boundary conditions can be set by using the SSM package. However, the default option of zero-dispersion/diffusion mass flux (heat in this case) is imposed for the boundaries. This Neumann condition ensures that the solute (/heat) can only leave the model by advection. Additionally, it is worth mentioning that, to try to reduce the computation time for the transport simulations, the active zone of the model was adjusted to an area covering 450 x 650 m around the wells. This can be justified because the change in temperature due to transport processes in the aquifer induced by the ATES system is not expected to reach beyond the new boundaries.

2.2.5.1.3. Simplifying hypotheses

Constructing a realistic and reliable groundwater model is a challenging and time-consuming task. Many parameters are involved and often a limited amount of available data leads to an uncertain estimation of those parameters. Hence it needs to be emphasized that simplifying hypotheses were made to create the model which will inevitably limit its predictive capacity to a certain extent (Yapparova et al., 2014). However, such simplifications can be justified for an initial feasibility study of the project which is an ATES system with no net abstraction in a (semi-)confined aquifer.

First of all, no horizontal anisotropy is considered. This means that the horizontal hydraulic conductivity is equal in all directions (Ky=Kx). Second, within each layer, no heterogeneity is taken into account. Worth clarifying is the difference between anisotropy and heterogeneity. Anisotropy is the change in the value of a parameter depending on the direction while heterogeneity is the change in the value of a parameter in space. Not accounting for heterogeneity in the subsurface is nevertheless an important bottleneck for designing and predicting ATES systems as it influences groundwater flow and transport. Taking this into consideration, it is evident that heterogeneity influences the distribution of warm and cold plumes (Bridger & Allen, 2014; Sommer et al., 2013, 2015). Consequently, also the efficiency of an ATES system may vary with local heterogeneity (Possemiers et al., 2015; Hermans et al., 2018). Even though the shown importance of heterogeneity, it was not included in the model because of the lack of data. As such, the principle of parsimony was used implying that the best solution is the one that requires the fewest possible assumptions to explain the data.

Third, neither surface topography, nor layer inclination, is accounted for in the conceptual model. This is as well for simplification purposes as it is expected that the model results will not vary much with the surface topography since the upper Quaternary layer does not correspond to the groundwater reservoir of interest. Also, the inclination of the layers was disregarded as the thickness of the layers of interest does not vary with the inclination i.e. the thickness remains constant. As such, here also the principle of parsimony applies.

Fourth, phenomena that could have an additional influence on the groundwater flow were not considered in this study. These coupled processes were assumed not to have a significant influence on the data. Examples

of coupled processes are geomechanical effects (subsidence due to drawdown) and thermal effects. The latter involves changes in hydraulic conductivity due to changes in viscosity (intrinsic permeability) and the induction of a density-driven flow due to density changes of the water. However, for the proposed ATES system only limited temperature changes of +/- 5 °C are considered. As a result, neglecting the thermal effects in the first instance is a valid assumption. It is indeed confirmed by Zuurbier et al. (2013) and Zeghici et al. (2015) that for most shallow ATES applications with limited temperature differences (< 15 °C), density differences are not significant as the free convection (driven by density differences) is much smaller than forced convection (driven by external sources e.g. hydraulic gradient).

Fifth, through the buffering effect of conduction, the value of thermal dispersion (in heat transport) is small in comparison with solute mechanical dispersion (in solute transport). As such, also the thermal dispersion is small in comparison with diffusion in heat transport. Hence, its effect was neglected as a heat transport process. Numerical dispersion will already occur due to simulation characteristics justifying the decision of not manually implementing dispersion as a model parameter.

Sixth, as mentioned earlier, initially no hydraulic gradient was imposed. Also, no seasonal variations were accounted for. Furthermore, only flow in the saturated zone was considered. Finally, regarding heat transport, no heat flux from the bottom or the atmosphere was accounted for as it would remain limited because the aquifer is confined.

2.2.5.2. Mathematical model

A system is transient if it is affected by non-constant factors such as extraction by pumping. But if all the stress factors remain constant the system will evolve towards a new equilibrium (steady-state). It was opted to start immediately with the transient-state simulation because of the interest in the evolution of the groundwater level with time. Also, the initial groundwater level in the study area was not determined using a steady-state simulation because the boundaries were set as constant head boundaries and the initial groundwater levels were measured in the field.

In transient conditions, the volume of water stored in the volume of the model can vary with time. As a result, inflow ≠ outflow anymore but an additional parameter has to be added to the equation of mass conservation i.e. the storage. For a confined aquifer the storage coefficient ($S = specific\ storage\ coefficient + specific\ yield$) can be simplified to only the specific storage coefficient because the specific yield is negligible. The specific yield is linked to a change in saturation which does not apply in a confined aquifer which remains fully saturated. This results in the following set of 3D equations (Langevin et al., 2017a):

Darcy's Law for 3D movement of groundwater of constant density through porous earth material:

$$\boldsymbol{q} = -\boldsymbol{K}\nabla\boldsymbol{h} = -\begin{pmatrix} \boldsymbol{K_{xx}} & \boldsymbol{0} & \boldsymbol{0} \\ \boldsymbol{0} & \boldsymbol{K_{yy}} & \boldsymbol{0} \\ \boldsymbol{0} & \boldsymbol{0} & \boldsymbol{K_{zz}} \end{pmatrix}\nabla\boldsymbol{h} \qquad \{5\}$$

Water balance on a small volume:

$$\boldsymbol{inflow - outflow = change\ of\ storage\ with\ time}$$

$$-\boldsymbol{div}(\boldsymbol{\rho_w q}) - \boldsymbol{\rho_w q'} = \boldsymbol{\rho_w S_s}\frac{\boldsymbol{\partial h}}{\boldsymbol{\partial t}} \qquad \{6\}$$

{5} in **{6}**: Partial-differential equation that describes the distribution of the hydraulic head:

$$\frac{\boldsymbol{\partial}}{\boldsymbol{\partial x}}\left(\boldsymbol{K_{xx}}\frac{\boldsymbol{\partial h}}{\boldsymbol{\partial x}}\right) + \frac{\boldsymbol{\partial}}{\boldsymbol{\partial y}}\left(\boldsymbol{K_{yy}}\frac{\boldsymbol{\partial h}}{\boldsymbol{\partial y}}\right) + \frac{\boldsymbol{\partial}}{\boldsymbol{\partial z}}\left(\boldsymbol{K_{zz}}\frac{\boldsymbol{\partial h}}{\boldsymbol{\partial z}}\right) - \boldsymbol{q'} = \boldsymbol{S_s}\frac{\boldsymbol{\partial h}}{\boldsymbol{\partial t}} \qquad \{7\}$$

Where:

q	: fluid-flux vector/ Darcy's velocity [m/s]
K	: hydraulic conductivity tensor [m/s]
K_{xx}, K_{yy}, K_{zz}	: values of the hydraulic conductivity along the x, y, and z coordinate axes (assumed parallel to the major axes of hydraulic conductivity [m/s]
h	: hydraulic head [m]
∇h	: head-gradient vector
q'	: sink/source term [m/s]
ρ_w	: density of water [kg/m3]
S_s	: specific storage coefficient [1/m]
t	: time [s]

For an unconfined aquifer, this 3D equation must be simplified to a 2D equation as only flow in the saturated zone is considered. In 2D equations, the hydraulic conductivity is replaced by the transmissivity. The transmissivity is defined as the integral of the hydraulic conductivity over the thickness of the aquifer. In an unconfined aquifer, the thickness depends on the hydraulic head, thus the transmissivity will also depend on the hydraulic head. Next, the specific storage has to be replaced by 'Ss* thickness of the aquifer'. However, in an unconfined aquifer, the specific storage can be disregarded because it is negligible in comparison with the specific yield. This results in the following equation:

$$\frac{\partial}{\partial x}\left(T_x \frac{\partial h}{\partial x}\right) + \frac{\partial}{\partial y}\left(T_y \frac{\partial h}{\partial y}\right) + \frac{\partial}{\partial z}\left(T_z \frac{\partial h}{\partial z}\right) - q' = Sy \frac{\partial h}{\partial t} \qquad \{8\}$$

Where:

T_x, T_y, T_z	: values of the transmissivity along the x, y, and z coordinate axes [m2/s]
S_y	: specific yield [m3/m3]

When the output of the groundwater flow simulations (based on MODFLOW) has been generated, MODPATH can be used to calculate the three-dimensional flow paths (Pollock, 2012). MODPATH is a particle-tracking post-processing program designed to compute paths for imaginary "particles" of water moving through the simulated groundwater system. In addition, the time of travel of the particles is calculated. The path can be computed by tracking the particle from one cell to the next until it reaches a boundary, an internal sink/source, or satisfies another termination criterion. The computation of these paths can be forward or backward. To calculate these pathlines, the values of the principal components of the velocity vector at every point in the flow field must be calculated based on the intercell flow rates from the finite difference model. To do this, a simple linear interpolation method can be used. For transient-flow simulations, the shortly described particle-tracking algorithm for steady-state flow can be extended considering that transient simulations behave as a series of steady-state flow periods during which the flow remains constant and the storage changes within cells. As stated by Pollock (2012): "For each time step particle paths are computed just as for the steady-state case until the end of the time step is reached. A new velocity distribution is then calculated for the next time step and the computation of the paths is resumed.". To consult the set of equations used by MODPATH, the reader is referred to Pollock (2012).

Next, to simulate the extent of the warm and cold plumes induced by the ATES system, transport equations must be used. Heat transport can be translated into a mathematical problem using the following equation (Zheng, 2010):

$$\left(1 + \frac{1-\theta_t}{\theta_t}\frac{\rho_s}{\rho_w}\frac{c_s}{c_w}\right)\frac{\partial(\theta_t T)}{\partial t} = \nabla\left(\theta_t\left(\frac{k_0}{\theta_t \rho_w c_w} + D_{mech}\right)\times \nabla T\right) - \nabla(qT) + q_s T_s \qquad \{9\}$$

$$with \quad k_0 = k_w\theta + k_s(1-\theta)$$
$$\rho_b = \rho_s(1-\theta_t)$$

Where:

θ_t	= 35	: total porosity [%]
ρ_b	= 1716	: bulk density [kg/m3]
t	-	: time [s]
q	-	: specific discharge vector [m/s]
q_s	-	: volumetric flow rate per unit volume of the aquifer representing sources or sinks [m/s]
ρ_s	= 2640	: density of the solid [kg/m3]
ρ_w	= 1000	: density of the water [kg/m3]
c_s	= 710	: specific heat capacity of the solid [J/(kg°C)]
c_w	= 4183	: specific heat capacity of the water [J/(kg°C)]
T	-	: temperature [°C]
k_0	= 2.153	: bulk thermal conductivity [W/(m°C)]
k_w	= 0.58	: thermal conductivity of the water [W/(m°C)]
k_s	= 3	: thermal conductivity of the solid [W/(m°C)]
D_{mech}	-	: mechanical dispersion coefficient tensor [m2/s]
T_s	-	: source temperature

The values for the different parameters above are the ones used by Vandenbode et al. (2011) in a shallow heat injection and storage experiment in the same study area. They were in turn derived from Langevin et al. (2007). They represent values of quartz sediment. These parameters have a smaller range for different sediments than for example the hydraulic conductivity. Hence they can be considered representative of the aquifer.

The first term on the right-hand side of the equation represents heat transport by conduction and thermal dispersion. The second and third terms respectively represent the heat transport by groundwater flow and the thermal sinks/sources. On the left-hand side of the equation, the heat storage with time and the effect of thermal retardation due to conduction between the solid and the fluid is reported.

Because of the similarity between solute and heat transport and because of the disregarding of density/viscosity effects, MT3D-USGS could be used to model heat transport processes (Zheng, 2010; Hecht-Méndez et al., 2010; Sommer et al., 2013; Possemiers, 2014). Indeed, when comparing the solute transport equation {10} with the heat transport equation {9}, the heat transport by conduction and thermal dispersion is analogous to molecular diffusion and mechanical dispersion in the solute transport equation.

Next, the transport of heat by groundwater flow is analogous to the advection term in the solute transport equation (Zheng, 2010).

$$\left(1+\frac{\rho_b}{\theta_e}K_d\right)\partial\left(\frac{\theta_e C}{\partial t}\right)=\nabla(\theta_e D\times\nabla C)-\nabla(qC)+q_s C_s+\sum R_n \qquad \{10\}$$

Where:

K_d : distribution coefficient [m3/kg]
C : concentration of the solute [kg/m3]
D : hydrodynamic dispersion coefficient tensor [m2/s] = mechanical dispersion coefficient tensor (Dmech) + molecular diffusion coefficient (Dm)
C_s : concentration of the source or sink flux [kg/m3]
R_n : chemical reaction term

To implement this in MT3D-USGS, the (thermal) distribution coefficient (K_d^t) and the molecular diffusion coefficient (D_m^t) must be defined as follows (Zheng, 2010):

$$K_d^t=\frac{c_s}{c_w\rho_w}=1.69*10^{-4}\ m^3/kg \qquad D_m^t=\frac{k_0}{\theta_t\rho_w c_w}=1.47*10^{-6}\ m^2/s \qquad \{11\}\ and\ \{12\}$$

The distribution coefficient can be used as input for the first sorption parameter when the RCT (chemical reaction) package in MT3D-USGS is selected. The molecular diffusion coefficient can be implemented in the tab 'Layer Groups' when the DSP (dispersion) package in MT3D-USGS is selected.

To end, the heat transfer process between the fluid and the solid (conduction) results in a retardation of the movement of the warm/cold temperature plume in comparison to the average linear groundwater flow velocity (equation 13) (Zheng and Wang, 1999; Vandenbohede et al., 2011).

$$thermal\ retardation\ factor=1+\frac{\rho_b}{\theta}K_d^t=1.83 \qquad \{13\}$$

2.2.5.3. Numerical model

2.2.5.3.1. ModelMuse

For this project, the freely available USGS MODFLOW 6 software was used (Langevin et al., 2017a, 2017b). This is the most widely used software for groundwater models. The model itself was built using the software ModelMuse which is only a graphical interface to MODFLOW (Winston, 2019). Also, MODPATH was used to simulate advective transport (Pollock, 2012). Finally, MT3D-USGS was used to model the full transport processes (Bedekar et al., 2016).

2.2.5.3.2. Numerical methods

The natural neighbour method was used for interpolation of the thickness of the Gentbrugge Fm in the study area. This method applies a weight to all the closest neighbours based on proportionate areas.

MODFLOW uses the control-volume finite-difference method to solve the mathematical equation numerically. This means that firstly the continuous domain was subdivided into a finite number (*n*) of cells. Using this control-volume finite-difference approach, a cell (which is not necessarily rectangular) can be hydraulically connected to any number of surrounding cells. Secondly, the partial derivative equations are replaced by a set of *n* discretized finite-difference equations, one for each cell of the grid. In short, the derivatives are replaced by the finite difference between neighbouring cells. In each cell of the grid, an unknown is present: the hydraulic head. The goal is to solve the new system of *n* equations in order to calculate the variable at each location of the grid (*n unknowns*). In the block centred finite difference method only the solution at the

nodes is calculated (no interpolation is done between nodes). The node is the central point of a cell which is considered homogeneous. The derivatives are approximated by finite differences. The system of equations is then solved iteratively using an initial value. This version of Modflow ensures the continuity of fluxes towards any adjacent cell and the difference equations are based on the mass conservation in each cell. For more details on the implementation of the control-volume finite-difference method in Modflow, the reader is referred to Langevin et al. (2017a).

In the transient equation, time is an important parameter: the values of the parameters in the cells (like the hydraulic head) are changing over time. As a result, the system of equations mentioned above has to be solved at each time step. To solve this equation using the (control-volume) finite-difference method an explicit method, an implicit method or a semi-implicit method can be used. In these methods, the value of the parameters is respectively considered at time t, at time t+Δt and at a time between t and t+Δt. Modflow makes use of a semi-implicit method. This method aims to stabilise the solution.

To solve the heat transport equation, the third-order TVD (Total Variation Diminishing) method was used (Zheng and Wang, 1999). This Eulerian method uses a fixed axis system (i.e. it does not move along the streamline). The TVD method is comparable with the finite difference method, but the former has a higher order of precision to solve advection-dominated transport problems. In 1D, four nodes (three neighbours) are needed to calculate the solution. It is better to use a backward approximation and use two neighbours upstream and one downstream because more information is available upstream (this is where the warm/cold plume comes from). The Generalized Conjugate Gradient (GCG, convergence criterion of 10^{-10}) Solver is used to implicitly solve the dispersion, sink/source and reaction terms with a finite-difference method. Finally, a linear sorption isotherm was selected in the RCT package. It accounts for the heat transfer process between the fluid and the solid (conduction).

2.2.5.3.3. Grid discretization

As mentioned earlier, the continuous domain of the model was subdivided into a finite number of cells. For this project, a structural grid was used (DIS package) (Langevin et al., 2017a). Each of the 8 layers consists of squares and/or rectangles. For the ease of implementing georeferenced shapefiles and images, the vertices that define the edges of the active zone of the model are expressed in Belgian Lambert 72 coordinates (EPSG: 31370). This is the projected coordinate system for Belgium - onshore. The bottom left corner was assigned ‘101550,188280’ and the upper right corner was assigned ‘106550, 193280’. This results in a grid of 5 by 5 kilometres as the coordinates are expressed in meters. The z-axis of the model is defined in mTAW.

The smaller the cell size, the more accurate the approximation will be. However, a balance between cell size and computation time must be found. To improve the solution but avoid an exaggerated computation time, the grid was only refined where the solution was expected to change rapidly, i.e. where a steep gradient is expected. With such kind of irregular grid, the ratio of the width of adjacent cells should not be larger than 1.5. Besides, the ratio of the horizontal cell size and the vertical cell size shouldn’t be larger than 10. For this project, the largest grid size was 100 m. This grid size was set smaller when approaching the well area. It decreases to 5 m, to 0.5 m and finally approximates the drilling diameter of the wells (roughly 0.25 m) (Figure 9). To meet the above-discussed criteria, the grid was smoothed. Furthermore, the grid was adjusted several times during the project because the focus was on the well area which shifted in space during different steps of the project. However, the grid size itself remained about the same. Only for heat transport the smallest grid size was 1 m around the well area. The previously smaller cell size was needed for calibration and to limit numerical dispersion for the advective transport simulation but not for heat transport simulations where diffusion is much more important.

Next, to solve transient equations, also the time is discretized in time steps. In that case, it has to be ensured that the advective path during a time step is smaller than the grid cell size, otherwise smaller times steps have to be chosen. This condition is defined by the 'Courant number' and is automatically verified by Modflow/MT3D-USGS. For the flow simulations for this project, the maximum length of the first time step was set to 60 s and the multiplier, which is the incrementation of the time step size, was set to 1.3.

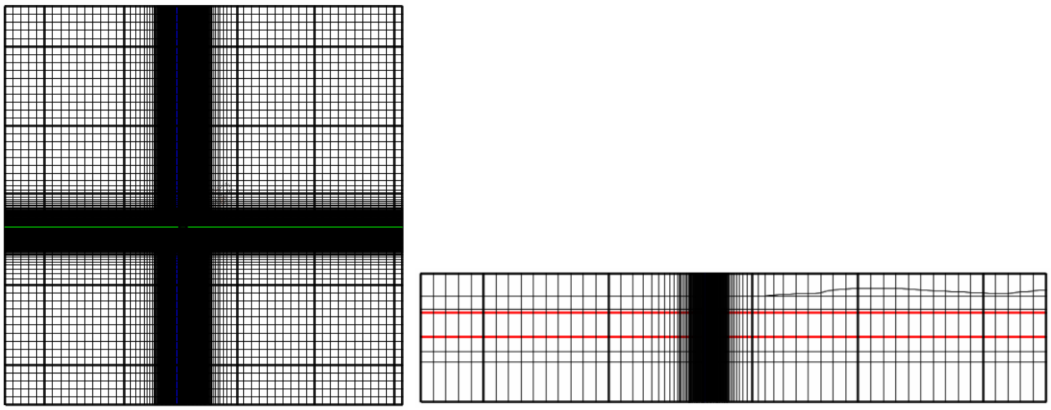

*Figure 9: Example of the used grid (5*5 km) and a cross-section through the grid which is refined around the well area.*

2.2.5.4. Calibration

Model calibration is needed to ensure that the model will approximate the reality as close as possible. The results from the calibration are the values of the set of hydraulic parameters that had to be defined (K_x, K_z, S_s, S_y, porosity). In practice, because Lebbe et al. (1992) gathered a lot of valuable data in the study area, the values of their already calibrated model were used to first simulate the triple pumping test with the newly constructed model. This was done to ensure that the model works in the appropriate way. However, to do this, first, the hydraulic resistance from Table 1 has to be converted to the vertical hydraulic conductivity (K_z). Because the resistance is calculated between the nodes (i.e. central point of a homogeneous cell) of two consecutive layers, this was done using the following equation (after Langevin et al., 2017a):

$$\boldsymbol{Hydraulic\ resistance\ between\ layer\ a\ and\ b\ (in\ days)} = \frac{L_a/2}{K_{z,a}} + \frac{L_b/2}{K_{z,b}} \qquad \{14\}$$

Where:

L_a, L_b : thickness of layer a and b [m]

$K_{z,a}$, $K_{z,b}$: vertical hydraulic conductivity of layer a and b [m/d]

This equation can be used to iteratively determine K_z for all layers when imposing an initial K_z for a particular (pervious) layer (Table 3). Here a K_z of 0.05 m/d was chosen for layer 6.

Table 3: Hydraulic parameters used as input for the model (after Lebbe et al., 1992).

Layer	Kx (m/s)	Kz (m/s)	Ss (1/m)	Sy (m^3/m^3)	Porosity
8 (Quaternary)	2,89E-06	4,73E-09	5,50E-05	9,84E-03	0,3
7 (Gentbrugge Fm.)	2,89E-06	4,73E-09	5,50E-05	9,84E-03	0,3
6 (Yd 6)	9,94E-06	5,79E-06	5,50E-05	9,84E-03	0,3
5 (Yd 5)	2,31E-07	2,44E-07	5,50E-05	9,84E-03	0,3
4 (Yd 4)	1,28E-05	1,13E-05	3,60E-05	9,84E-03	0,3
3 (Yd 3)	2,31E-08	8,61E-09	3,60E-05	9,84E-03	0,3
2 (Yd 2)	1,46E-05	1,14E-08	3,80E-05	9,84E-03	0,3
1 (Yd 1)	4,63E-07	3,11E-07	1,20E-05	9,84E-03	0,3

Next, in essence, the drawdown with time in the nine observation wells in the study area (implemented in the model using the OBS package) was simulated and compared to the measured drawdown in the field. When there was good accordance between the results of the new model and the results by Lebbe et al. (1992) (Figure 6), it was decided to simulate the pumping/injection test that was performed in light of this study. To check whether the model simulates the reality well, the method proposed by Cooper and Jacob (1953) was used. This is a graphical technique for the determination of the hydraulic properties (transmissivity and storage coefficient) of non-leaky confined aquifers. It is based on the Theis' equation (Theis, 1935) which could also be translated to a graphical method but this needed the computation of a special 'type-curve' for each used observation of drawdown (Cooper and Jacob, 1953). The straight-line method by Cooper and Jacob (1953) involves that, when sufficient time has elapsed after a confined well has begun discharging at a steady rate, the drawdown within a given distance increases approximately in proportion to the logarithm of the time since the discharge began, and decreases in proportion to the logarithm of the distance from the well. As such a straight line can be matched to the semi-logarithmic plot of the observed drawdown.

2.2.5.5. Well placement

To design an ATES system, first the energy demand of the building, both for heating and cooling, that must be fulfilled by geothermal energy must be determined. With this knowledge, the volume of water to be extracted and the resulting temperature change in the groundwater reservoir can be estimated. As such, knowing the maximum pumping/injection rate for a single well pair, the number of well pairs can be calculated. This is illustrated by the following equations, ignoring in first instance the coefficient of performance of the heat pump (Glassley, 2015):

$$\boldsymbol{E = V \times c \times \Delta T} \qquad \{\mathbf{15}\}$$

$$\boldsymbol{Q = \frac{V}{t} \leftrightarrow Q = \frac{E}{tc\Delta T} = \frac{P}{c\Delta T}} \qquad \{\mathbf{16}\}$$

$$\boldsymbol{N = \frac{Q}{Q_{max}}} \qquad \{\mathbf{17}\}$$

Where:

- E : thermal energy that can be stored/extracted from a given volume of water [J]
- V : volume of water [m^3]
- c : the heat capacity of water [4.178 * 10^6 J/m^3K]
- ΔT : the difference in temperature between the extracted and injected water [K]
- Q : the total flowrate of the system [m^3/s]
- t : time [s]
- P : power [W]
- N : the number of well pairs (each pair consists of 2 drillings)
- Q_{max} : the maximum pumping/injection rate for a single well pair [m^3/s]

From these equations, it is apparent that the produced power is proportional to the flow rate and the temperature difference. This again justifies the need for groundwater modelling to design an ATES system sustainably.

Additionally, optimal use of (sub)surface space and an optimal storage efficiency should be realized. One of the parameters which influences this performance, besides the groundwater flow and pumping rate, is the well placement (Yapparova et al., 2014). Many studies have been carried out related to this topic. In short, it was shown that storage efficiency decreases with decreasing distance between the warm and cold well

areas. The storage efficiency also decreases with increasing hydraulic conductivity (Kim et al., 2010; Yapparova et al., 2014). As such, the relatively low hydraulic conductivity in the study area might be an advantage in this project which can be used to choose a smaller distance between the wells. Hence, optimizing the usage of space without compromising the storage efficiency. The fact that the storage efficiency decreases with increasing hydraulic conductivity can be explained by a short-circuit between the cold and warm well areas. This is also often called a thermal breakthrough (Kim et al., 2010; Gao et al., 2013; Yapparova et al., 2014; Bloemendal et al., 2018). It means that the outlet temperature of the pumped water will change with the inlet temperature of the injected water as the water mixes, resulting in a gradual attenuation of the ATES efficiency (Gao et al., 2013). In theory, it is sufficient to ensure that the distance between the cold and warm wells in the design of the system is sufficient. This safe distance can be estimated from the thermal radius of influence (R_{th}) (Bloemendal et al., 2018; Bloemendal and Olsthoorn, 2018). Considering this, the well group arrangement mode is essential (Gao et al., 2013). Different arrangements exist such as a cluster (i.e. a group of wells) of the warm wells and one of the cold wells, an arrangement in rings, or a number of parallel lanes (alternately consisting of warm and cold well groups). However, Gao et al. (2013) showed that after a long period of operation of an ATES system in a ring arrangement, the pumping wells become easily surrounded by injection water augmenting the risk for a thermal breakthrough. The row/lane type well arrangement where the warm and the cold wells are clustered might be a better option (Gao et al., 2013; Bloemendal et al., 2018). While the clustered well placement might be a better option considering the storage efficiency, the opposite might be beneficial for the hydraulic head. The latter must also be taken into account as it must be able to maintain a low enough pressure in the injection wells to avoid damaging the confining clay layer and increasing the risk of flooding. As a rule of thumb, the efficiency of a well is about 70%. This results in an increase in water level in the well of 10/7 in comparison to the theoretical increase. Next, the increase in water level above the ground should be lower than 1/5 of the thickness of the confining layers above the aquifer (Simpson, personal communication). As such, compared to a clustered well arrangement, the drawdown will remain more limited when pumping and injection wells are placed alternately in a checkboard pattern because the superposition principle applies in a confined aquifer. The latter implies that the resulting drawdown at a location is the algebraic sum of the effect of multiple pumping/injection wells in the neighbourhood.

For the project, since the area is limited by the relatively small available space for many wells, different well arrangements will be tested to effectively store heat while using the available space efficiently. Furthermore, the suggestion by Bloemendal et al. (2018) saying that the distance between wells of the opposite and same type should be $2.5*R_{th}$ and $1*R_{th}$ respectively will be taken into account. To do this in practice, first the hydraulic radius of influence was estimated analytically using the Thiem-Dupuit method for a confined aquifer in steady-state (Dupuit, 1863, Thiem, 1906):

$$\boldsymbol{R = 10^{\frac{s \times 2\pi Ke}{Q}} \times x} \qquad \{18\}$$

Where:

- R : the hydraulic radius of influence [m]
- s : the drawdown at a certain location x due to pumping/injecting [m]
- K : horizontal hydraulic conductivity of the medium [m/s]
- e : the thickness of the groundwater reservoir [m]
- Q : pumping/injection rate [m^3/s]
- x : location at a certain distance from the well

Interesting to point out is that this method for the calculation of the hydraulic radius of influence (R) differs from the one used by Bloemendal et al. (2018). The latter calculates the radius of a cylinder around the well that would correspond to the quantity of water injected in one cycle, considering the filter screen length

(depending on the available aquifer thickness). This will result in a smaller radius than the one that would be calculated using the proposed Thiem-Dupuit method which actually gives the size of the cone of depression for steady-state conditions. Hence, the used approach should add a factor of safety. Additionally, it must be pointed out that the aquifer used for this project is heterogeneous (i.e. layered). As such, the radius of influence will differ significantly according to the layer which is considered. As Yd 4 is the thickest and most permeable layer and hence expected to have the largest radius of influence, it was chosen to calculate R. Also, for the analytical calculation of R, instead of using only a part of the pumping rate, the full pumping rate was extracted from Yd 4. In reality, this flow rate would be distributed over the three pervious layers (Yd 2, Yd 4, Yd 6) according to their transmissivity This should again add an additional factor of safety.

Next, this estimation of R (in Yd 4) can be validated/adjusted with the groundwater model by simulating a well pair of one injecting and one pumping well for six months and by using particle tracking to visualise whether there is a connection between the wells. If there is, the distance between the wells should be adjusted until there is no connection anymore. Finally, using the earlier defined thermal retardation factor, the thermal radius of influence ($R_{th} = hydraulic\ radius\ /\ thermal\ retardation\ factor$) can be estimated.

Knowing this, to determine a possible well configuration for the future ATES system, different well arrangements will be tested for a short period of time (6 months – 2 years). They will be evaluated based on the resulting hydraulic head and heat storage efficiency. The wells will be placed within the available area of Campus Sterre according to the future plans for 2038 (Figure 10).

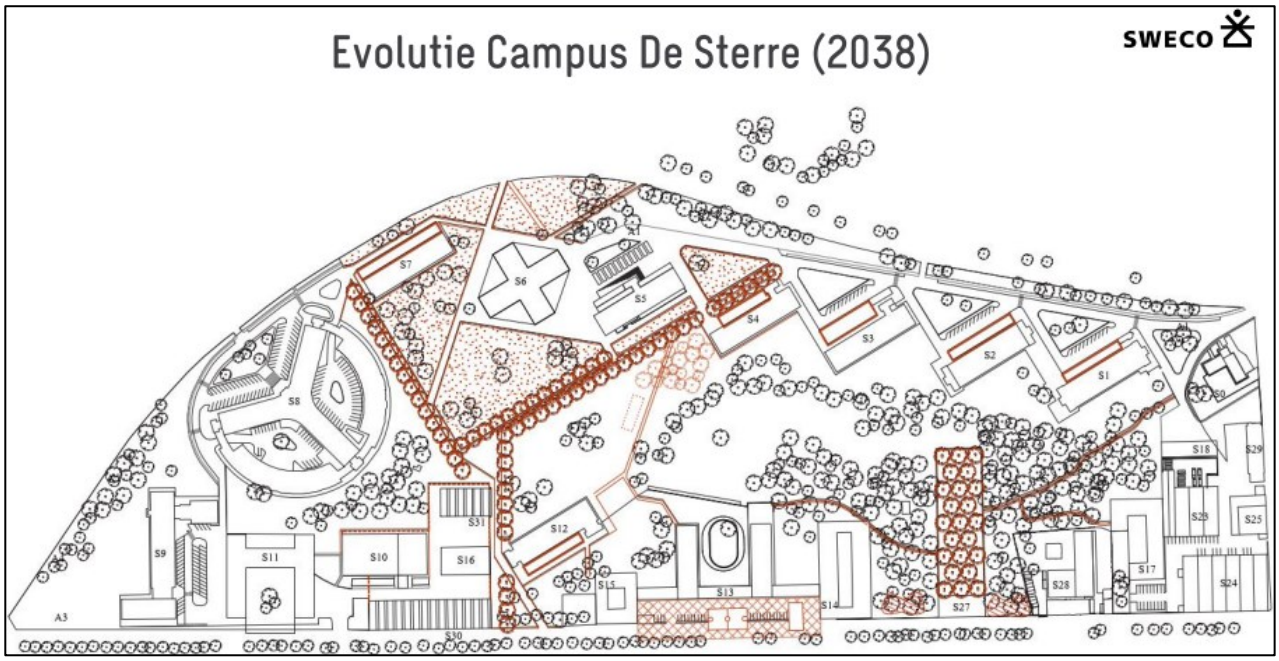

Figure 10: Future plan of Campus Sterre made by SWECO. The available space for ATES wells is mostly limited to the left side of the campus because the vegetational area on the right side is preferably maintained.

In practice, the wells will be screened from the bottom of Yd 1 to the top of Yd 6 (like PB JE in the pumping test). In the groundwater model this is implemented using a WEL package only in Yd 4, which is the thickest permeable layer, and assigning a very high value for the hydraulic conductivity (vertical and horizontal) from Yd1 to Yd 6 at the location of the well. In this way, for a given abstraction rate, the discharge is distributed to the different pervious layers according to the transmissivity and drawdown of each layer.

2.2.5.6. Modelling scenario

Subsequently, an ATES system with the above discussed well configuration was modelled using a scenario with the maximum pumping/reinjection rate in the study area when pumping/injection would be done in all pervious units simultaneously (i.e. in fully screened wells). This rate was determined using the pumping tests that were carried out (see 'Pumping tests'. The modelled scenario was evaluated for a period of 20 years. Within each year warm water injection is assumed to take place in summer (6 months) and cold water injection is assumed to take place in winter (6 months). These long periods represent an extreme scenario. The temperature of the injected water was imposed in the model while the temperature of the extracted water varies according to heat transport processes. The injection temperature is normally approximately +5°C for the warm well area and -5°C for the cold well area (relative to the natural groundwater temperature of 13.8 °C). Furthermore, a yearly balance between heating and cooling demand from the underground was assumed. Next, as the natural groundwater flow also influences the geothermal energy storage, a gradient in the study area was imposed for the modelled scenario (Gao et al., 2013; Yapparova et al., 2014; Bloemendal and Olsthoorn, 2018). In practice, this was done by adjusting the boundary conditions of the model. The Eastern and Western boundaries were changed to zero-flux boundaries using the WEL package. For the Northern and Southern boundaries the initial values of the specified head boundaries (CHD package) were changed. The values were chosen based on the available groundwater level monitoring network of VMM available in DOV ('Databank Ondergrond Vlaanderen', n.d.). As the amount of data points within the study area is very limited, a triangular interpolation method was done using data points located in the area of 20*20 km around Campus Sterre. Also, for each data point, the mean of all available monitoring data of several years was selected. As such, the uncertainty increases about the true water level at the boundaries of the model. According to the data, the water level in the north is 8 mTAW while in the south it is about 15 mTAW. Nevertheless, the gradient itself remained within realistic limits for the study area i.e. 7 m/5 km or 0.14%.

In the end, the resulting water level and heat transport could be visualised with ModelMuse. The storage efficiency was assessed using a plot showing the temperature variation of the warm well area, the cold well area and the temperature difference in function of time (Fleuchaus et al., 2020).

Noteworthy is the role of the servers in the ATES system. As they are producing a considerable amount of heat all year long, they represent the largest share of the cooling demand. The heat which they produce will be added to the warm well area to increase the efficiency for the upcoming years. More specifically, in summer, cooling will be foreseen by the circulating groundwater. The water will eventually acquire the excess heat and will be injected into the warm well area. In winter, on the other hand, the heat produced by the servers can be used directly to preheat the water that will be used to warm up the building. Also in this way the servers will be cooled. The coupling with the servers was already made in the calculation for the heating/cooling demand so no specific injection temperature adjustment was made in the model itself.

2.2.6. Economic analysis

From an economical perspective, the high investment cost must be worthwhile despite geological uncertainties such as the estimated thermal and hydraulic conductivity of the subsurface. To focus on the main advantage of an open-loop ATES system over a closed-loop BTES system, the investment cost of both systems was compared. For the BTES system this was done based on an initial estimation provided by SWECO a couple of years ago. The investment cost of an ATES system, which should produce the same power, was estimated based on data provided by IFTECH.

3. Results and discussions

To improve the readability, the choice was made to do the discussion right after presenting the results of each section. This was done because the results of an analysis were used to carry on with the next one.

3.1. Pumping tests

Results

The highest pumping rate could be obtained in pumping well PP 4. A pumping rate of 5 m^3/h was too high as air bubbles started to show. This means that this pumping rate was above the critical flow rate as an unsaturated zone could be established. It will not be possible to reach a new equilibrium in the aquifer using such a high pumping rate in PP 4. Pumping with a rate of 4.2 m^3/h could be possible however the drawdown in PP 6 significantly increased. As such the absolute maximum pumping rate in PP 4 is estimated to be about 4 m^3/h. Using this pumping rate, a new equilibrium could be reached and a stable drawdown could be observed. In PP 6, a pumping rate of 1 m^3/h could be reached. In PP 2, a pumping rate of 0.9 m^3/h could be sustained. These results will be used in the discussion to estimate the maximum pumping rate in a well that is filtered over the entire aquifer depth. The maximum injection rate in PB 2.y is estimated to be about 0.5-0.65 m^3/h. The maximum injection rate in PB 6.y was estimated to be even lower than 0.2 m^3/h. More tests were attempted to determine the precise injection rate in the piezometers (and to make the comparison with injection in a pumping well) but could not go through due to difficulties with the pumping installation. The maximum pumping and injection rate in the currently available wells was estimated to be 3.8 m^3/h. Using this injection rate no flooding of the surface could be observed. Considering this, a pumping rate of 3.8 m^3/h was chosen to carry out the pumping-reinjection test.

As mentioned earlier, the pumping tests started on 25/10/2021. This can be observed in the graphs as a drop in the water level (Figure 11). The drop is the largest in PP 4 because it is the pumping well itself. Next, in well PB 2.1 the drop is not clearly visible, however, it might be attributed to the fact that the installed diver only started monitoring the water level after the pumping had already started. Further, it must be noted that the data in PB JE should best be disregarded until 15h40 (25/10/2021) because the diver was only submerged from the moment the injection started (when reinstalling the divers on 5/11/2021 this issue was eliminated.) Nevertheless, in PB JE and PP 2, a drop can be observed during a short period of time after which a rise in water level can be seen. At first sight, this might be explained by the fact that the pumping started first and the injection dominates the response only afterwards. However, when looking in greater detail at the data, this drop already occurs around 07h00 on 25/10/2021. This cannot be due to the pumping but it might be attributed to a change in atmospheric pressure. This is illustrated in Figure 12. Also, the measuring station 'Boekhoute_ME (ME03_017)' of Waterinfo confirmed that a different atmospheric pressure was measured by the barodiver. This was accounted for in further data analysis. Furthermore, this drop which does not result from pumping can also be observed in PP4 and PP6. Interesting to point out is that the drop in water level due to pumping can thus only be observed in PP 4, PP 6, PB 6.1 and PB 6.2.

The injection in PB JE started shortly after the pumping was initiated. Despite the fact that PB JE is filtered from the top of Yd 6 to the bottom of Yd 1 (Figure 5), the influence of the injection (i.e. a rise in water level) could only be observed in PB JE, PP 2, and PB 2.1. On 28/10/2021 the MFI test was carried out and the pumping/injection was disturbed. This can be observed as a positive peak in the wells influenced by the pumping and a negative peak in the wells influenced by the injection. Also on 29/10/2021, a negative peak can be observed in PB JE. This might be attributed to external disturbance (perhaps due to a curious passer-by). From 5/11/2021 on, only monitoring results in PP 4 and PB JE are available. Some troubles due to the pump itself can be observed from November 5 to 9. Also, on November 9, the programmed pumping rate of 3.8 m^3/h seemed too high because PB JE was almost overflowing. The pumping rate had to be reduced to 3.05 m^3/h.

When equilibrium has been reached after the injection and pumping started, the water level remained relatively stable. However, in PP 2 and PB 2.1, the water level seems to keep rising (Figure 11). This trend, even though less pronounced, can also be observed in the other wells. Furthermore, a variation of the water level of maximum 0.5 m with first a decreasing and afterwards an increasing trend can be seen in PB JE (November-December).

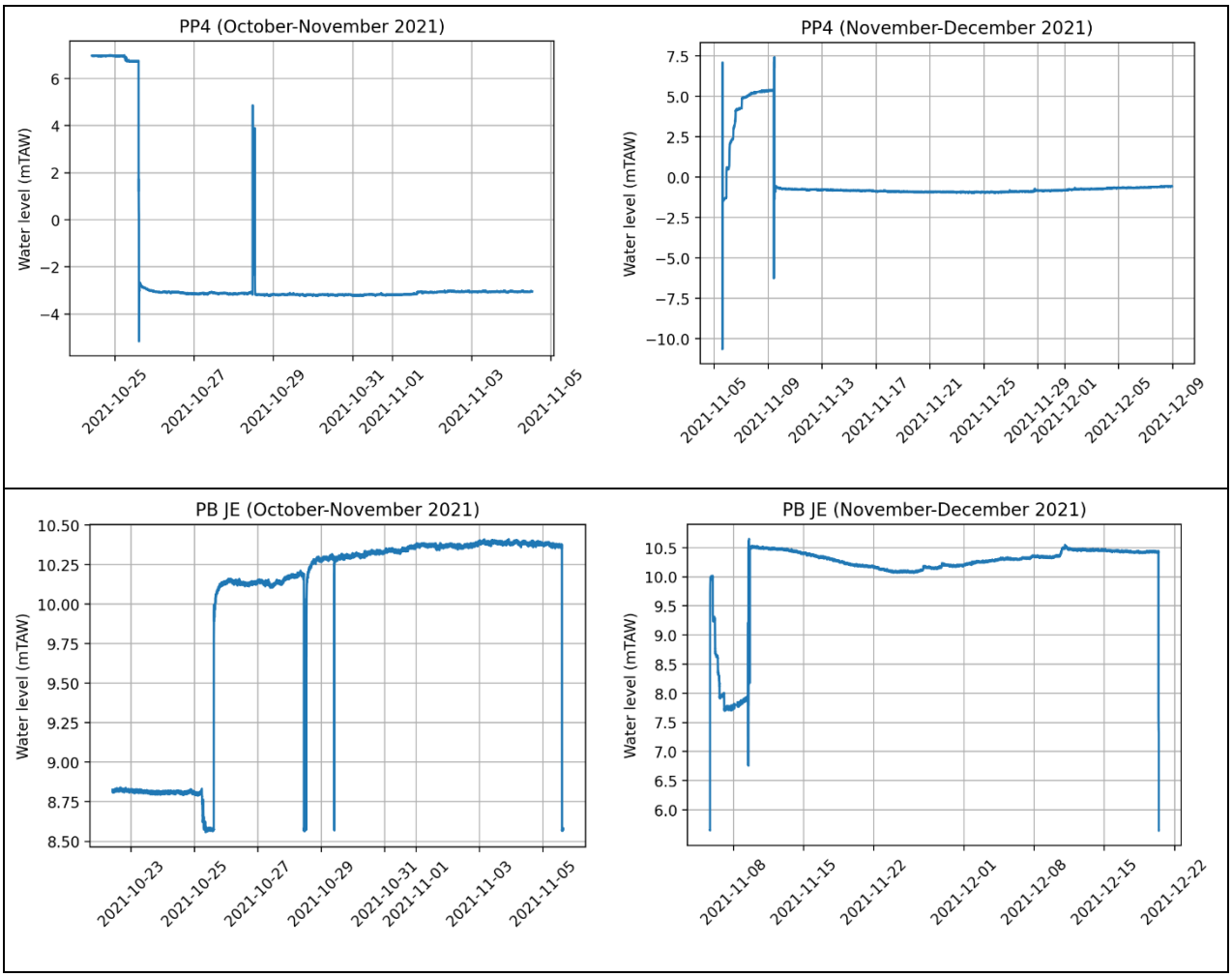

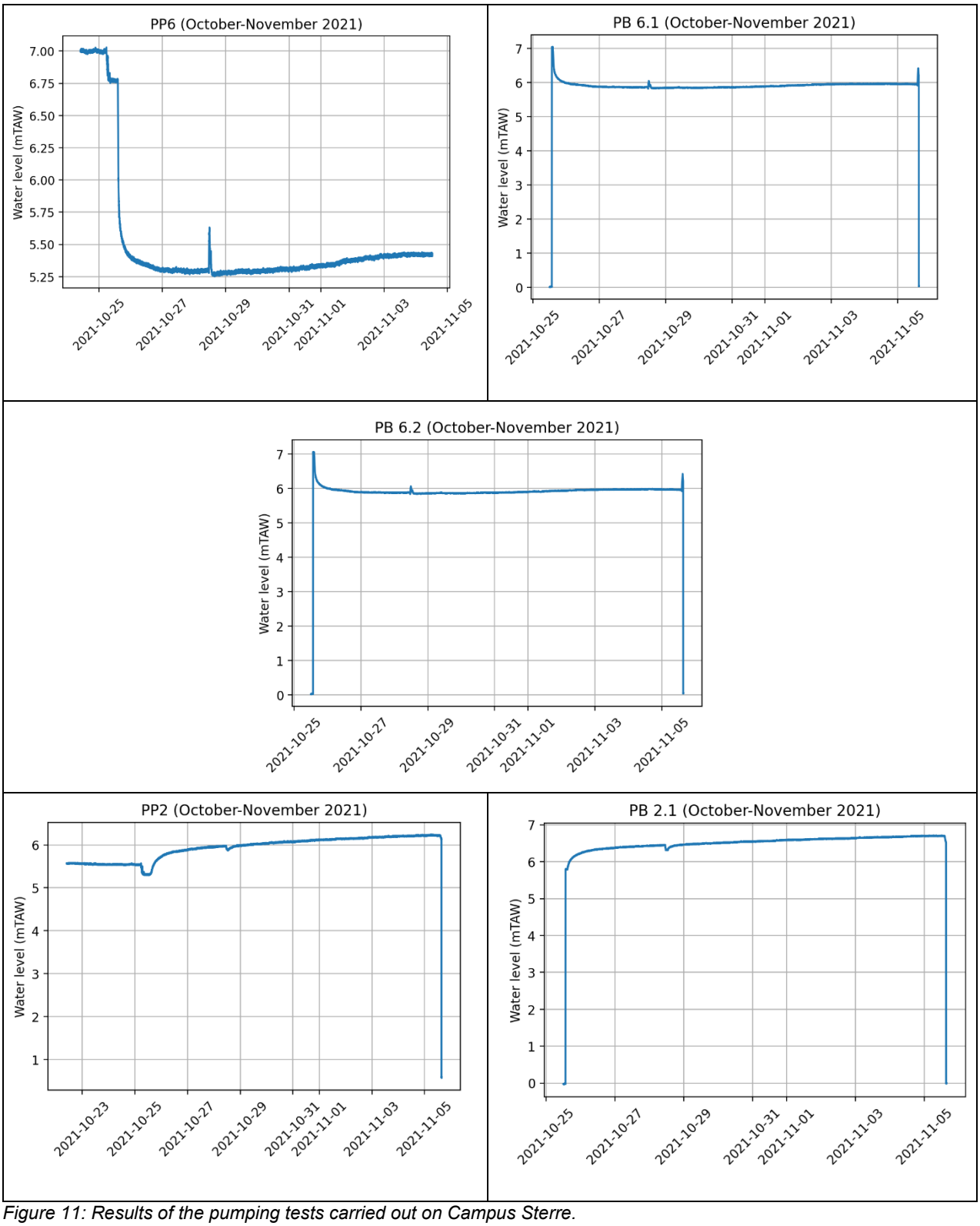

Figure 11: Results of the pumping tests carried out on Campus Sterre.

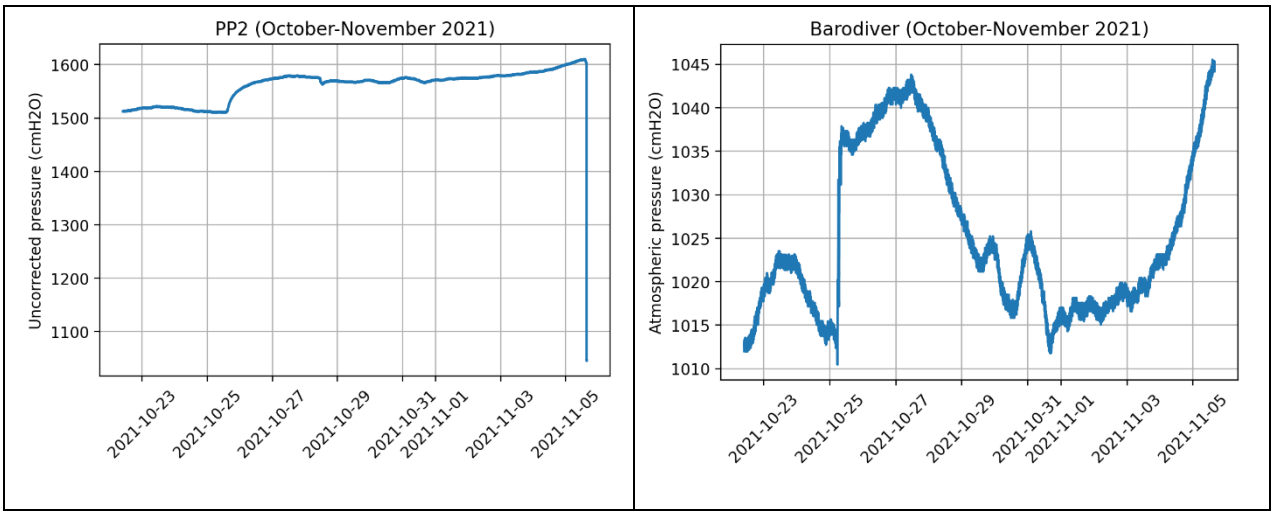

Figure 12: Uncorrected results of the water level monitoring in PP2 during the pumping tests (left) and the atmospheric pressure that was used for correction (right). This illustrates that the drop in water level which could be observed in the corrected graph of PP2 in Figure 11 is not due to pumping but might be attributed to a change in atmospheric pressure.

After the pumping and reinjection stopped, the divers installed in PP 4 and PB JE measured the fluctuations of the natural groundwater level until May 2nd (Figure 13). The fluctuations measured in both wells have a similar trend which was also expected. The graphs in Figure 13 show that, from December until May, the water level fluctuates within a range of 0.5 m. The maximum natural water level is about 7.5 to 7.6 mTAW.

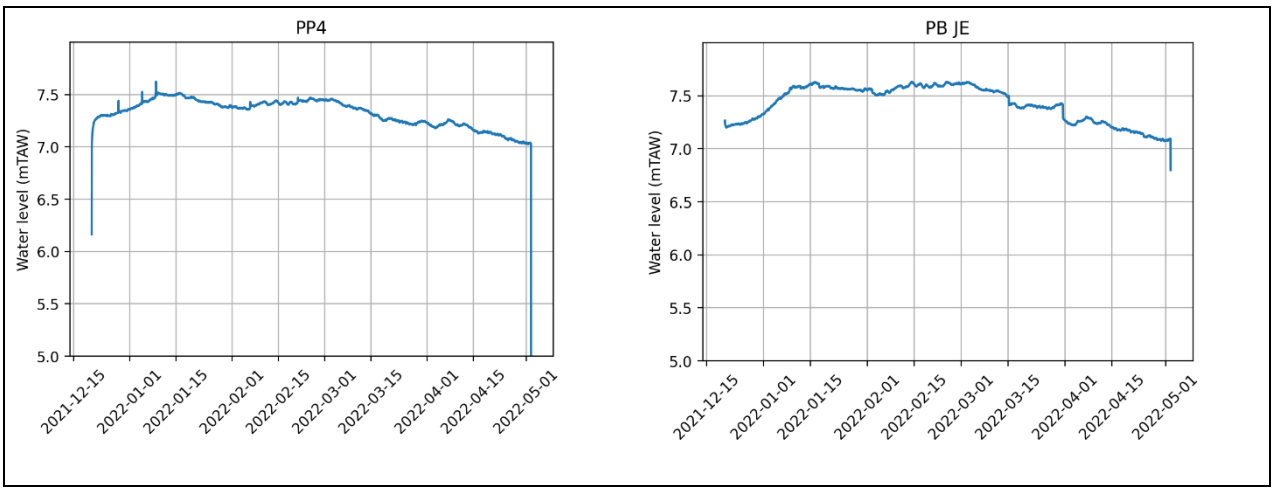

Figure 13: Monitoring results of the seasonal variations of the water level in PP 4 and PB JE from December 20 (2021) until May 2 (2022).

Discussion

The drop in water level due to pumping could only be observed in Yd 6 and Yd 4. This might illustrate that the semi-pervious layer Yd 5 does not prohibit the connection between Yd 6 and Yd 4. Indeed, when looking at Figure 5, Yd 5 is present as a thin layer which cannot prevent water from flowing from Yd 6 to Yd 4 when pumping is initiated. In Yd 2, no drop in water level could be observed due to the pumping which on the one hand might illustrate that no connection is made between Yd 2 and Yd 4. On the other hand, the influence of the injection might be dominant in Yd 2, masking the influence of the pumping. Given the larger distance between PP 2 and PB JE than the distance between PP 2 and PP 4, it can be safely stated that the influence on Yd 2 due to pumping in Yd 4 is limited in comparison to the influence of the injection. Also, when looking at Figure 6, the last hypothesis can be strengthened. When pumping in Yd 4 or Yd 6, a significant drawdown

can be seen from the beginning on in Yd 4 and Yd 6. However, in Yd 2, this drawdown is also present but only later on and it is less significant. Also, when pumping in Yd 2, a strong drawdown can be observed in Yd 2, and a weaker one in Yd 4 and Yd 6. This illustrates that there is indeed also a connection between Yd 2 and Yd 4, however in the pumping tests that were carried out for this project, it could not be observed because the injection was dominant. However, in practice for the actual ATES system, this effect would be counterbalanced because there will also be pumping in Yd 2. Furthermore, the influence of the injection, even though in all layers simultaneously, could only be observed in Yd 2 as a rise in water level. This might as well be attributed to the fact that in Yd 4 and Yd 6 the pumping is dominant. Also, the further away from the injection well, the less steep the gradient will be and the less influence the injection will have on the change in water level.

Next, in this setting, the injection rate is the limiting factor due to the high groundwater level below the surface (and probably also due to the smaller diameter of the well as the used injection well was not constructed as a pumping well but as a piezometer). Roughly two weeks after the pumping and injection started, the pumping rate had to be lowered due to a risk of overflow in PB JE. This risk of overflow is probably not the result of seasonal variations as they remain relatively limited and they would not be the cause of a necessary significant decrease of the pumping rate from 3.8 m^3/h to 3.05 m^3/h. On the one hand, this decrease in injection capacity might be attributed to the state of the well which is not ideal anymore. Therefore, maybe the well could have been silting up again. On the other hand, the problems encountered with the pump could also explain the situation. The latter was attributed to a reduction of the section of the pipe due to pinching, which led to an irregular flow rate and injection of air. It is therefore possible that air might have been injected into the well surrounding, affecting the permeability. Consequently, this might have significantly decreased the injection capacity.
Meanwhile, the other curves show a slight increase in the water level with time. This trend is most pronounced in PP 2 and PP 2.1. There, the new equilibrium resulting from injection might not have been reached yet at the end of the period, as suggested by modelling results (Appendix B). However, it might also be the result of natural conditions such as seasonal variations or a combination of both. The variations remain indeed limited to the range that was determined in Figure 13. Furthermore, first a decreasing and afterwards an increasing trend could be seen in PB JE (November-December). The decreasing trend might be attributed to the response of the aquifer due to the decrease in the pumping rate. The increasing trend might be related to clogging due to air affecting the permeability but can probably also be attributed to seasonal variations which indicate an increase in the natural groundwater level.

Ideally, new pumping wells with filter screens in the three pervious layers would be more suitable to determine the maximum capacity of the aquifer, but due to time constraints, it was not possible to install them. As such, the maximum pumping rate in a fully screened well in the layered aquifer had to be estimated by using the principle of superposition. This principle assumes that each pervious layer is fully confined. On the one hand, this assumption seems acceptable for Yd 2 and Yd 4. On the other hand, it was shown that a strong connection between Yd 4 and Yd 6 exists indicating that Yd 5 is not a good confining layer. Hence, the maximum pumping rate in Yd 6 and Yd 4 combined is most likely smaller than the sum of their individual rates. Also, in Lebbe et al. (1992) a pumping rate of 1.66 m^3/h could be reached in PP 2, while we were limited to a rate of 1 m^3/h by our equipment. Assuming that PP 6 can only account for 10 % of its estimated maximum pumping rate (i.e. 0.1 m^3/h), a maximum pumping rate in PP 4 of about 4 m^3/h and the maximum pumping rate of 1.66 m^3/h in PP 2 estimated by Lebbe et al. (1992), a total maximum pumping rate of 5.76 m^3/h could be estimated in a fully screened well in the layered aquifer.

To summarize, the maximum pumping rate in the currently available wells was estimated to be 4 m^3/h in Yd 4. With the contribution of Yd 2 and Yd 6, probably a higher pumping rate of about 5.8 m^3/h could be reached. It is however not recommended to exploit a well at the maximum rate, especially for a long period of time such as in an ATES system. Therefore the rate will be limited to 5 m^3/h for the rest of the study. The injection

well PB JE was the limiting factor during the field test as it was constructed as a piezometer with a small diameter. The current maximum injection rate was estimated at 3.8 m^3/h with a water level reaching the surface (but without flooding it). A higher rate could be reached when using wells, especially the injection well, in a better state and with a larger diameter. To have an idea, to be able to inject 5 m^3/h in a fully-screened injection well with a larger diameter, there must be an increase in capacity of about 30% relative to injecting 3.8 m^3/h in a fully-screened piezometer with a smaller diameter. It was attempted to test this using PP 4 as pumping well and PP 2 and PB 2.1/2.2 as injection wells. However, as also noted earlier, the test could not go through due to troubles with the pumping installation. It is advised to carry this test out again in the future. Another possibility to increase the injection rate would be to maintain the injection at a higher pressure. However, as mentioned above, such an injection rate would cause a water pressure extending above the ground level. When excessive, this might cause flooding and/or instability of the clay layer (Gentbrugge Fm) between Yd 6 and the Quaternary. This risk will be evaluated later on using the groundwater model.

3.2. Chemical analysis

Results

The results of the analysis with the multi-parameter probe in August show that the groundwater temperature in the study area is rather warm (14.8-15.9 °C) (Table 4). However, the divers which monitored the groundwater temperature for a longer period of time (October 2021-May 2022) indicate a slightly lower temperature (13.5-13.7 °C in PP 4) and a trend of a slightly increasing temperature from November until December (Figure 14). Next, the oxidation-reduction potential (ORP) has a negative value for all three pumping wells. Moreover, the trend of a decreasing redox potential with depth can be observed from Yd6 to Yd4. The ORP of Yd 4 is lower than the ORP of Yd 2.

The results of the chemical analysis in the lab are also reported in Table 4. The charge balance error was checked for validating the data quality (relative deviation in Table 4). All deviations are positive indicating a higher concentration of cations than anions. The deviations remain within the limits of +/- 5%. Only for PP 6, the deviation is relatively high. This might indicate an error. Indeed, when looking at the sulphate concentration it is similar for PP 2 and PP 4 but much lower for PP 6. If the sulphate concentration of the latter is changed (to 230 mg/l, as is the case for PP 2 and PP 4), the charge balance error becomes similar for all three samples.

The pH was measured both with the multi-parameter probe as well as in the lab. The latter is expected to be more reliable and has a value of 7 and is thus neutral. Additionally, in general, the water can be classified as a Ca-HCO_3 -water type according to the Stuyfzand classification (Stuyfzand, 1986): Ca^{2+} is the most abundant cation in all water samples and HCO^{3-} is the most abundant anion (except in PP2 where SO_4^{2-} is the most abundant one but the difference is small). Furthermore, the chloride level remains below the limit of freshwater which is 150 mg/l. The total hardness, which is a measurement of calcium and magnesium, is 45 to 55 °F ($Hardness\ (°F) = 5*(Ca^{2+} + Mg^{2+})\ (in\ meq/l)$). This is characteristic of very hard water (Stuyfzand, 1986). Considering this, it will be worth discussing the risk for calcite precipitation due to temperature changes. Next, when looking at the Total Dissolved Solids (TDS), the groundwater can be classified as moderately to weakly fresh when taking into account the quality class limits of De Moor and De Breuck (1969). Finally, the results of the chemical analysis were compared to the environmental quality standards for groundwater as were drawn up in appendix 2.4.1. (2019) of Vlarem II (Appendix A) by Vlaamse Milieumaatschappij (1995). Only the nitrite concentration is higher than the maximum admissible concentration of 0.1 mg/l.

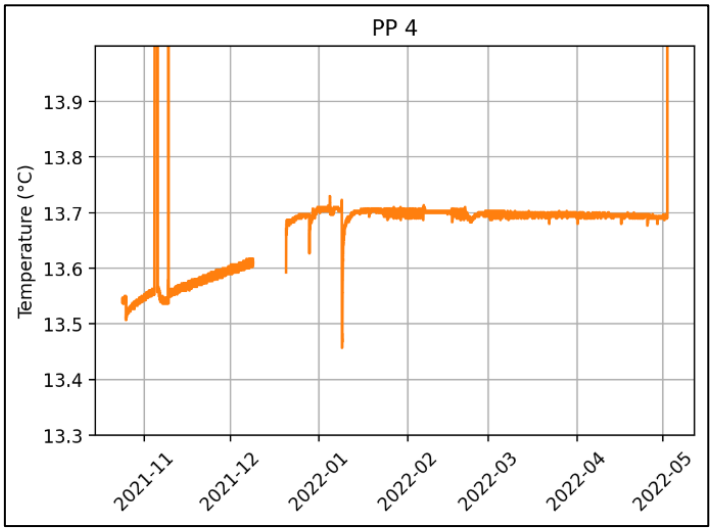

Figure 14: Variations in groundwater temperature monitored in PP 4 from October 24 (2021) until May 2 (2022). Outliers are attributed to disturbances by intermediate retrievals of the diver.

Table 4: Results of the analysis of the groundwater in the pervious layers Yd 2, Yd 4, and Yd 6 with the multi-parameter probe in a flow-through cell and results of the chemical lab analysis of water samples that were taken on August 5, 2021.

Chemical parameters	**PP2**		**PP4**		**PP6**	
Results multi-parameter probe						
TEMP (°C)	14,8		15,9		14,8	
ORP (mV)	114.6 (negative)		175.6 (negative)		85.3 (negative)	
PH	8,03		7,87		7,85	
DO (% sat)	0		0		0	
DO (mg/l)	0		0		0	
EC (µs/cm)	2080		2485		866	
TDS (mg/l)	1353		1615		561	
SAL (PSU)	1,05		1,25		0,36	
Results TA-TAC titration						
Titration (HCl, 0.01 molarity, added)	3,52		6,6		7,87	
carbonate [CO_3^{2-}] (mg/l)	0		0		0	
bicarbonate [HCO_3^-] (mg/l)	214,72		402,6		480,07	
Results chemical analysis						
PH	7,1		7,04		6,9	
COND	810		966		880	
	mg/l	***meq/l***	***mg/l***	***meq/l***	***mg/l***	***meq/l***
Na^+	17,068	0,743	21,133	0,92	18,814	0,819
K^+	11,048	0,283	3,376	0,086	3,194	0,082
Ca^{2+}	154,523	7,711	230,624	11,508	222,231	11,089
Mg^{2+}	15,195	1,25	3,717	0,306	3,376	0,278
Fe^{2+}/Fe^{3+}	1,206	0,043	2,382	0,085	2,688	0,096
Mn^{2+}	0,105	0,004	0,162	0,006	0,112	0,004
Al^{3+}						
NH^{4+}	0,2234	0,012	0,2452	0,014	0,2048	0,011
Cl^-	36,739	1,036	12,505	0,353	16,728	0,472
SO_4^{2-}	231,86	4,827	232,96	4,85	80,196	1,67
NO_3^-	0,2098	0,003	0,0769	0,001	0,0414	0,001
NO_2^-	0,2644	0,006	0,4911	0,011	0,2663	0,006
HCO_3^-	215,94	3,54	399,55	6,55	384,91	6,31
CO_3^{2-}		0		0		0
PO_4^{2-}	0,2905	0,005	0,4251	0,007	0,1177	0,002
OH^-		0		0		0
TDS	684,6721		907,6473		732,8792	
TOTAL CATIONS (meq/l)	10,046		12,925		12,379	
TOTAL ANIONS (meq/l)	9,417		11,772		8,46	
ABS DEVIATION (meq/l)	0,628		1,153		3,919	
REL DEVIATION (%)	3,229		4,67		18,808	
	mg/l	***meq/l***	***mg/l***	***meq/l***	***mg/l***	***meq/l***
fluoride mg/l	0,293	0,015	0,192	0,01	0,191	0,01

Discussion

Taking into account the temperature measurements in August and the monitoring results in PP4, a mean annual groundwater temperature of 13.82 °C was estimated. Additionally, it was shown from the pumping tests that due to the pumping/injection necessary for the implementation of an ATES system, the mixing of water of the different layers that constitute the main groundwater reservoir will occur. However, the risk of affecting the groundwater quality will probably remain limited because the groundwater of all 3 layers has a similar composition which is in line with the regulations drawn up in Vlarem II (2019) (Appendix A, Vlaamse Milieumaatschappij, 1995). It was shown that the water is moderately fresh, very hard water. As such, precipitation of calcium, induced by temperature changes, might significantly reduce the porosity and permeability of the aquifer. However, it was shown that when the temperature rise is limited, as is the case for most current ATES systems with a temperature range of 5-20 °C, calcium precipitation does not occur (Drijver, 2011; Hartog et al., 2013; Possemiers et al., 2014). Hartog et al. 2013 showed that there is a limited impact for such small temperature changes in ATES systems with an underground thermal balance as the effect of temperature on equilibrium constants is opposite for temperature increases and decreases (Possemiers et al., 2014). Next, reportedly, in the study area, there is also no knowledge of the presence of a drinking water catchment area that is sensitive to slight changes in groundwater quality, or a contaminated area where pollutants might be mobilized. The former would also be vulnerable to biological activity which might be induced due to a temperature change in the aquifer (Bonte et al., 2011; Todorov et al., 2020). Next, in the groundwater reservoir, the conditions are reducing (i.e. a decreasing redox potential, also no dissolved oxygen (DO) is present). The ORP of Yd 2 was expected to be lower than the ORP of Yd 4 when extrapolating the decreasing redox potential from Yd 6 – Yd4, however, this was not the case. This could probably be attributed to the fact that the connection between Yd 2 and Yd 4 is not fully present due to the presence of the semi-pervious layer Yd 3. If the water would come in contact with the atmosphere, the iron present in the groundwater reservoir would be oxidized and rust might form. This would be detrimental to the steel casing and could induce well clogging. Also, the sulphates present could cause corrosion. However, plastic tubes would be used for the ATES system. Moreover, the system will also be closed and will remain pressurized so there will be no contact with the atmosphere which might influence these chemical equilibria. As a result, it can be concluded that the impacts on the groundwater quality and the efficiency of the system due to the implementation of an ATES system will most probably remain limited. As such, this project did not focus on the chemical/ biological equilibria that would be affected due to the implementation of the shallow geothermal system.

3.3. Membrane Filtering Index test

Results

The results of the MFI tests can be seen in Figure 15 and Figure 16. No sand could be visibly observed in the mesh netting with a mesh size of 70 µm, during the test. The slope of the two graphs is 5.2 and 8.3 respectively. Usually, the curves are expected to increase significantly at the end of the test due to compaction on the filter. However, this could not be observed. The curve of the second MFI test even started to decline after some time. In the first graph, a dip can be observed, this is a measurement error. Further, the filters of both MFI tests are visibly still relatively clean, which is a good indicator that the low MFI values measured are reliable.

Additionally, the long-term pumping and reinjection test had to be interrupted because in PB JE there was a risk of flooding as the injection capacity seemed to have declined over time. As also mentioned earlier, the pumping/injection rate had to be lowered from 3.8 m^3/h to 3.05 m^3/h.

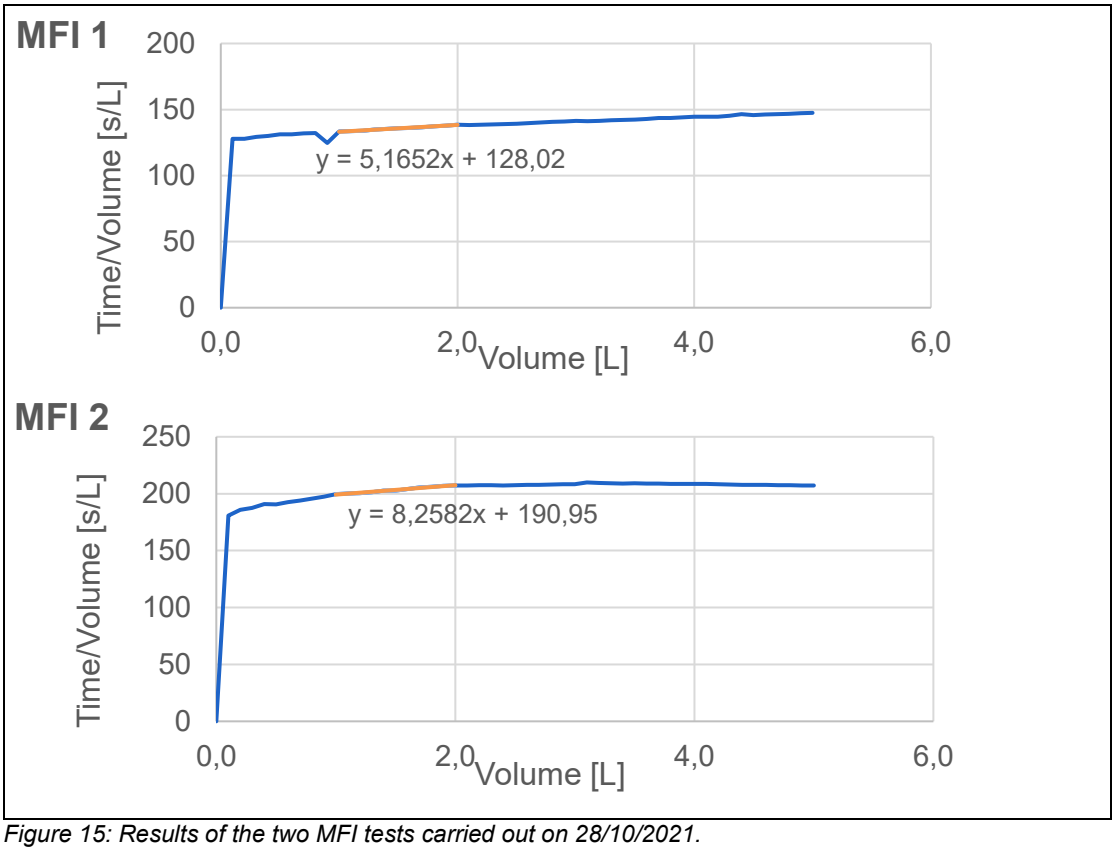

Figure 15: Results of the two MFI tests carried out on 28/10/2021.

Figure 16: The sediment particles on the filters after the two MFI tests were carried out.

Discussion

When carrying out the MFI test, poor results were expected because the groundwater reservoir consists of a lot of clay and silt. However, the results were above expectations. The slopes of the two curves are lower than 10 which means that the result is good and allow for injection to take place in the aquifer. The MFI results could be enhanced in the future with new wells with an adapted filter.

The curves usually steepen significantly in the end due to the compaction of particles on the filters. This could not be noticed and the second curve even started to decline after some time. This might be explained by a water leak alongside the filter or when pumping for a longer time, fewer particles are left to be loosened and moved to the filter. Nevertheless, the results are still reliable since the slope was calculated using only the initial part of the curve.

The long-term pumping and reinjection test showed that there was probably a decrease in the injection capacity with time. However, as already discussed above, this can probably be attributed to the fact that the test set-up was shut down for a while because of problems with the pump itself. Probably, air entered the tubes and, when the system was turned on again, this air could not escape the well anymore. This can significantly reduce the injection capacity as it is a type of clogging reducing the permeability. This explanation is further confirmed by the fact that the reduction did not occur gradually, as would be the case for clogging by fine particles, but immediately after the problems with the pump. Additionally, no further reduction of capacity was observed during the long-term injection test. Injection of air is not expected to happen in the actual ATES system as the pressure in the system will always be maintained. In case it would happen, it could be easily resolved by pumping in the well. As the initial pumping/reinjection rate of 3.8 m^3/h could be sustained for about two weeks without any decrease in injection capacity and without flooding of the surface, no decrease in injection capacity with time due to well clogging is expected for the actual ATES system.

3.4. Model results analysis and prediction

3.4.1. Calibration

Results

As mentioned earlier, the calibration of the groundwater model was done in two steps. First, the model results were compared to the results of the model of Lebbe et al., 1992 (Figure 6, Figure 17). These results show a good level of agreement which indicates that the new numerical model is a good proxy for the model of Lebbe.

Second, using the same model parameters, the simulated drawdowns were compared to the drawdowns observed during the pumping tests that were carried out for this project (Figure 18). A positive drawdown means a drop in water level while a negative drawdown indicates a rise in water level. For PB 6.1 and PB 6.2, there is a very good agreement. Also for PB 2.1, the agreement is satisfactory even though the model slightly overestimated the negative drawdown. The pumping and injection well (respectively PP 4 and PB JE), as well as PP 6 and PP 2, show a larger discrepancy. In PP 4 and PP 6, the simulated (positive) drawdown was underestimated while the (negative) drawdown in PB JE and PP 2 was overestimated in the model results. As such, in general, there is a good agreement for the observation wells (PB x.y) but a less good agreement for the pumping wells (PP x and PB JE). However, when looking at the graphs where the time is plotted on a logarithmic scale, the curves of the observed and the simulated drawdowns are relatively parallel. Considering the Cooper and Jacob (1953) method, this shows that both curves represent the same groundwater reservoir.

Pumping test on PP 2

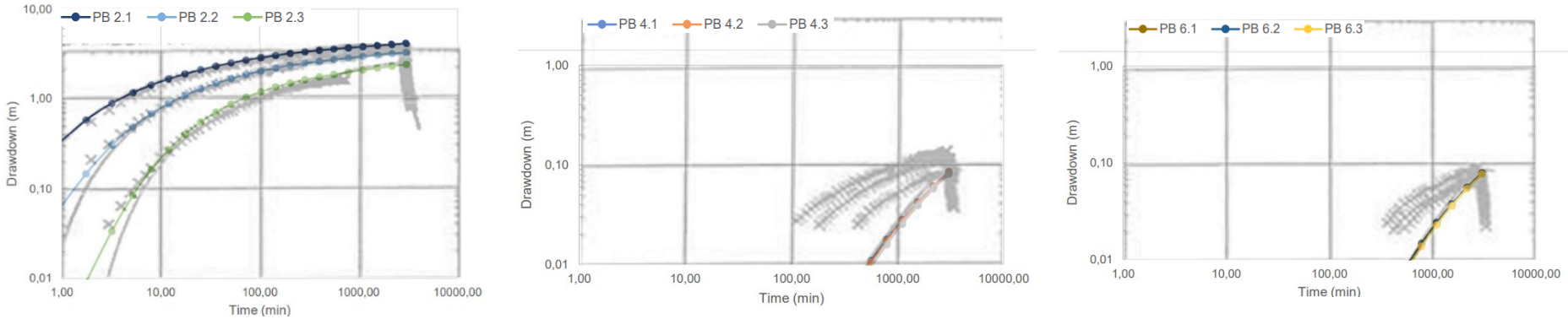

Pumping test on PP 4

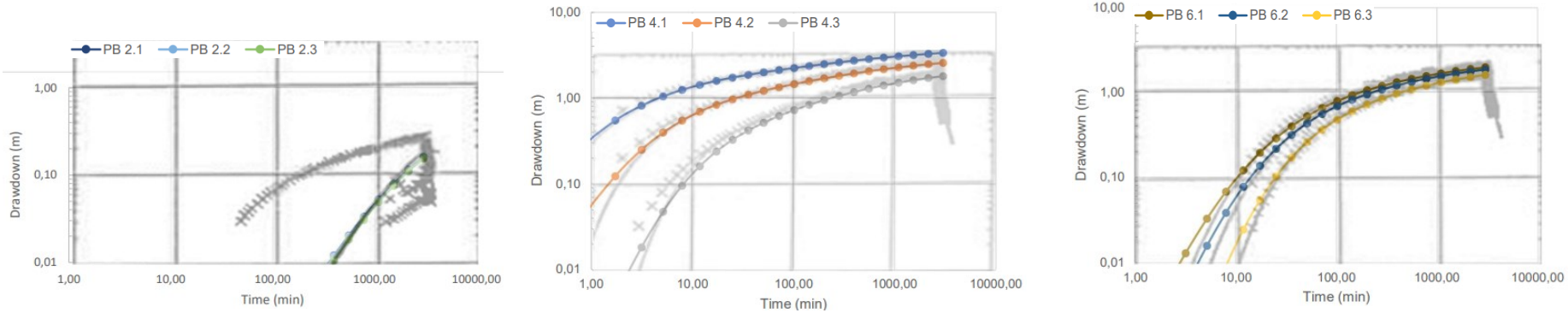

Pumping test on PP 6

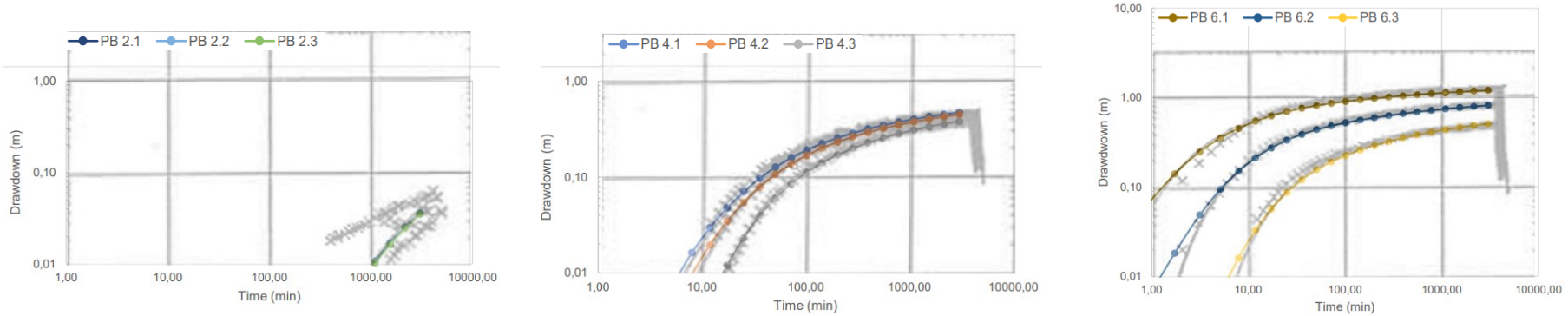

Figure 17: Comparison of the results of the groundwater model (coloured) with the results of Lebbe et al. (1992) (grey).

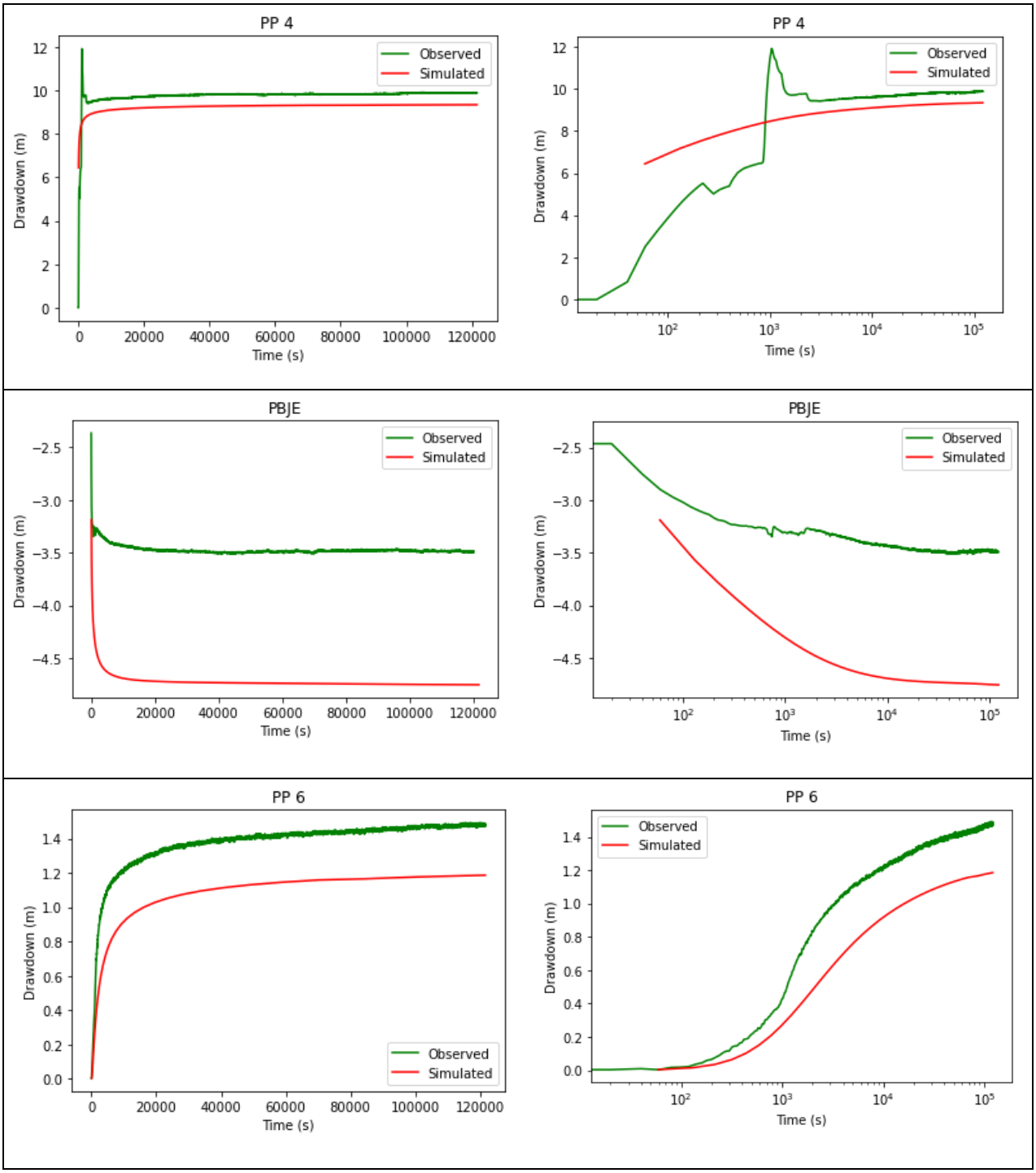
PP 4
Observed
Simulated
Drawdown (m)
Time (s)
PP 4
Observed
Simulated
Drawdown (m)
Time (s)
PBJE
Observed
Simulated
Drawdown (m)
Time (s)
PBJE
Observed
Simulated
Drawdown (m)
Time (s)
PP 6
Observed
Simulated
Drawdown (m)
Time (s)
PP 6
Observed
Simulated
Drawdown (m)
Time (s)

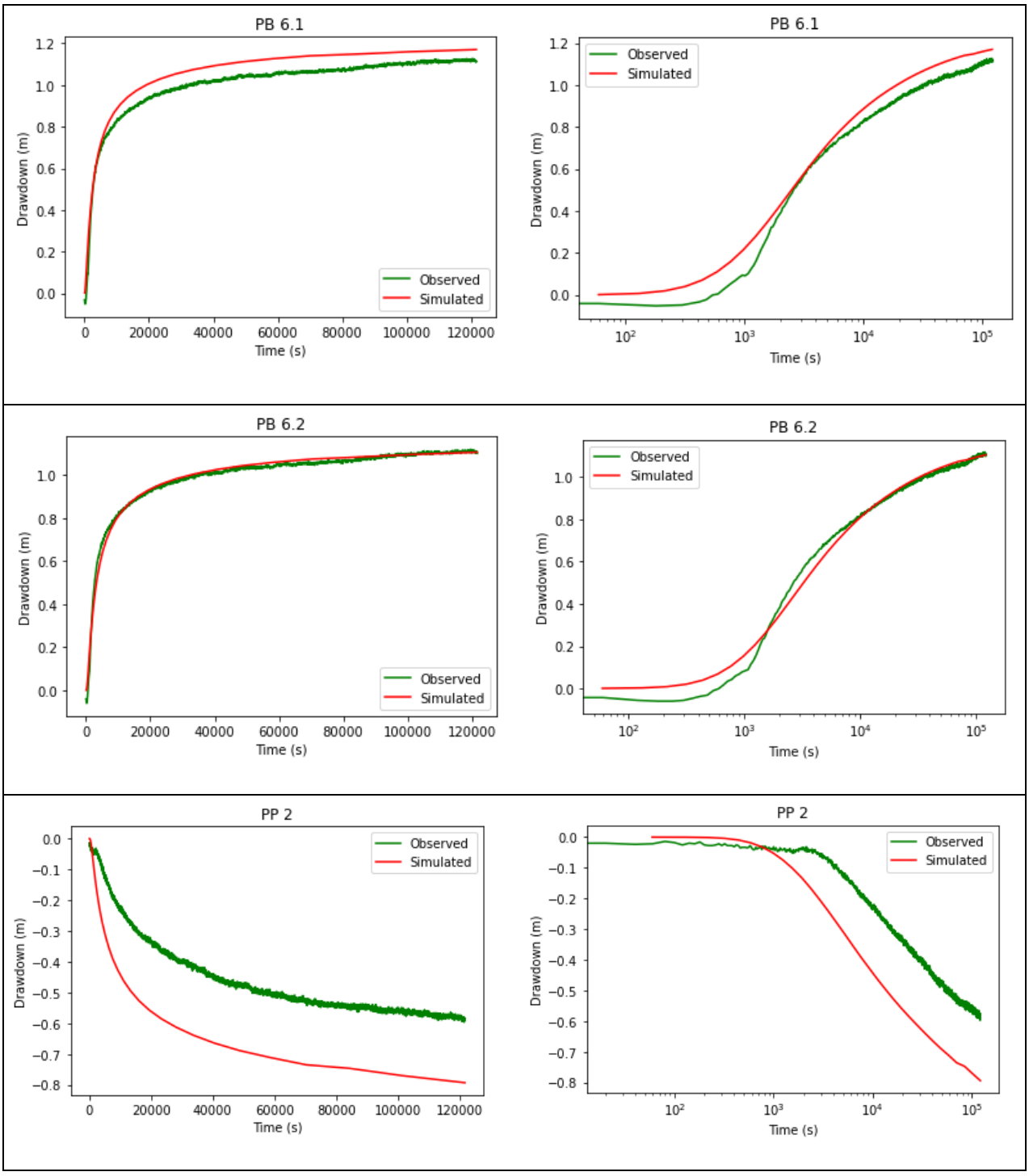
PB 6.1
Drawdown (m)
Time (s)
Observed
Simulated
PB 6.1
Drawdown (m)
Time (s)
Observed
Simulated
PB 6.2
Drawdown (m)
Time (s)
Observed
Simulated
PB 6.2
Drawdown (m)
Time (s)
Observed
Simulated
PP 2
Drawdown (m)
Time (s)
Observed
Simulated
PP 2
Drawdown (m)
Time (s)
Observed
Simulated

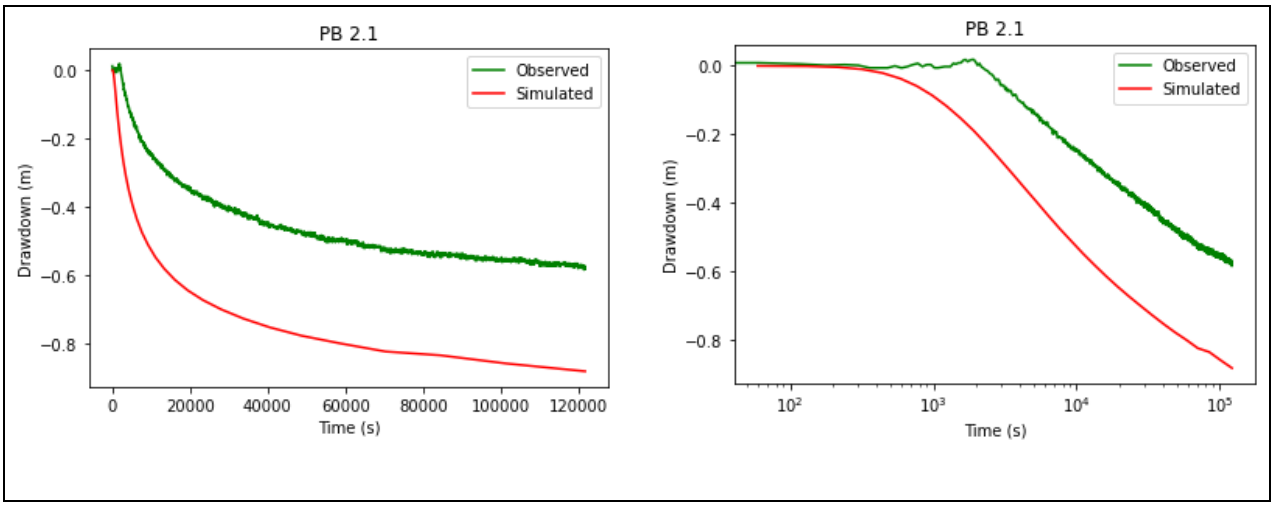

Figure 18: Comparison of the simulated drawdown to the observed drawdown. The drawdown is positive when the water level decreases and negative when the water level increases. On the right side, this is plotted using a logarithmic time scale to visualise the straight-line method by Cooper and Jacob (1953).

Discussion

The comparison of the simulated drawdowns of the triple pumping test with the results of Lebbe et al. (1992) in Figure 17 shows a good agreement. This indicates that the model is well-calibrated and approximates the reality well, at least for the area around the pumping well. As no data is available beyond this zone, this means that no indication of horizontal heterogeneity is present and therefore could not be included in the model (homogeneous layers). The validity of the model at a larger scale could only be validated when new data becomes available on the site.

When comparing the simulated drawdowns with the observed ones for the pumping/injection test in Figure 18, it was shown that, in general, the fit is relatively good for the observation wells (PB x.y) but less good for the pumping wells (PP x and PB JE). It is important to keep in mind that the pumping test is only representative of a small part of the study area as no horizontal heterogeneity is taken into account. The area of influence is larger when injection occurs simultaneously to pumping, with potential lateral heterogeneity playing a role. Even though including lateral heterogeneity might improve the fit, especially around PB JE, adjusting the hydraulic parameters to improve the fit was not attempted. This choice was made because local sensitivity analysis showed that changing the hydraulic parameters (while keeping to realistic limits) could not induce a significant change in the simulated value, while including lateral heterogeneity would be highly speculative and not relevant to the final scale we are aiming for (simulation of ATES system at the scale of the campus). A large impact of the model parameters on the calculated drawdown would be needed to improve the fit significantly as there is still a relatively large discrepancy between the observed and the simulated values in the pumping wells (PP x). Hence, the discrepancy should be explained in a different way.

Near a pumping/injection well the hydraulic gradient is steep and it has the shape of a cone with the pumping (/injection) well as the centre. When using a small grid size this steep gradient could be clearly observed in the model. With distance from the well, the gradient becomes less steep. However, modelling the well itself is more difficult. The presence of water in the well instead of sediment was simulated by setting the value of the hydraulic conductivity (vertical and horizontal) very high at the location of the well. This will decrease the water pressure at that location when injecting. Nevertheless, the positive skin factor, which is a reduction of the permeability in the immediate vicinity of the well due to drilling/well completion/production processes, was not implemented in the model (Van Everdingen, 1953). In general, by reducing the permeability the drawdown in the well itself would be larger and the cone of depression would be steeper (when increasing the permeability this would have the opposite effect). As such, at the pumping well PP 4, a positive skin factor

could be present, this causes the observed drawdown to be larger than the simulated one as observed in Figure 18. At the injection well PB JE, a positive skin factor would cause the negative drawdown to be larger (in absolute values) than the simulated one (injecting water in the aquifer would be more difficult because of reduced near-wellbore permeability). However, the opposite is observed in the results (Figure 18). Maybe there is an increased permeability, i.e. a negative skin factor, in the immediate vicinity of the well due to the gravel that was used in the well completion, due to the flushing of the well or due to local heterogeneity. Another explanation is that the injection well, which is crossing several aquifer layers is not properly represented in the model, which is corroborated by the higher discrepancy compared to PP 4 (a discrepancy of roughly 1.5 m in comparison to about 1 m PP 4. Modelling a pumping/injection well is always difficult as numerical models are not designed to represent heterogeneity in hydraulic conductivity at this scale. Since the pressure drop or increase at the location of the well itself due to pumping and injection respectively was correctly monitored by the divers, the interpretation of the model results at those locations should be made with care. Hence, relying on observations, an injection rate between 3 and 4 m^3/h does not result in an excessive increase in the water level which was in this case taken as the ground surface. As such for the calibration, the focus was on the observation wells where the gradient is less steep and hence more accurately modelled. For PB 6.1 and 6.2, the agreement between the observed and simulated values is good. In PB 2.1 a larger difference of about 30 cm between both curves can be observed. This might be attributed to the fact that it is more strongly influenced by the injection as well as the pumping which results in a more complex situation to model. The pumping wells PP 6 and PP 2 which were used as observation wells show a similar deviation as PP 4 and PB JE. They are both located close to the pumping well where the gradient is steep. All monitoring results have in common that the simulated pressure at the bottom of the well is too high when compared to the observed one. Maybe the deviation could also be attributed to the sealing of the semi-pervious layers which was not ideal as was already mentioned by Lebbe et al., (1992). Nevertheless, when looking at the graphs on a logarithmic timescale, it was shown that the curves are relatively parallel. As such, since the Cooper and Jacob method (1953) describes that the transmissivity and the storage coefficient can be derived from the slope, it is can be shown that the model simulates the real behaviour of the aquifer relatively well. The beginning of the curves is more influenced by the wellbore effect.

It can be concluded that, when only pumping is considered in the triple pumping test, the model simulates the reality quite well, but when also injection is implemented it becomes more difficult to model a more complex reality. Nevertheless, the parallel graphs plotted in the logarithmic timescale indicate a good agreement between the behaviour of the groundwater reservoir in the model and the reality. Also, as the drawdown in the pumping and injection wells are largely influenced by the well resistance, it is normal that the absolute drawdowns in the wells are not reproduced perfectly. However, for the simulation of ATES systems, this is of minor importance. In practice, the well resistance will depend largely on the design and installation of the wells, which can be optimized during installation. The model is therefore considered valid for further simulations.

3.4.2. Well placement and modelled scenario

3.4.2.1. Hydraulic and thermal radius of influence

Results

As mentioned above, a pumping/injection rate of 5 m^3/h per well will be used to model the ATES system for the project.

The hydraulic radius of influence in Yd 4 for one pumping well with a pumping rate of 5 m^3/h was analytically estimated to be 36 m. This was calculated taking into account a drawdown of 1.56 m at a distance of 5 m from the well as was indicated by a simulation of 6 months. The particle tracking simulated for six months in MODPATH shows that no connection between the injection and the pumping well is established when the distance between the wells is 62 m (Figure 19). This was shown by increasing the distance between the wells

step-by-step starting from 36 m. The distribution of the hydraulic head resulting from this single well pair can be consulted in Figure 19. Accounting for the thermal retardation factor of 1.83 (equation 13), the thermal radius of influence in Yd 4 is about 20 m. This was also estimated by using the model (Figure 20). There is a small discrepancy of about 3.5 m between the analytically estimated thermal radius of influence and the modelled one. Because of the limited availability of space, the thermal radius of 20 m was chosen for further analysis.

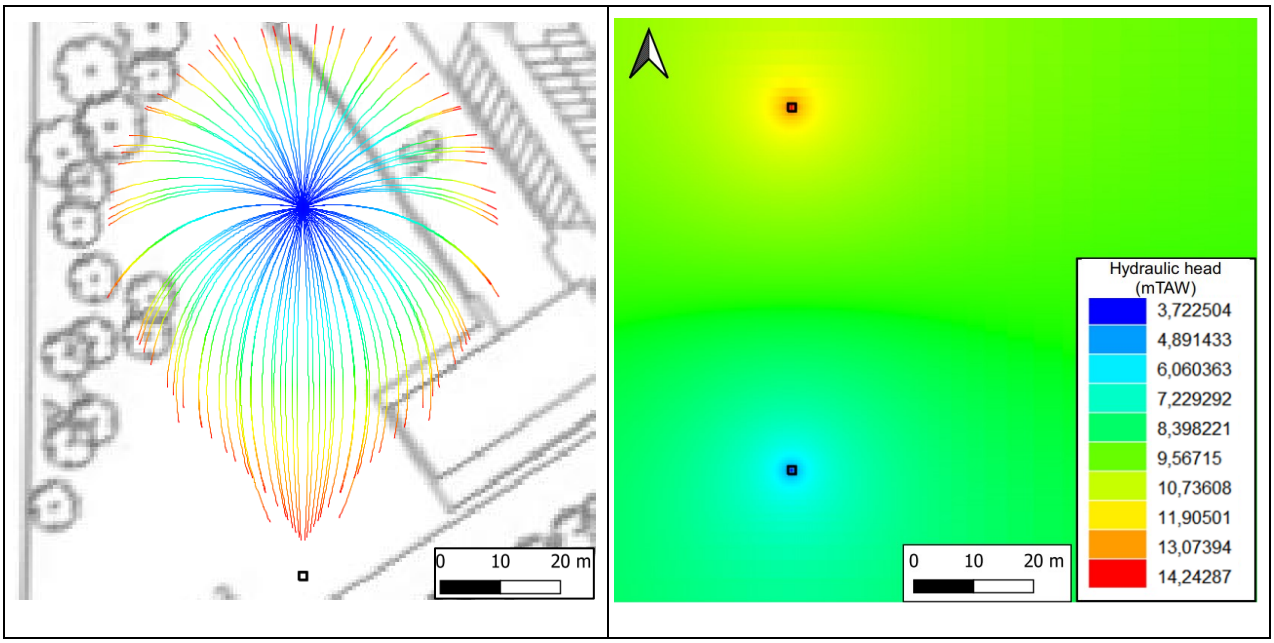

Figure 19: Particle tracking (left) and distribution of the hydraulic head (right) in Yd 4 for 6 months for a well pair consisting of one injection well (upper) and one pumping well (lower). The pumping-reinjection rate is 5 m^3/h and the distance between the wells is 62 m.

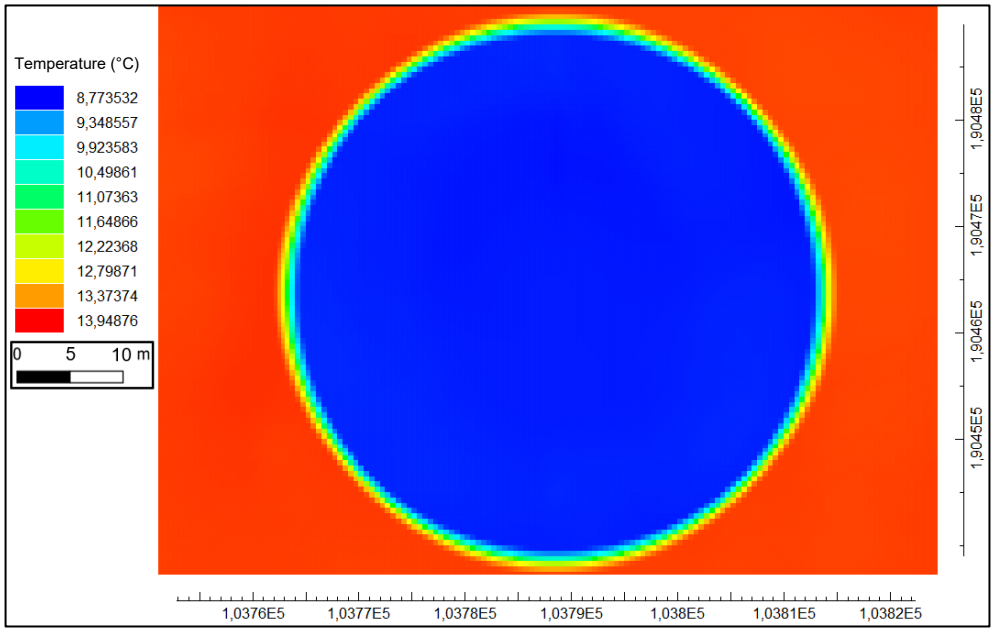

Figure 20: Visualization of the thermal radius of influence in Yd 4 after a simulation period of 6 months.

In an ATES system with multiple well pairs, the interaction between the pairs must also be analysed. In particular here, where the maximum flow rate per well pair is the limiting factor (in comparison to the commonly accepted cut-off rate of 10 m^3/h), it is important to check that the proposed configuration is feasible both hydraulically and thermally. To test this in practice, a double well pair was simulated for six months with a distance between the two clusters of 62 m and a distance between the wells of the same cluster of 20 m. The drawdown remained within limits and also no thermal breakthrough was observed (Figure 21).

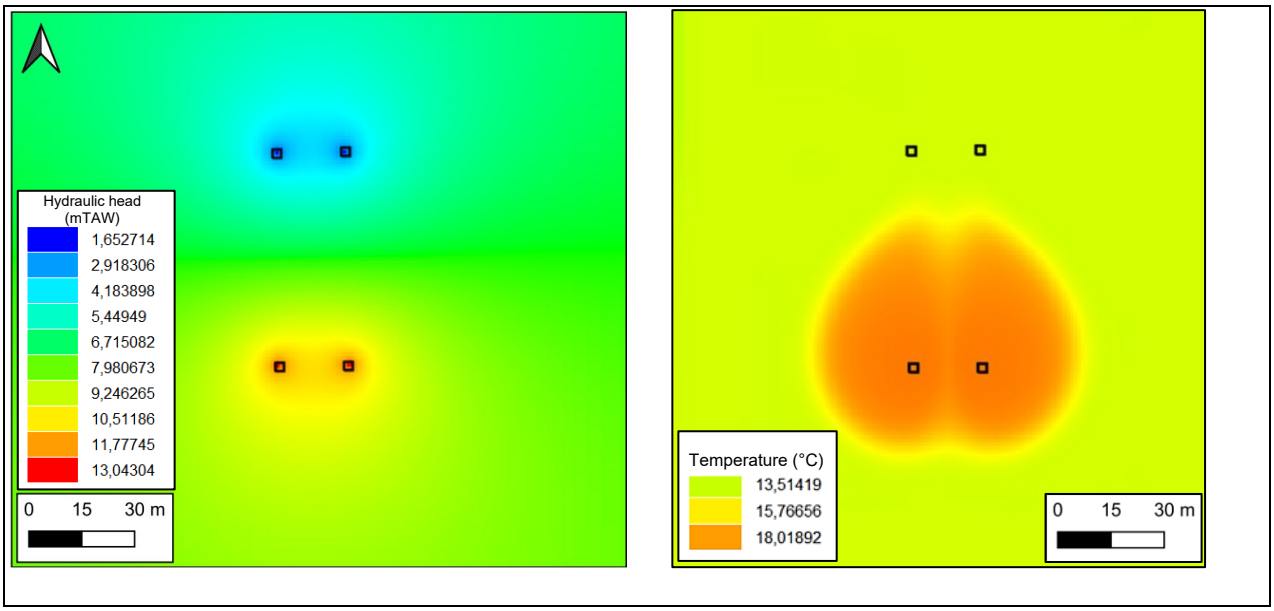

Figure 21: Simulation of the distribution of the hydraulic head (left) and the thermal influence (right) for a double well pair after six months. The distance between the clusters is 62 m, the distance between wells from the same cluster is 20 m.

Discussion

The particle tracking showed that the minimum distance between a well pair must be at least 62 m to avoid a connection between them. However, it must be noted that this is highly dependent on the value of the porosity. If the porosity decreases, the advection velocity increases and the distance between the two clusters will be larger. This indicates that a thorough sensitivity analysis should be carried out in the future because the porosity, which was not yet accurately estimated by Lebbe et al. (1992), has a direct significant influence on the well placement. Geophysical well logging methods (for instance nuclear magnetic resonance logging) might as well be used to better estimate the porosity in the study area. The difference between the thermal radius of influence that was analytically estimated and the one that was simulated might be attributed to the fact that the actual flow field is not uniform.

It was shown that for 1 and 2 well pairs the guidelines drawn up by Bloemendal et al. (2018) work relatively well. The injection pressure in the injecting wells was not too high. Nevertheless, the distribution of the hydraulic head in Figure 21 illustrates the effect of superposition. Namely, the combination of on the one hand two injection wells close to each other and on the other hand two pumping wells close to each other results in a larger radius of influence than was previously simulated for a single well pair. Also, the drawdown in between the clusters remained more limited as the injection counteracts the extraction because their hydraulic radii of influence overlap.

As mentioned earlier, a well efficiency of 70% must be taken into account when estimating the water pressure in the injection well using the model. However, from Figure 18 it was shown that the model already overestimates the pressure (an overestimation of about 1.2 m on an actual negative drawdown of roughly 3.5 m which is about 34%). As such this well efficiency of 70% was not taken into account. Furthermore, the

increase in water level above the ground should be lower than 1/5 of the thickness of the confining layers above the aquifer (Simpson, personal communication). This depends on the thickness of the Gentbrugge Fm which is variable and not well known in the study area. Also, the Quaternary on top might contain some clay layers which might be taken into account for the calculation. As such, as a rough estimation, the modelled increase of the water level above the ground level should best remain limited to 1 or 2 meters. Furthermore, the short heat transport test with 2 well pairs also showed that no thermal breakthrough occurred.

3.4.2.2. Simulations of an ATES system

Results

Considering the power requirement of 0.63 MW and a standard temperature difference between the extracted and the injected water of 5°C, the required total pumping rate can be calculated as follows (equation 16):

$$Q = \frac{P}{1.16 \times \Delta T} = 108.62\ m^3/h$$

Assuming a pumping rate of 5 m^3/h per well, this results in the need for 22 well pairs and hence 44 wells (equation 17).

Subsequently, when the distance between the wells was validated, first a well arrangement in two clusters (i.e. one group of cold wells and one group of warm wells) was simulated (Figure 22 A). This was done to have an idea of what happens when the occupied space by the ATES system would remain limited. This implies that here the campus configuration was considered to be a constraint. It was shown that the total absolute increase in water level resulting from a cluster of injection wells is about 53 m. The total absolute drawdown resulting from a cluster of pumping wells is about 46 m. Considering the guidelines discussed above, this is too large and not acceptable in practice. Additionally, other clustered well arrangements were tested, but the simulated (negative and positive) drawdown remained too high. Respectively a minimum increase in water level of about 31 m due to injection and a minimum drawdown of roughly 28 m was simulated (Figure 22). The reason for these excessive drawdowns (positive and negative) will be discussed later on. Furthermore, for these well configurations, a warning message popped up saying that some cells went dry at the end of the simulation period.

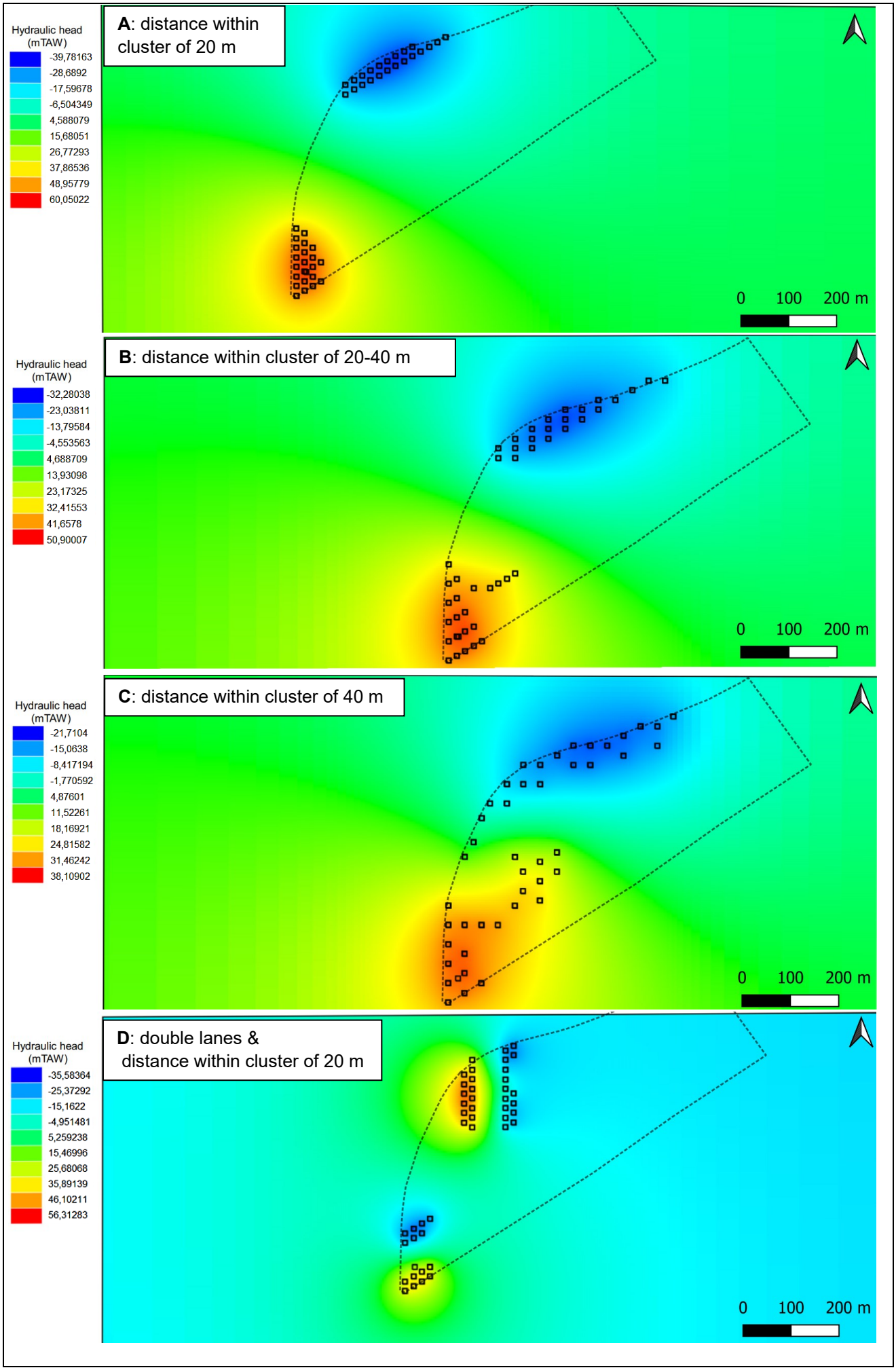

Figure 22: Hydraulic head distribution after 6 months for different well arrangements. The dotted line indicates Campus Sterre.

Due to the large drawdown when a well configuration in clusters was used, it was chosen to carry on with a well configuration in lanes for the project. As mentioned earlier in the methodology, this should effectively limit the drawdown and hence also the injection pressure by the principle of superposition. According to Bloemendal et al. (2018) the distance between the warm and cold well area should at least be 2.5*R_{th}. Taking into account the chosen thermal radius of influence of 20, this results in a distance of 50 m between the lanes. This was tested for a period of 6 months, but it was shown that a thermal breakthrough between the warm and cold well area was established (the cause will be discussed later on). This means that the distance between the lanes was too small. Consequently, the distance between the lanes was incrementally adjusted. For a distance of 80 m, it can be seen that the warm plume almost reaches the cold well area in the NE (Figure 23). As such, a safer distance of 90 m between the lanes was chosen and tested for a simulation period of 2 years. It was shown that the drawdown and the injection pressure were not as pronounced as in previous simulations (Figure 24). The maximum increase in water at the injection wells is about 15 m (extending 12 m above the ground surface). However, it must be pointed out that the hydraulic head in the injection wells in the SW is significantly higher than in the NE. As discussed above, the model also tends to overestimate the injection pressure.

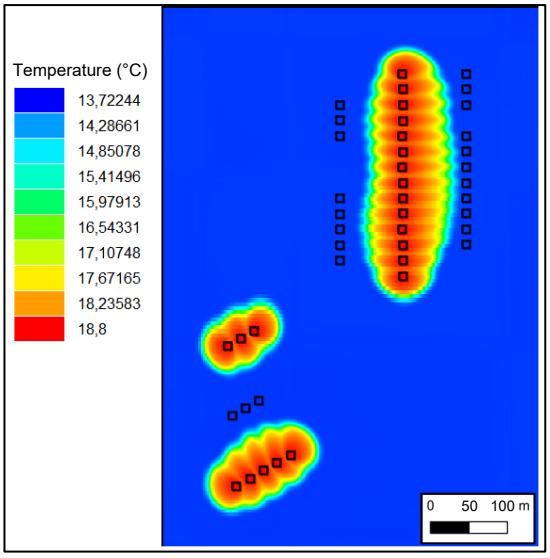

Figure 23: Thermal influence after 6 months of injection of warm water and pumping in the cold well area. The distance between the wells of the same lane is 20 m, while the distance between the lanes is 80 m.

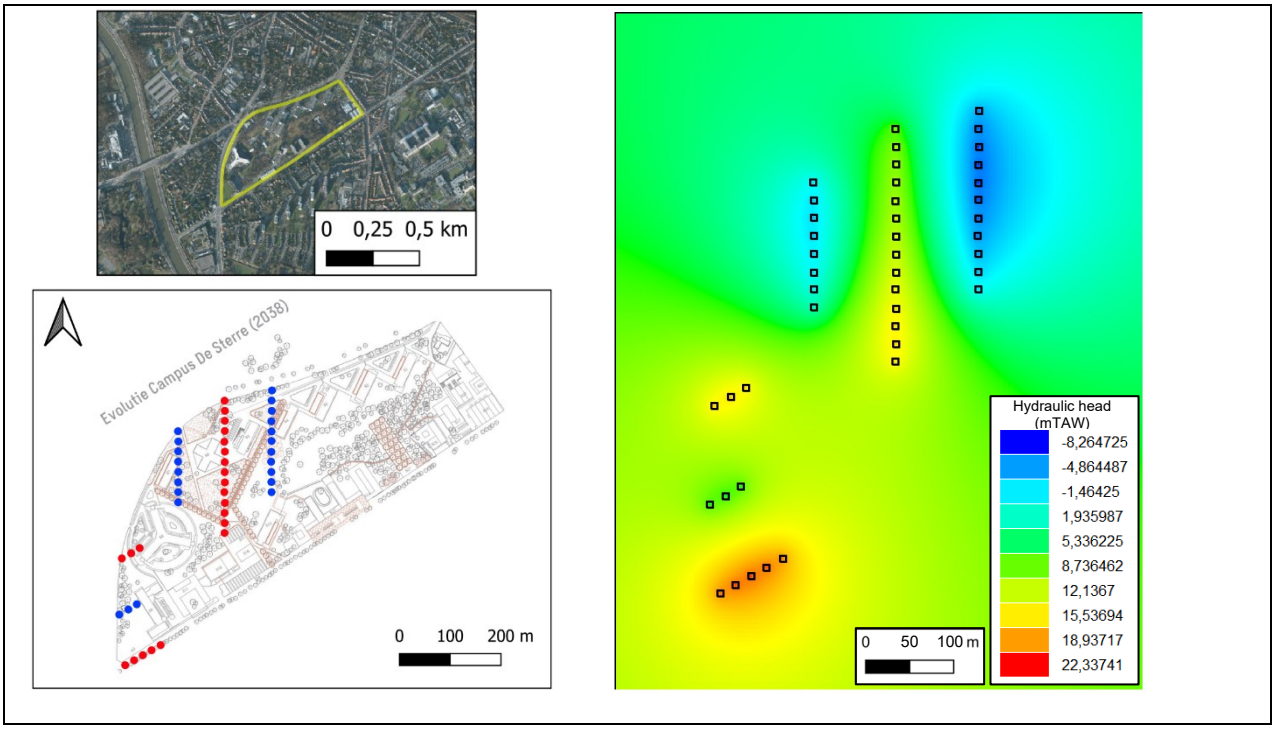

Figure 24: Well arrangement used for the project where the distance between wells within the same lane is 20 m and the distance between the lanes is 90 m (left) and the distribution of the hydraulic head resulting from this arrangement (right).

Next, from a thermal point of view, no breakthrough occurred after the simulated period. Hence, this well configuration was tested for 20 years to determine the storage efficiency of the ATES system (see methodology for 'Modelling scenario'). The result at the observation locations can be seen in Figure 25.

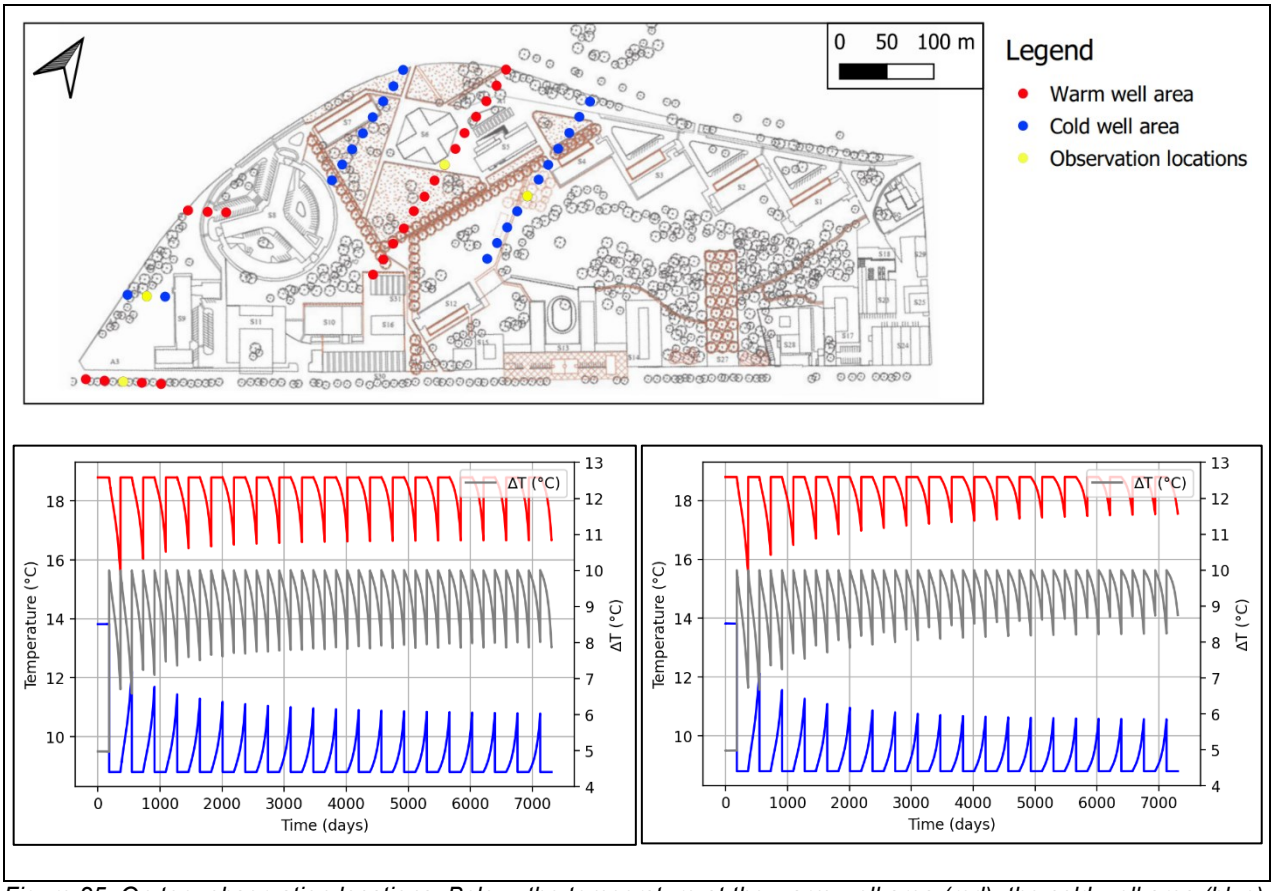

Figure 25: On top: observation locations. Below: the temperature at the warm well area (red), the cold well area (blue), and the temperature difference (grey) at the observation locations in the NE of the well area (left) and the SW of the well area (right) after 20 years of using an ATES system in the lane-type configuration.

The maximum temperature of the cold well area tends to decrease with time to roughly 10.5°C while the minimum temperature of the warm well area tends to increase to roughly 17°C (Figure 25). The minimum temperature difference between the warm well area and the cold well area also tends to increase with time. Furthermore, for the latter, a difference between the seasons of roughly 0.5 °C can be observed. A limited difference in temperature between the observation locations in the NE and SW can be seen.

It was demonstrated that because of the relatively low hydraulic capacity of the aquifer, a high amount of well pairs is needed for the ATES system. These wells, placed in different clusters, interact with each other. Mostly the interaction within the same cluster leads to high pressures or drawdowns. The pressures might be too high for the clay layer to sustain hence increasing the risk of soil outburst (or flooding). To try to overcome this issue, an extra scenario was simulated using a well configuration in a checkerboard pattern. As in this pattern, the injection and extraction wells are alternating, it should be the best one to limit the change in the hydraulic head considering the principle of superposition. As this is a supplementary modelled scenario, the wells were placed as far as possible from each other, disregarding the buildings, within the available space of Campus Sterre (Figure 26, Figure 27). This results in a well spacing of minimum 80 m. Figure 26 indeed illustrates that the hydraulic head remains more limited. However, again a difference between the NE and the SW can be observed. The plot in Figure 27 also shows that the minimum temperature of the warm well area increases while the maximum temperature of the cold well area decreases. The minimum temperature difference also increases with time.

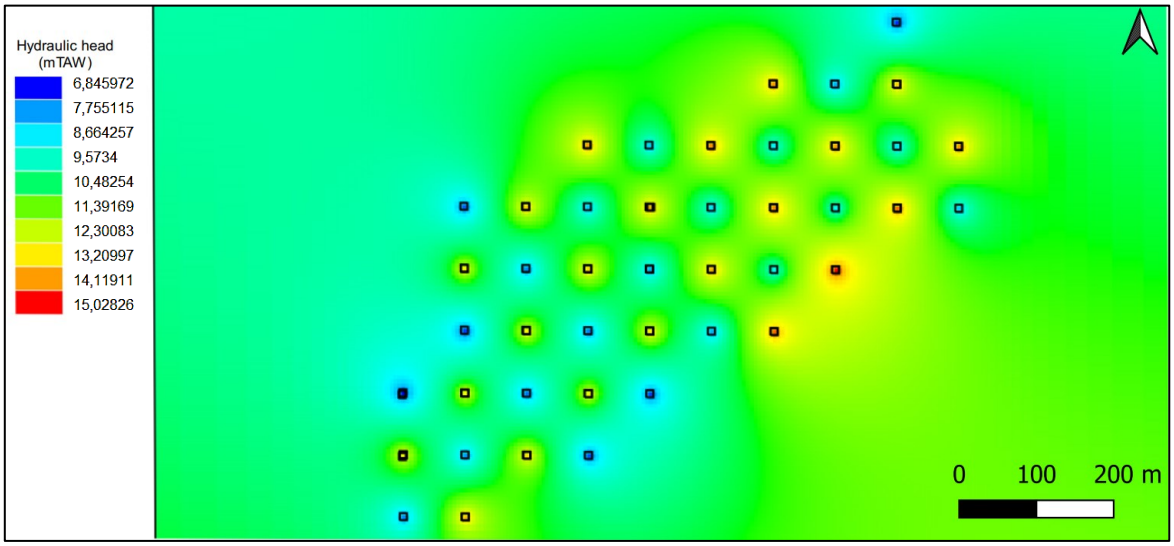

Figure 26: Distribution of the hydraulic head after a simulation period of six months when the wells are placed in a checkerboard pattern with a distance between the wells of 80 m.

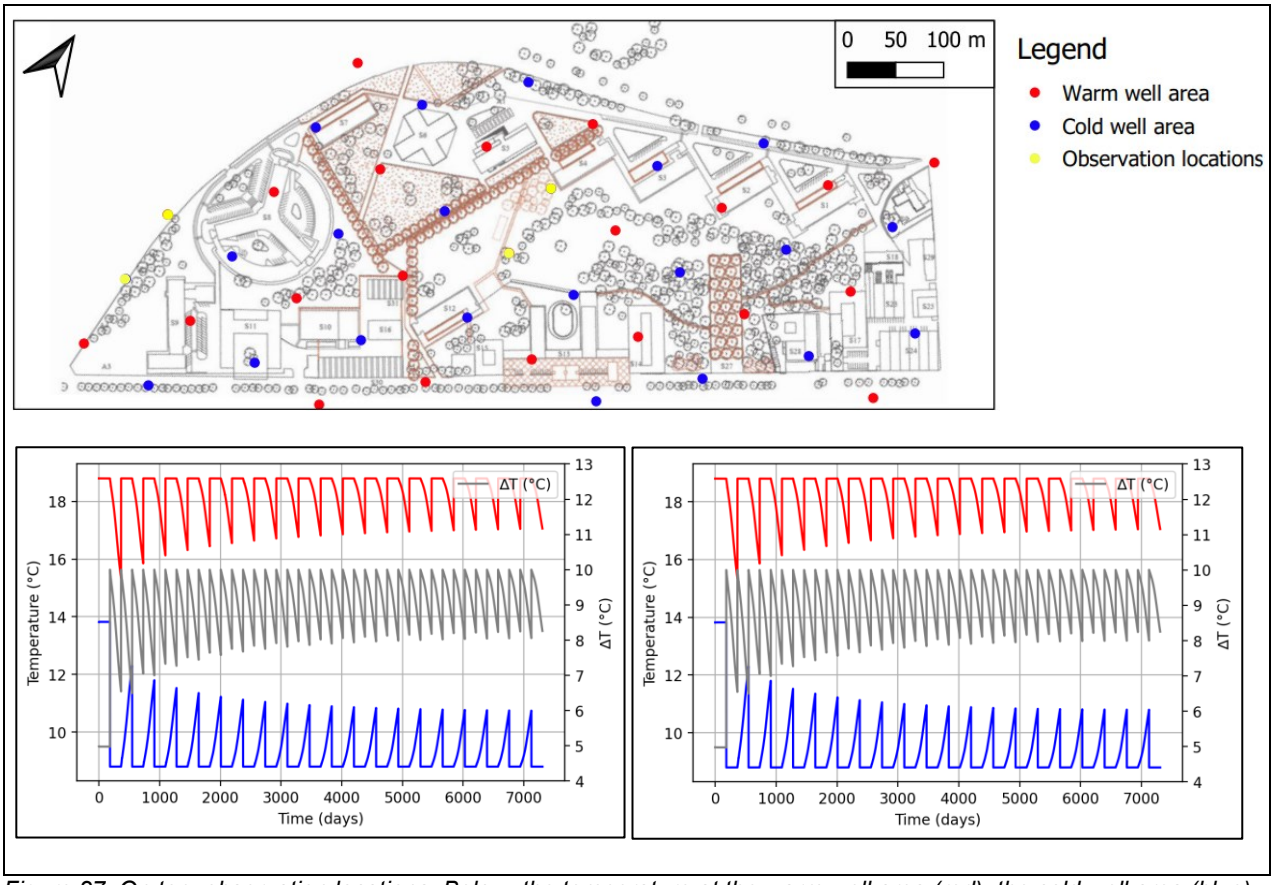

Figure 27: On top: observation locations. Below: the temperature at the warm well area (red), the cold well area (blue), and the temperature difference (grey) at the observation locations in the NE of the well area (left) and the SW of the well area (right) after 20 years of using an ATES system in the checkerboard-type configuration.

Discussion

When the wells for the future ATES system were arranged in 2 (or 4) large clusters, the model showed that the hydraulic head at the location of the injection wells and the drawdown at the extraction wells would be too large (Figure 22). As such, this is not considered a feasible option for the future ATES project. This results from the principle of superposition which implies that the resulting hydraulic head at a certain location is the combination of all influences (resulting from different pumping/injection wells) at that same location. When many wells are grouped into one cluster with an inter-well distance which is less than the hydraulic radius of influence and when combining the influences of all wells in a cluster, this will result in an excessive drawdown (positive or negative). Even though the model tends to overestimate the injection pressure, an increase in water level of minimum 31 m relative to the natural groundwater level is not acceptable. Using such a configuration flooding will likely occur around the injection wells and the confining clay layer might not be able to withstand such high pressures. Also, the minimum drawdown of about 28 m at the pumping wells is not feasible as this would probably cause the aquifer to become partly unsaturated and consequently might cause the necessary pumping rate of 5 m^3/h per well not to be reached anymore.

When implementing these well arrangements with two or 4 large clusters, the model also showed a problem with dry cells in the Southwestern corner of the well area. This is probably related to the location of the border for the occurrence of the Gentbrugge Fm (Merelbeke Mb) (Figure 28). As mentioned earlier, it was set using the catalogue of Geopunt Vlaanderen. This boundary crosses Campus Sterre. As a result, where the clay layer does not occur, Yd 6 is phreatic and in connection with the Quaternary. In a phreatic aquifer, the superposition principle for the estimation of the hydraulic head due to pumping in more than 1 well does not apply anymore and the resulting drawdowns are larger. Also, this would be a disadvantage for the injection of water since it could more easily result in wetting of the ground surface. The data set that was used is the result of interpolation. Hence, the boundaries might be inaccurate. As such, the occurrence of this border must be verified in the future using available borehole descriptions in the neighbourhood, cone penetration tests, and/or geophysical well logging methods such as gamma-ray logging. For this thesis, however, due to time constraints, it was decided to carry on with the modelling using the initial boundary for the occurrence of the Gentbrugge Fm. Also, in this way, an idea can be made of the response of the aquifer due to the implementation of an ATES system as well as with a phreatic upper part of the Ypresian Aquifersystem (in the SW of the campus) as with a fully confined upper part (in the NW of the campus).

Figure 28: Indicated in white is the border for the occurrence for the Paniselian Aquiftardsystem (Gentbrugge Fm, Merelbeke Mb) which occurs in the NE of the study area.

Next, the arrangement of wells in several lanes showed that a distance of 90 m between the lanes was necessary to avoid thermal breakthrough. This is significantly larger than the guidelines of Bloemendal et al. (2018) proposed. It can probably be attributed to the fact that the increase of the water level around the injection wells is larger for an entire lane than for only 1 or 2 wells. This can again be attributed to the interaction of wells within a cluster/lane. The radii of influence which were deduced for a single well pair are not valid anymore when hydraulically the wells are adding up. This results in an extra pressure which moves the water (and the temperature front) forwards. The lane arrangement showed an overall improvement of the hydraulic head at the location of the injection wells due to the closeness of wells of the opposite type. However, it also showed that the hydraulic head in the SW of the well area is significantly higher than in the

NE. It might be the result of the fact the warm lanes in the SW are not located in between two cold lanes which counterbalance the increase in hydraulic head.

From a thermal point of view, Figure 25 showed that no thermal breakthrough occurred. This would show as a drop in temperature of the warm well area below the natural groundwater temperature of 13.8 °C (and it would show as the reverse for the cold well area. Due to the injection of warm and cold water during summer and winter respectively a temperature difference is created between the warm and cold well areas. As such, during the next cycle water can be extracted at respectively a higher (in winter) and lower temperature (in summer) relative to the natural groundwater temperature. This concept of storing energy increases the efficiency of the system. Additionally, as the minimum temperature of the warm well area increases and the maximum temperature of the cold well area decreases, the efficiency of the system increases with time and the temperature reaches a dynamic equilibrium. The former is the result of not extracting all heat/cold during the extraction season for the wells. The increasing efficiency can also be seen in the minimum temperature difference which increases with time. The change of about 0.5 °C in temperature difference between the summer and winter seasons is normal and is relatively limited. The small difference between the temperature at the observation locations in the NE and SW might be explained by the fact that in the NE the lanes consist of more wells close to each other, slightly decreasing the storage efficiency. Furthermore, the influence of the imposed natural groundwater gradient of 0.14% (see 'Modelling scenario') did not seem to be an issue for heat storage as the cold and warm plumes are not moving away significantly with the natural groundwater flow.

From the above it is evident that the injection pressure (i.e. the increase of the hydraulic head at the location of the injection well) is the limiting factor in the design of this particular ATES system. It is not surprising as the pumping/injection rate (5 m^3/h) is close to the estimated maximum rate for this aquifer (about 5.8 m^3/h). Consequently, an additional well arrangement in a checkerboard pattern was simulated as, considering the principle of superposition, it should be the best approach to limit the hydraulic head in the injection wells. However, this pattern is less optimal for efficiently using the available space and hence less cost-efficient when considering the piping and installation costs. In addition, on the one hand, it might also increase the risk of a thermal breakthrough. On the other hand, as the injection pressure is more limited, it should also slightly decrease the thermal radius. This additional scenario, also modelled for 20 years, served to give a first idea of the difference between the two well configuration approaches. The checkerboard pattern indeed showed a more limited increase in the hydraulic head at the location of the injection wells which confirms its purpose. The hydraulic head was higher in the NE of the study area than it was in the SW. This is opposite to what could be observed in the lane-type arrangement but it can probably be attributed to the border of occurrence of the Paniselian Aquitardsystem. This well configuration was also validated from a thermal point of view. No thermal breakthrough occurred in the 20-year simulation and the efficiency of the system tends to increase with time. It must be pointed out that when looking at the diagonals in the checkerboard pattern it resembles the lane-type well arrangement but with a larger distance between the wells of the same cluster (lane). Based on these results and taking into account that the drawdown/injection pressure remains more limited by using the checkerboard pattern, this configuration can easily be adapted in the future to accommodate the buildings and optimize the usage of the available space. As such, it is plausible that the distance between the wells might be decreased to about 60 m without significantly increasing the risk for thermal breakthrough. To summarize, the lane-type well arrangement should effectively store heat and cold in the subsurface for the implementation of an ATES system on Campus Sterre. However, it was shown that the injection pressure is the limiting factor in the design of the system. For future well placement it is therefore suggested to use the hydraulic radius of influence instead of the thermal radius as a starting point to derive the optimal well placement when using the guidelines drawn up by Bloemendal et al. (2018). Furthermore, it must be pointed out that currently a temperature difference of 5 °C was used between the warm and cold injected water. This could be adapted to 6 °C reducing the required pumping rate (equation 16) and hence the required amount of well pairs.

3.5. Economic analysis

Results

SWECO estimated that for the implementation of a BTES system which can provide the power requirement of 0.63 MW, about 175 drillings of each 100 m deep would be needed. This results in a total occupied area of 4370 m^2 when considering 25 m^2 per drilling. The investment cost for such a BTES system is roughly € 3 500 000 (estimated by SWECO). Taking into account 10% inflation, this results in an initial investment cost of € 3 850 000.

The estimation of the investment cost of an ATES system was made based on the data provided by IFTECH a couple of years ago at approximately the same time the estimation by SWECO was made (Table 5). These prices may vary according to the final length of the pipes used (and hence depends on the well arrangement). Additionally, for the future system, a heat pump with a lower capacity (and a lower cost) might be used than the one which is used for the estimation. Altogether, the initial investment cost of an ATES system consisting of 44 wells is estimated to be about € 1 600 000.

Table 5: Estimated cost of the ATES system of 44 wells with data provided by IFTECH.

	Unit price (€)	Unit price + 10% inflation (€)	Amount	Total (€)
Drillings (depth 35 m)	8801,50	9681,65	44	425992,6
Pumps	1523,55	1675,905	44	73739,82
Finishing wells	5906,52	6497,172	44	285875,6
Hydraulic and electrical connection	655,17	720,687	44	31710,23
Pipes (/m)	50,76	55,836	2000	111672
Cables	202160,00	222376	1	222376
Excavation work	32,06	35,266	1	35,266
Heat exchanger (1330 kW)	105000,00	115500	1	115500
Collectors	111081,60	122189,76	1	122189,8
Other components	11752,73	12928,003	1	12928
Control box	174867,40	192354,14	1	192354,1
Total investment cost				1 594 373

Discussion

The estimated initial investment cost for an ATES system is about 2.4 times lower than the estimated initial investment cost for a BTES system. The cost for the piping and installation could be higher than estimated because many wells need to be installed with a relatively large spacing in between them (for ATES). This is a significant difference in investment cost and, considering the currently rising energy costs, it might become even more cost-efficient in the future in comparison to traditional heating and cooling systems. However, more geological uncertainties arise for an ATES system such as the estimated hydraulic and thermal conductivity. As such, for such large investment costs, it is worth the effort to limit those uncertainties in advance. This can be done by carrying out new field tests in the study area. Nevertheless, if opted for the BTES system, some extra field tests should be performed anyway. A thermal response test to validate the thermal conductivity of the subsurface is always advised for such a large project and the natural groundwater gradient must also be accurately estimated. Afterwards, if the additional field tests show that an ATES system might be feasible, a thorough economic analysis should be commissioned to estimate the costs and benefits of the ATES system in comparison to other systems. For such a large project, it should also be taken into account in the economic analysis that an environmental impact assessment might have to be made.

If the ATES system is deemed to be the most suitable option, an extension of the system to provide more cooling/heating according to the demand might be possible in the future depending on the space that can be occupied by the system and the confirmed maximum pumping/reinjection rate.

4. Conclusion

For the implementation of aquifer thermal energy storage on Campus Sterre, the layered groundwater reservoir, which is part of the Ypresian Aquifersystem, is the only possibility. Although the latter is commonly disregarded as a possible aquifer for ATES as it has a limited permeability and thickness in the study area, for such large projects with high investment costs it was worthwhile to carry out a feasibility study. The Ypresian Aquifer system can be subdivided into six units which are alternately pervious or semi-pervious. From bottom to top they are numbered from Yd 1 to Yd 6 respectively (the even numbers being the pervious layers).

Several aspects were considered to evaluate the feasibility and sustainability of an ATES system on Campus Sterre. First, and most importantly, the pumping tests showed that a pumping and reinjection rate of 3.8 m^3/h is possible when pumping in a pumping well which is only screened in Yd 4 and reinjecting in a piezometer which is filtered over the entire depth of the studied groundwater reservoir. Applying the principle of superposition, it was analytically estimated that a pumping and reinjection rate of 5 m^3/h should be feasible in a fully-screened pumping and reinjection well with a suitable diameter. This requires an increase in injection capacity of about 30% relative to injecting in a fully-screened piezometer with a smaller diameter. In this setting, the injection rate will be the limiting factor as the hydraulic head in the injection well cannot extend too much above the ground level and the confining layer on top of the aquifer must be able to withstand the increased pressure without rupturing. If not, it might cause wetting and/or flooding of the ground surface.

Second, the Membrane Filtering Index test served to predict whether the fine sediment particles might clog the wells. It was shown that the risk of clogging remains within acceptable limits and allows for reinjection to take place while maintaining the pressure in the injection wells low enough to avoid flooding. Despite some difficulties with the pumping installation itself, the capacity for long term injection was also verified. As a result, no risk for decreased capacity and efficiency due to well clogging is expected for the ATES system. If in the future, new well pair(s) would be constructed for additional field tests, it is advised to install filters only in Yd 2, Yd 4 and Yd 6 as the other layers are semi-pervious and contain a considerable amount of small particles which are more prone to clog the injection wells.

These two aspects, on the one hand the pumping/reinjection rate and on the other hand the capacity for long-term injection without clogging, validate the hydraulic conditions needed for the implementation of an ATES system. Subsequently, after estimating the hydraulic and thermal radius of influence, several well configurations were tested to use the available space in an optimal way and to effectively store the thermal energy. The power requirement of 0.63 MW resulted in a simulation of 22 well pairs in a lane-type arrangement of alternately warm and cold lanes. This well placement was chosen because it successfully limits the injection pressure as the extraction and injection counterbalance each other through the principle of superposition. The distance between the wells from the same lanes was 20 m and the distance between adjacent lanes was 90 m to avoid thermal interference. The average low permeability of the study area limits the thermal radius for one well pair. However, when placing several wells at a relatively short distance from each other in a lane, the injection pressure, and hence also the thermal radius, increased again. As such, this shows that the low permeability in the study area is neither an advantage nor a disadvantage in this specific case where many wells had to be implemented for an ATES system. Next, it was proven that, for the chosen well arrangement in lanes, the efficiency of the ATES system tends to increase with time which is a good prospect. It indicates that the system would work well and could provide the necessary power.

As it was demonstrated that the injection rate and the resulting pressure build-up are the liming factors in the design of the system, a well configuration in a checkerboard pattern was also tested. This served to have an idea of what is possible when using the theoretically optimal well arrangement to limit the injection pressure. Not taking into account the aspect of using the available space optimally, a distance between the wells of 80 m was used. This encompasses the entire Campus Sterre (not taking into account buildings). The results

showed that the pressure at the injection wells indeed remained significantly lower, similar to what is observed for a single well pair, and that the storage efficiency still increased with time. Combined with the well arrangement in lanes, these results can be used afterwards, when more field tests will have been carried out, to optimize the well configuration. Furthermore, it was proven that the hydraulic radius of influence is more limiting than the thermal radius of influence in this case. As such, it is suggested to use the former to apply the guidelines for the well placement drawn up by Bloemendal et al. (2018) when looking to further optimize the well configuration. This is justified, as it was demonstrated that, when using the thermal radius of influence for the guidelines, the distance between the lanes still had to be significantly increased (from 50 to 90 m) to avoid thermal interference.

Next, the limited knowledge about lateral heterogeneity in the study area indeed turned out to be a bottleneck to design the ATES system. For instance, the exact location of the boundary for the occurrence of the Paniselian Aquitardsystem (Gentbrugge Fm, Merelbeke Mb) was not known. According to the used data set, the boundary divides Campus Sterre into two areas: one in the Northeast where the unit occurs, and one in the Southwest where the unit is absent. However, this is based on interpolation and might not be accurate at the borders. Also, the thickness of the unit is not precisely known. Nevertheless, because heterogeneity influences both groundwater flow and transport it might influence the results. As such, if the Paniselian Aquitardsystem is not present at some locations of the study area, the semi-pervious layer Yd 6 will be phreatic. This will result in an increased risk of wetting the ground surface when reinjection takes place and could impact heat storage by inducing some loss towards the atmosphere. Therefore it can be concluded that in the future it is suggested to have a better idea of the lateral heterogeneity on campus.

It is important to mention that no sensitivity analysis was carried out for the used model. The hydraulic conductivity and storage coefficient for all layers were already accurately estimated by Lebbe et al. (1992) who also carried out a thorough analysis of the results. As such, this was not repeated for this thesis. However, if in the future the newly created model will still be used, a detailed sensitivity analysis should be carried out for the porosity and dispersion parameters. Especially, the former has a direct impact on the calculation of the hydraulic and thermal radius and could therefore strongly impact well placement.

Third, although it was not the focus of this thesis, a short chemical analysis was carried out. The groundwater of the three pervious layers will be mixed in an ATES system. Nevertheless, it was estimated that the risk for chemical reactions which might be detrimental to the groundwater ecology will remain limited as the three pervious layers approximately already have the same composition. The risk that chemical reactions, induced by temperature changes, will influence the ecology and the efficiency of the system will also be limited. This could be justified by the fact that the temperature changes will be small (about +/- 5 °C).

Fourth, the brief economic analysis showed that an ATES system would be roughly 2.4 times more cost-efficient than a BTES system. This proves that it is worthwhile considering an ATES system for large projects even when traditionally it is disregarded for low permeable sediments. However, the cost of further field tests to limit uncertainties should also be taken into account. As the high investment cost must still be worthwhile despite the remaining uncertainties which are specific to many projects, an additional safety coefficient could be applied in the design. Options to make the ATES system more efficient could also be searched for. For instance, the well placement can be optimized to reduce the piping and installation costs. Also, a temperature difference of 6 °C could be used to limit the required total pumping rate i.e. reducing the required amount of wells (or reducing the pumping rate per well when maintaining the initial estimated amount of wells).

To conclude, this thesis showed that implementing an ATES system on Campus Sterre is probably feasible and more cost-efficient than a BTES system. Even though the sustainability of shallow geothermal resources cannot always be guaranteed since many aspects are to be considered, uncertainties can be limited by

carrying out additional field tests. Considering this, a list of recommendations can be made based on the priority of the actions that must be taken for this project in the future:

1. To confirm the estimated pumping/reinjection rate and the radius of influence it is essential that new pumping/reinjection tests are carried out using at least one newly constructed, fully-screened well pair with an adapted filter and diameter. These wells can be reused if the ATES system is installed.

2. Also, if two new well pairs would be constructed for additional field tests, they can be used for the assessment of the heterogeneity. This can be supported by cone penetration tests across the study area, which preferably also measure the conductivity. These tests also have the purpose of better locating the boundary for the occurrence of the Panisilian Aquitardsystem and better estimating its thickness.

3. In practice, the ideal location for the filter placement of the new wells should be determined during drilling or with geophysical logging methods. Optimal placement will limit the risk of clogging the wells with fine sediment particles of the semi-pervious layers. Also, new MFI tests as well as a long-term pumping/reinjection experiment (of preferably 6 months) should be carried out in the new wells to confirm the capacity for long-term injection.

4. Heat tracer experiments should also be carried out to validate the porosity and thermal parameters. A thermal response test should be carried out to validate the thermal conductivity of the subsurface. On top of lab analysis, the total and effective porosity could be estimated using nuclear magnetic resonance logging.

5. The ATES system should be refined using the hydraulic radius for the guidelines for well placement of Bloemendal et al. (2018) and the results of this thesis. Additionally, a heat loss could be introduced in the model by adapting the boundary conditions for heat transport. The system could also become more efficient when using a temperature difference of 6 °C (instead of 5 °C). This would result in less required well pairs and hence less occupied space. It might also allow for an extension of the system. Using the initial amount of well pairs but operating at a higher temperature difference could also be a sort of safety factor. However, it would reduce the efficiency of the heat pump.

6. Making a thorough economic analysis for the ATES project.

7. Evaluating the influence on the ecology of the groundwater due to the implementation of an ATES is closely related to an eventual environmental impact assessment that might have to be made when the project would be implemented in reality. This would include not only the impact on the groundwater but also the impact on other aspects of the environment.

This thesis demonstrated the importance, but also the limitations, of numerical simulations and it proved that field tests are indispensable to complement this. It was shown that, for large-scale projects, the positive environmental goal of having a minimal CO_2 output might also be reached using an ATES system instead of a BTES system in low permeable sediments.

5. Reference list

Aalten, T., Witteveen, H., 2015. Protocol zand- en slibhoudendheidsmetingen, versie 1.0. BodemenergieNL. Last accessed May 19, 2022 from https://docplayer.nl/48776639-Protocol-zand-en-slibhoudendheidsmetingen.html

Bedekar, V., Morway, E.D., Langevin, C.D., and Tonkin, M., 2016, MT3D-USGS version 1.0.0: Groundwater Solute Transport Simulator for MODFLOW: U.S. Geological Survey Software Release, 30 September 2016. Last accessed May 19, 2022 from http://dx.doi.org/10.5066/F75T3HKD

Bloemendal, M., 2018. The hidden side of cities: Methods for governance, planning and design for optimal use of subsurface space with ATES. PhD thesis, Delft University of Technology. Last accessed May 19, 2022 from https://doi.org/10.4233/uuid:0c6bcdac-6bf7-46c3-a4d3-53119c1a8606

Bloemendal, M., Olsthoorn, T., 2018. ATES systems in aquifers with high ambient groundwater flow velocity. Geothermics, 75 (January), 81–92. Last accessed May 19, 2022 from https://doi.org/10.1016/j.geothermics.2018.04.005

Bloemendal, M., Jaxa-Rozen, M., Olsthoorn, T., 2018. Methods for planning of ATES systems. Applied Energy, 216, 534–557. Last accessed May 19, 2022 from https://doi.org/10.1016/j.apenergy.2018.02.068

Bonte, M., Stuyfzand, P.J., Hulsmann, A., Van Beelen, P., 2011. Underground thermal energy storage: environmental risks and policy developments in the Netherlands and European Union. Ecology and Society **16**(1): 22. Last accessed May 19, 2022 from http://www.ecologyandsociety.org/vol16/iss1/art22/

Bridger, D.W., Allen, D. M., 2014. Influence of geologic layering on heat transport and storage in an aquifer thermal energy storage system. Hydrogeology Journal, 22(1), 233–250. Last accessed May 19, 2022 from https://doi.org/10.1007/s10040-013-1049-1

Cooper, H.H., Jacob, C.E., 1953. A generalized graphical method of evaluating formation constants and summarizing well-field history. Groundwater notes hydraulics, No. 7, 90-102. Last accessed March 31, 2022 from https://www.nrc.gov/docs/ML1429/ML14290A600.pdf

Databank Ondergrond Vlaanderen – Vlaamse Overheid. (n.d.). Verkenner. Last accessed April 19, 2022 from https://www.dov.vlaanderen.be/portaal/?module=verkenner

De Moor, G., De Breuck, W., 1969. De freatische waters in het Oostelijk Kustgebied en in de Vlaamse Vallei. Natuurwet. Tijdschr. 1969, 51, 3-68. Last accessed May 19, 2022 from https://www.vliz.be/nl

De Zwart, A.H., 2007. Investigation of clogging processes in unconsolidated aquifers near water supply wells. Proefschrift. Hydrology and Ecology Section and Petroleum Engineering Section, Department of Civil Engineering and Geosciences, Delft University of Technology. Last accessed May 19, 2022 from https://repository.tudelft.nl

Drijver, B.C., 2011. High Temperature Aquifer Thermal Energy Storage (HT-ATES): water treatment in practice. 1e Nationaal Congres Bodemenergie, Utrecht, Nederland, pp 5. Last accessed May 19, 2022 from https://www.researchgate.net

Dupuit, J.É.J., 1863. Études Théoriques et Pratiques sur le Mouvement des Eaux Dans les Canaux Découverts et à Travers les Terrains Perméables: Avec des Considérations Relatives au Régime des

Grandes Eaux, au Débouché à leur Donner, et à la Marche des Alluvions dans les Rivières à Fond Mobile; Dunod: Paris, France, 1863.

Edmunds, W.M., Shand, P., 2008. Natural groundwater quality. Blackwell Publishing Ltd. Last accessed May 19, 2022 from https://doi.org/10.1002/9781444300345

European Commission, 2012. Roadmap 2050 Low Carbon Europe. Last accessed May 19, 2022 from https://doi.org/10.2833/10759

European Commission,2019. Heating and cooling. Comprehensive assessment. https://ec.europa.eu/energy/en/topics/energy-efficiency/heating-and-cooling

Fleuchaus, P., Godschalk, B., Stober, I., Blum, P., 2018. Worldwide application of aquifer thermal energy storage – A review. Renewable and Sustainable Energy Reviews, 94(November 2017), 861–876. Last accessed May 19, 2022 from https://doi.org/10.1016/j.rser.2018.06.057

Fleuchaus, P., Schüppler, S., Godschalk, B., Bakema, G., Blum, P., 2020. Performance analysis of Aquifer Thermal Energy Storage (ATES). Renewable Energy, Volume 146 (February 2020), pp. 1536-1548. Last accessed May 19, 2022 from https://doi.org/10.1016/j.renene.2019.07.030

Gao, Q., Zhou, X.Z., Jiang, Y., Chen, X.L., Yan, Y.Y., 2013. Numerical simulation of the thermal interaction between pumping and injecting well groups. *Applied Thermal Engineering*, *51*(1–2), 10–19. Last accessed May 19, 2022 from https://doi.org/10.1016/j.applthermaleng.2012.09.017

Geopunt Vlaanderen – Vlaamse Overheid, 2019. H3Dv2 A0700, voorkomen Paniseliaan Aquitardsysteem. Last accessed March 30, 2022 from https://www.geopunt.be/catalogus/datasetfolder/9ffe28f7-ffa4-4e12-b1ca-498ef48ed4ca

Glassley, W.E., 2015. Geothermal energy: Renewable energy and the environment, Third edition. CRC Press, inc.

Hähnlein, S., Bayer, P., Ferguson, G., Blum, P., 2013. Sustainability and policy for the thermal use of shallow geothermal energy. Energy Policy, 59, 914–925. Last accessed May 19, 2022 from https://doi.org/10.1016/j.enpol.2013.04.040

Hartog, N., Drijver, B., Dinkla, I., Bonte, M., 2013. Field assessment of the impacts of Aquifer Thermal Energy Storage (ATES) systems on chemical and microbiological groundwater composition. European Geothermal Congress, pp 8. Last accessed May 19, 2022 from https://www.iftechnology.com

Hecht-Méndez, J., Molina-Giraldo, N., Blum, P., Bayer, P., 2010. Evaluating MT3DMS for heat transport simulation of closed geothermal systems. *Ground Water*, *48*(5), 741–756. Last accessed May 19, 2022 from https://doi.org/10.1111/j.1745-6584.2010.00678.x

Hermans, T., Nguyen, F., Klepikova, M., Dassargues, A., Caers, J., 2018. Uncertainty Quantification of Medium-Term Heat Storage From Short-Term Geophysical Experiments Using Bayesian Evidential Learning. Water Resources Research, 54(4), 2931–2948. Last accessed May 19, 2022 from https://doi.org/10.1002/2017WR022135

Jenne, E., Andersson, O., Willemsen, A., 1992. Well, hydrology, and geochemistry problems encountered in ATES systems and their solutions. SAE Technical Paper (1992). Last accessed May 19, 2022 from https://www.osti.gov/servlets/purl/10187570

Kim, J., Lee, Y., Yoon, W.S., Jeon, J.S., Koo, M.H., Keehm, Y., 2010. Numerical modeling of aquifer thermal energy storage system. *Energy*, *35*(12), 4955–4965. Last accessed May 19, 2022 from https://doi.org/10.1016/j.energy.2010.08.029

Langevin, C.D., Thorne, D.T., Dausman, A.M., Sukop, M.C., Guo, W., 2007. SEAWAT Version 4: A Computer Program for Simulation of Multi-species Solute and Heat Transport, US Geol. Surv. Tech. Methods, Book 6, US Geological Survey Reston, VA (Chapter A22). Last accessed May 19, 2022 from https://doi.org/10.3133/tm6A22

Langevin, C.D., Hughes, J.D., Banta, E.R., Niswonger, R.G., Panday, S., Provost, A.M., 2017a. Documentation for the MODFLOW 6 Groundwater Flow Model: U.S. Geological Survey Techniques and Methods, book6, chapter A55, 197p. Last accessed May 19, 2022 from https://doi.org/10.3133/tm6A55

Langevin, C.D., Hughes, J.D., Banta, E.R., Provost, A.M., Niswonger, R.G., and Panday, S., 2017b. MODFLOW 6 Modular Hydrologic Model: U.S. Geological Survey Software. Last accessed May 19, 2022 from https://doi.org/10.5066/F76Q1VQV

Lebbe, L., Mahauden, M., De Breuck, W., 1992. Execution of a triple pumping test and interpretation by an inverse numerical model. International Journal of Applied Hydrogeology, volume 1 4/1992, pp. 20-34.

Muela Maya, S., García-Gil, A., Garrido Schneider, E., Mejías Moreno, M., Epting, J., Vázquez-Suñé, E., Marazuela, M.Á., & Sánchez-Navarro, J.Á., 2018. An upscaling procedure for the optimal implementation of open-loop geothermal energy systems into hydrogeological models. Journal of Hydrology, 563(May), 155–166. Last accessed May 19, 2022 from https://doi.org/10.1016/j.jhydrol.2018.05.057

Meng, B., Vienken, T., Kolditz, O., Shao, H., 2019. Evaluating the thermal impacts and sustainability of intensive shallow geothermal utilization on a neighborhood scale: Lessons learned from a case study. Energy Conversion and Management. Last accessed May 19, 2022 from https://doi.org/10.1016/j.enconman.2019.111913

Olsthoorn, T.N., 1982. The clogging of recharge wells, main subjects; KIWA Communications 72, Rijkswijk. Last accessed May 19, 2022 from https://library.wur.nl/WebQuery/hydrotheek/2108784

Parsons, M.L., 1970. Groundwater Thermal Regime in a Glacial Complex. Water Resources Research, 6(6), 1701–1720. Last accessed May 19, 2022 from https://doi.org/10.1029/WR006i006p01701

Perego, R., Viesi, D., Pera, S., Dalla, G., Cultrera, M., Visintainer, P., Galgaro, A., 2020. Revision of hydrothermal constraints for the installation of closed-loop shallow geothermal systems through underground investigation , monitoring and modeling. Renewable Energy, 153, 1378–1395. Last accessed May 19, 2022 from https://doi.org/10.1016/j.renene.2020.02.068

Pollock, D.W., 2012. User Guide for MODPATH Version 6 – A Particle-Tracking Model for MODFLOW. US Geol. Surv. Techniques and Methods 6 – A41. Last accessed May 19, 2022 from https://doi.org/10.3133/tm6A41

Possemiers, M., 2014. Aquifer thermal energy storage under different hydrochemical and hydrogeological conditions. PhD Thesis, Faculty of Science, KU Leuven. Last accessed May 19, 2022 from https://limo.libis.be

Possemiers, M., Huysmans, M., Batelaan, O., 2014. Influence of Aquifer Thermal Energy Storage on groundwater quality: A review illustrated by seven case studies from Belgium. Journal of Hydrology: Regional Studies, Volume 2, pp 20-34. Last accessed May 19, 2022 from https://doi.org/10.1016/j.ejrh.2014.08.001

Possemiers, M., Huysmans, M., Batelaan, O., 2015. Application of multiple-point geostatistics to simulate the effect of small scale aquifer heterogeneity on the efficiency of aquifer thermal energy storage. Hydrogeology Journal, 23(5), 971–981. Last accessed May 19, 2022 from https://doi.org/10.1007/s10040-015-1244-3

Ramos-Escudero, A., García-cascales, M.S., Cuevas, J.M., Sanner, B., Urchueguía, J.F., 2021. Spatial analysis of indicators affecting the exploitation of shallow geothermal energy at European scale. Renewable Energy, 167, 266–281. Last accessed May 19, 2022 from https://doi.org/10.1016/j.renene.2020.11.081

Schippers, J.C., Verdouw, J., 1979. De membraanfiltratie-index als kenmerk voor de filtreerbaarheid van water. H2O (12), nr.5, pp 104-109. Last accessed May 19, 2022 from https://edepot.wur.nl/398518

Schippers, J.C., Verdouw, J., 1980. The Modified-Fouling Index. A method for Determining the Fouling Characteristics of Water. Desalination 32, pp 137-148. Last accessed May 19, 2022 from https://doi.org/10.1016/S0011-9164(00)86014-2

Sommer, W., Valstar, J., Van Gaans, P., Grotenhuis, T., & Rijnaarts, H., 2013. The impact of aquifer heterogeneity on the performance of aquifer thermal energy storage. Water Resources Research, 49(12), 8128–8138. Last accessed May 19, 2022 from https://doi.org/10.1002/2013WR013677

Sommer, W., Valstar, J., Leusbrock, I., Grotenhuis, T., & Rijnaarts, H., 2015. Optimization and spatial pattern of large-scale aquifer thermal energy storage. Applied Energy, 137, 322–337. Last accessed May 19, 2022 from https://doi.org/10.1016/j.apenergy.2014.10.019

Stuyfzand, P.J., 1986. A new hydrogeochemical classification of water types: principles and application to the coastal dunes aquifer system of the Netherlands. Proceedings 9th Sea Water Intrusion Meeting (SWIM), Delft (The Netherlands), 641-656.

Theis, C.V., 1935. The relation between the lowering of the piezometric surface and the rate and duration of discharge of a well using groundwater storage. Am. Geophys. Union Trans., vol. 16, pp. 519-524. Last accessed March 31, 2022 from Last accessed May 19, 2022 from https://water.usgs.gov/ogw/pubs/Theis-1935.pdf

Thiem, G., 1906. Hydrologische Methoden: Dissertation zur Erlangung der Wurde eines; JM Gebhardt: Leipzig, Germany, 1906.

Todorov, O., Alanne, K., Virtanen, M., Kosonen, R., 2020. A method and analysis of aquifer thermal energy storage (ATES) system for district heating and cooling: A case study in Finland. Sustainable Cities and Society, 53(July 2019), 101977. Last accessed May 19, 2022 from https://doi.org/10.1016/j.scs.2019.101977

Vandenbohede, A., Hermans, T., Nguyen, F., Lebbe, L., 2011. Shallow heat injection and storage experiment: Heat transport simulation and sensitivity analysis. Journal of Hydrology, 409(1–2), 262–272. Last accessed May 19, 2022 from https://doi.org/10.1016/j.jhydrol.2011.08.024

Van Essen Instruments, 2016. Product manual Diver. Last accessed May 19, 2022 from https://www.vanessen.com

Van Everdingen, A.F., 1953. The Skin Effect and Its Influence on the Productive Capacity of a Well. Journal of Petroleum Technology, 5(06), 171–176. Last accessed May 19, 2022 from https://doi.org/10.2118/203-g

Waterinfo-Vlaamse Overheid, n.d. Retreived May 5, 2022 from https://www.waterinfo.be/Meetreeksen

Winston, R.B., 2019, ModelMuse version 4—A graphical user interface for MODFLOW 6: U.S. Geological Survey Scientific Investigations Report 2019–5036, 10 p., Last accessed May 19, 2022 from https://doi.org/10.3133/sir20195036

Yapparova, A., Matthäi, S., Driesner, T., 2014. Realistic simulation of an aquifer thermal energy storage: Effects of injection temperature, well placement and groundwater flow. Energy, *76*, 1011–1018. Last accessed May 19, 2022 from https://doi.org/10.1016/j.energy.2014.09.018

Zeghici, R.M., Oude Essink, G.H.P., Hartog, N., Sommer, W., 2015. Integrated assessment of variable density-viscosity groundwater flow for a high temperature mono-well aquifer thermal energy storage (HT-ATES) system in a geothermal reservoir. Geothermics, volume 55, pp 58-68. Last accessed May 19, 2022 from https://doi.org/10.1016/j.geothermics.2014.12.006

Zheng, C., and Wang, P.P., 1999. MT3DMS: A modular three-dimensional multi-species transport model for simulation of advection, dispersion and chemical reactions of contaminants in groundwater systems; Documentation and user's guide: Contract report SERDP-99-1: U.S. Army Engineer Research and Development Center, Vicksburg, MS, 169 p. Last accessed May 19, 2022 from https://hydro.geo.ua.edu/mt3d/mt3dmanual.pdf

Zheng, C., 2010. MT3DMS v5.3: Supplemental User's Guide. Department of Geological Sciences The University of Alabama, 51. Last accessed May 19, 2022 from https://hydro.geo.ua.edu/mt3d/mt3dms_v5_supplemental.pdf

Zuurbier, K.G., Hartog, N., Valstar, J., Post, V.E.A., van Breukelen, B.M., 2013. The impact of low-temperature seasonal aquifer thermal energy storage (SATES) systems on chlorinated solvent contaminated groundwater: modelling of spreading and degradation. J. Contam. Hydrol., pp 1-13. Last accessed May 19, 2022 from https://doi.org/10.1016/j.jconhyd.2013.01.002

6. Appendix

Appendix A

VLAREM II - bijlagen
Bijlagen

Bijlage 2.4.1. Milieukwaliteitsnormen en milieukwantiteitscriteria voor grondwater

Artikel 1. Als grondwaterkwaliteitsnormen gelden de richtwaarden, vermeld in de hier volgende tabellen:

A. Fysisch-chemische parameters

parameters	eenheid	Grondwaterkwaliteitsnorm	opmerkingen
1 temperatuur	°C	25	
2 zuurtegraad (pH)	pH-eenheid	5 <pH< 8,5	
3 elektrische geleidbaarheid	µS/cm bij 20 °C	1600	overeenkomend met de hoeveelheid mineralen in het water
4 chloride	mg/l Cl^-	250	
5 sulfaat	mg/l SO_4^{2-}	250	
6 calcium	mg/l Ca^{2+}	270	
7 magnesium	mg/l Mg^{2+}	50	
8 natrium	mg/l Na^+	150	
9 kalium	mg/l K^+	12	
10 aluminium	mg/l Al^{3+}	0,2	

B. Parameters voor ongewenste stoffen

Parameters	eenheid	Grondwaterkwaliteitsnorm	opmerkingen
11 nitraat	mg/l $NO3^-$	50	
12 nitriet	mg/l $NO2^-$	0,1	
13 ammonium	mg/l NH_4^+	0,5	
14 geëmulgeerde of opgeloste koolwaterstoffen (na extractie met ether) minerale oliën	µg/l	10	
15 fenolen (fenolgetal)	µg/l C6H5OH	0,5	met uitzondering van natuurlijke fenolen die niet op chloor reageren
16 boor	µg/l B^{3+}	1000	
17 ijzer	mg/l Fe2+/3+	20	
18 mangaan	mg/l Mn 2+/3+/4+/7+	1	

19 koper	µg/l Cu+/2+	100	
20 zink	µg/l Zn^{2+}	500	
21 fosfaat	mg/l PO4-/2/3-	1,34	
22 fluoride	mg/l F^-	1,5	
23 barium	mg/l Ba^{2+}	1	

C. Parameters voor toxische stoffen

Parameters	eenheid	Grondwaterkwaliteitsnorm	opmerkingen
24 arseen	µg/l As^{3}/3+/5+	20	
25 cadmium	µg/l Cd^{2+}	5	
26 cyanide	µg/l CN^-	50	
27 chroom	µg/l $_{Cr}$2+/3+/6+	50	
28 kwik	µg/l Hg+/2+	1	
29 nikkel	µg/l $_{Ni}$2+/3+	40	
30 lood	µg/l $_{Pb}$2+/4+	20	
31 antimoon	µg/l Sb^{3}/3+/5+	10	
32 seleen	µg/l Se^{2}/4+/6+	10	
33 pesticiden en aanverwante producten • per afzonderlijke stof • totaal	µg/l	0,1 0,5	Onder pesticiden worden onder andere insecticiden, herbiciden, fungiciden, nematiciden, acariciden, biociden en hun afbraakproducten verstaan. Onder aanverwante producten worden onder andere polychloorbifenylen (PCB), polychloorterfenylen (PCT) en hun afbraakproducten verstaan.
34 aromatische polycyclische koolwaterstoffen (totaal)	µg/l	0,2	referentiestoffen: •· fluoranteen •· benzo (a) pyreen •· benzo (b) fluoranteen •· benzo (g,h,i) peryleen •· benzo (k) fluoranteen •· indeno (1,2,3-cd) pyreen
35 tetrachlooretheen (PER) en trichlooretheen (TRI) (totaal)	µg/l	10	

D. Microbiologische parameters

Parameters		grondwaterkwaliteitsnorm

	uitkomsten: hoeveelheid van het monster in ml	membraanfiltermethode	meervoudige proefbuisjesmethode (MPN)
36 totaal aantal colibacteriën (1)	100	0	MWA < 1
37 fecale colibacteriën	100	0	MWA < 1
38 fecale streptokokken	100	0	MWA < 1
39 sulfietreducerende clostridia	20	-	MWA < 1

Art. 2. §1. Als achtergrondniveaus voor grondwater gelden de richtwaarden, vermeld in de volgende tabel:

parameter	pH min	pH max	Al 3+	$As^{3-/3+/5+}$	B^{3+}	Ca 2+	Cl^-	$Cr^{2+/3+/6+}$	$Cu^{+/2+}$	Ec	F^-	$Fe^{2+/3+}$	K^+	Mg 2+	$Mn^{2+/3+/4+/7+}$	Na^+	NH_4^+	$Ni^{2+/3+}$	NO^{2-}	$Pb^{2+/4+}$	$PO_4^{-/2-/3-}$
GWL / eenheid	(-) Sörensen		mg/l	µg/l	µg/l	mg/l	mg/l	µg/l	µg/l	µS/cm	mg/l	mg/l	mg/l	mg/l	mg/l	mg/l	mg/l	µg/l	mg/l	µg/l	mg/l
BLKS_0160_GWL_1M	6,4	7,4	*	18	210	180	79	*	*	970	0,3	17	15	29	1,6	50	2,5	9	*	*	1.0
BLKS_0160_GWL_1S	6,4	7,4	*	18	210	180	79	*	*	970	0,3	17	15	29	1,6	50	2,5	9	*	*	1.0
BLKS_0400_GWL_1M	6,3	7,4	*	6	43	190	89	*	*	1000	0,3	5,1	6,6	25	1,1	32	*	10	*	*	0.50
BLKS_0400_GWL_1S	6,3	7,4	*	6	43	190	89	*	*	1000	0,3	5,1	6,6	25	1,1	32	*	10	*	*	0.50
BLKS_0400_GWL_2M	6,2	8,4	0,08	10	3500	99	220	*	*	1500	2,0	2,1	27	25	0,26	390	1,2	6	*	*	1,8
BLKS_0400_GWL_2S	6,2	8,4	0,08	10	3500	99	220	*	*	1500	2,0	2,1	27	25	0,26	390	1,2	6	*	*	1,8
BLKS_0600_GWL_1	6,9	7,5	0,12	*	39	160	55	*	*	840	0,2	4,4	4,1	18	0,52	18	0,66	6	*	*	0,39
BLKS_0600_GWL_2	7,1	8,4	*	16	4100	93	2200	*	*	6100	1,4	3,1	32	22	0,12	1300	1,7	*	*	*	1,7
BLKS_0600_GWL_3																					
BLKS_1000_GWL_1S	6,8	7,4	*	*	79	190	83	*	*	1000	0,3	4,0	8,8	28	0,52	25	0,47	7	*	*	0,46
BLKS_1000_GWL_2S	7.0	8,3	*	*	450	130	35	*	*	800	0,8	1,7	18	23	0,11	150	0,69	*	*	*	0,83
BLKS_1100_GWL_1M	7.0	7,4	0,06	*	*	160	41	*	*	780	*	1,4	4,1	18	0,58	18	*	9	0,07	*	0,32
BLKS_1100_GWL_1S	7.0	7,4	0,06	*	*	160	41	*	*	780	*	1,4	4,1	18	0,58	18	*	9	0,07	*	0,32
BLKS_1100_GWL_2M	7.0	8,8	*	6	710	120	170	*	*	1100	1,0	1,4	19	27	0,08	180	0,81	*	*	*	0,33
BLKS_1100_GWL_2S	7.0	8,8	*	6	710	120	170	*	*	1100	1,0	1,4	19	27	0,08	180	0,81	*	*	*	0,33
CKS_0200_GWL_1	4,9	7,4	0,20	17	110	140	88	*	*	940	0,6	50	15	17	0,95	47	1,2	23	*	*	2,1
CKS_0200_GWL_2	5,6	7,7	*	9	170	86	37	*	*	600	0,3	21	18	12	0,51	25	1,2	9	*	*	1,1
CKS_0220_GWL_1	4,3	6,6	0,88	29	71	73	110	*	*	680	0,5	49	21	20	1,2	47	1,3	97	*	*	0,47
CKS_0250_GWL_1	5,9	7,2	0,07	8	43	70	68	*	*	490	0,6	20	5.0	8,3	0,83	31	*	13	*	*	0,78
CVS_0100_GWL_1	6,2	7,7	*	7	170	220	140	*	*	1400	0,4	7,3	15	35	1,4	110	0,95	19	*	*	0,75
CVS_0160_GWL_1	6,6	7,7	*	13	76	250	110	*	*	1300	0,4	12	11	23	1,6	65	4,6	10	*	*	1,2
CVS_0400_GWL_1	7,1	8,4	*	11	6600	75	380	*	5	2300	1,3	2,9	35	35	0,43	530	1,4	*	*	*	2,3
CVS_0600_GWL_1	5.0	7,6	0.10	7	94	190	130	*	*	1100	0,5	19	11	22	0,83	77	1,5	22	*	*	0,64
CVS_0600_GWL_2	7.0	8,6	0,07	11	4600	130	1400	*	6	5400	1,4	3,0	38	34	0,35	1200	1,8	*	*	*	1,4
CVS_0800_GWL_1	5,4	7,5	*	*	130	160	100	*	*	1000	0,4	16	14	23	0,89	97	1,0	30	*	*	0,95
CVS_0800_GWL_2	5,5	8,5	*	9	2900	180	490	*	*	3800	0,9	16	22	18	0,55	850	1,1	15	*	*	1,9
CVS_0800_GWL_3	5,9	7,6	0,12	6	67	200	87	*	5	1100	0,3	5,5	10	27	1,0	54	0,58	15	0,07	*	0,52
KPS_0120_GWL_1	6,9	7,9	*	15	860	240	190	*	*	1500	0,8	4,3	44	61	0,61	190	3,9	8	*	*	2,8
KPS_0120_GWL_2	6,9	7,9	*	15	860	240	190	*	*	1500	0,8	4,3	44	61	0,61	190	3,9	8	*	*	2,8
KPS_0160_GWL_1	6,7	7,8	*	46	3000	440	8500	12	8	24000	0,8	13	170	600	1,6	4800	35	20	*	*	16
KPS_0160_GWL_2	6,7	7,8	*	46	3000	440	8500	12	8	24000	0,8	13	170	600	1,6	4800	35	20	*	*	16
KPS_0160_GWL_3	6,7	7,8	*	46	3000	440	8500	12	8	24000	0,8	13	170	600	1,6	4800	35	20	*	*	16
MS_0100_GWL_1	4,9	7,1	0,13	13	43	83	70	*	*	610	0,4	30	7,7	14	0,82	37	0,81	27	0,09	*	0,63
MS_0200_GWL_1	4,9	6,9	0,13	12	41	51	64	*	*	480	0,5	20	8,4	10	0,63	29	*	49	0,09	*	0,54
MS_0200_GWL_2	5,3	7,1	*	14	61	69	68	*	*	550	0,3	20	6,3	15	0,93	33	0,61	19	0,10	*	0,61
SS_1000_GWL_1	7,2	8,8	*	18	3800	69	480	*	7	3500	6,4	1,6	24	17	0,4	860	0,82	8	*	*	2,2
SS_1000_GWL_2	7,2	8,8	*	18	3800	69	480	*	7	3500	6,4	1,6	24	17	0,4	860	0,82	8	*	*	2,2
SS_1300_GWL_1	7,3	9,3	*	8	1400	78	84	17	*	1100	4,7	1,5	19	33	0,07	240	0,86	*	*	*	0,41
SS_1300_GWL_2	7,1	8,3	*	6	660	110	57	*	*	750	1,7	1,1	22	27	0,09	88	0,52	*	*	*	0,31
SS_1300_GWL_3	7,7	9,8	0,10	20	3600	62	650	*	6	3800	6,9	1,1	24	11	0,11	920	1,3	8	*	*	1,1
SS_1300_GWL_4	7,7	9,8	0,10	20	3600	62	650	*	6	3800	6,9	1,1	24	11	0,11	920	1,3	8	*	*	1,1
SS_1300_GWL_5	7,7	9,8	0,10	20	3600	62	650	*	6	3800	6,9	1,1	24	11	0,11	920	1,3	8	*	*	1,1

Opmerkingen:
Een asterisk geeft aan dat de richtwaarde niet bepaalbaar is omdat het achtergrondniveau onder de rapporteringsgrens ligt. Bij de berekening van de drempelwaarden wordt in dit geval met een waarde van 0 gerekend.
Voor BLKS_0600_GWL_3 is de berekening van een richtwaarde voor de achtergrondniveaus niet mogelijk omdat de VMM-meetnetten maar één filter met kwaliteitsmetingen binnen dat grondwaterlichaam bevatten.

§2. De achtergrondniveaus worden vastgesteld door de afdeling, bevoegd voor grondwater, per grondwaterlichaam op basis van de metingen van het primair en freatisch grondwatermeetnet van de afdeling. De temperatuur wordt geothermisch bepaald.

Art. 3. Als drempelwaarden voor grondwater gelden de richtwaarden, vermeld in de volgende tabel:

parameter	As3-/3+/5+	Cd 2+	Cl^-	Ec	F-	K+	NH4+	Ni 2+/3+	NO2-	Pb 2+/4+	$PO4^{-}$/2-/3-	SO4 2-	Zn 2+
GWL / eenheid	µg/l	µg/l	mg/l	µS/cm	mg/l	mg/l	mg/l	µg/l	mg/l	µg/l	mg/l	mg/l	µg/l
BLKS_0160_GWL_1M	19	2,5	160	1300	0,9	15	2,5	25	0,07	10	1,17	190	300
BLKS_0160_GWL_1S	19	2,5	160	1300	0,9	15	2,5	25	0,07	10	1,17	190	300
BLKS_0400_GWL_1M	13	2,5	170	1300	0,9	9	0,35	25	0,07	10	0,92	220	310
BLKS_0400_GWL_1S	13	2,5	170	1300	0,9	9	0,35	25	0,07	10	0,92	220	310
BLKS_0400_GWL_2M	15	2,5	240	1600	2,0	27	1,2	23	0,07	10	1,80	190	270
BLKS_0400_GWL_2S	15	2,5	240	1600	2,0	27	1,2	23	0,07	10	1,80	190	270
BLKS_0600_GWL_1	10	2,5	150	1200	0,9	8	0,66	23	0,07	10	0,87	200	270
BLKS_0600_GWL_2	18	2,5	2200	6100	1,5	32	1,7	20	0,07	10	1,70	150	260
BLKS_0600_GWL_3	10	2,5	150	1200	0,9	8	0,66	23	0,07	10	0,87	200	270
BLKS_1000_GWL_1S	10	2,5	170	1300	0,9	10	0,49	24	0,07	10	0,90	210	270
BLKS_1000_GWL_2S	10	2,5	140	1200	1,2	18	0,69	20	0,07	10	1,09	170	260
BLKS_1100_GWL_1M	10	2,5	150	1200	0,8	8	0,35	25	0,09	10	0,83	170	260
BLKS_1100_GWL_1S	10	2,5	150	1200	0,8	8	0,35	25	0,09	10	0,83	170	260
BLKS_1100_GWL_2M	13	2,5	210	1400	1,3	19	0,81	20	0,07	10	0,84	160	260
BLKS_1100_GWL_2S	13	2,5	210	1400	1,3	19	0,81	20	0,07	10	0,84	160	260
CKS_0200_GWL_1	19	2,5	170	1300	1,1	15	1,2	32	0,07	10	2,10	230	360
CKS_0200_GWL_2	15	2,5	140	1100	0,9	18	1,2	25	0,07	10	1,22	180	270
CKS_0220_GWL_1	29	2,5	180	1100	1,0	21	1,3	97	0,07	10	0,91	260	410
CKS_0250_GWL_1	14	2,5	160	1000	1,1	9	0,35	27	0,07	10	1,06	170	330
CVS_0100_GWL_1	14	2,5	200	1500	1,0	15	0,95	30	0,07	10	1,05	280	310
CVS_0160_GWL_1	17	2,5	180	1500	1,0	12	4,6	25	0,07	10	1,27	250	280
CVS_0400_GWL_1	16	2,5	380	2300	1,4	35	1,4	20	0,07	10	2,30	230	260
CVS_0600_GWL_1	14	2,5	190	1400	1,0	12	1,5	31	0,07	10	0,99	290	290
CVS_0600_GWL_2	16	2,5	1400	5400	1,5	38	1,8	20	0,07	10	1,40	210	260

CVS_0800_GWL_1	10	2,5	180	1300	1,0	14	1,0	35	0,07	10	1,15	280	320
CVS_0800_GWL_2	15	2,5	490	3800	1,2	22	1,1	28	0,07	10	1,90	340	260
CVS_0800_GWL_3	13	2,5	170	1400	0,9	11	0,58	28	0,09	10	0,93	220	310
KPS_0120_GWL_1	18	2,5	220	1600	1,2	44	3,9	24	0,07	10	2,80	230	260
KPS_0120_GWL_2	18	2,5	220	1600	1,2	44	3,9	24	0,07	10	2,80	230	260
KPS_0160_GWL_1	46	2,5	8500	24000	1,2	170	35	30	0,07	10	16,0	400	280
KPS_0160_GWL_2	46	2,5	8500	24000	1,2	170	35	30	0,07	10	16,0	400	280
KPS_0160_GWL_3	46	2,5	8500	24000	1,2	170	35	30	0,07	10	16,0	400	280
MS_0100_GWL_1	17	2,5	160	1100	1,0	10	0,81	34	0,1	10	0,99	210	310
MS_0200_GWL_1	16	2,5	160	1000	1,0	10	0,35	49	0,1	10	0,94	200	350
MS_0200_GWL_2	17	2,5	160	1100	0,9	9	0,61	30	0,10	10	0,98	170	340
SS_1000_GWL_1	19	2,5	480	3500	6,4	24	0,82	24	0,07	10	2,20	370	270
SS_1000_GWL_2	19	2,5	480	3500	6,4	24	0,82	24	0,07	10	2,20	370	270
SS_1300_GWL_1	14	2,5	170	1400	4,7	19	0,86	20	0,07	10	0,88	190	260
SS_1300_GWL_2	13	2,5	150	1200	1,7	22	0,52	20	0,07	10	0,83	160	260
SS_1300_GWL_3	20	2,5	650	3800	6,9	24	1,3	24	0,07	10	1,22	420	260
SS_1300_GWL_4	20	2,5	650	3800	6,9	24	1,3	24	0,07	10	1,22	420	260
SS_1300_GWL_5	20	2,5	650	3800	6,9	24	1,3	24	0,07	10	1,22	420	260

Art. 4. Om te bepalen of de kwantitatieve toestand van de grondwaterlichamen goed is, gelden de volgende criteria:

1° Wijzigingen in het grondwatersysteem hebben geen significante negatieve effecten [...] op de actuele of beoogde natuurtypen van de grondwaterafhankelijke terrestrische ecosystemen, in het bijzonder in beschermde gebieden en in waterrijke gebieden;

2° De winningen veroorzaken geen zoutwaterintrusie;

3° De gespannen lagen behouden hun spanningskarakter zodat ze niet geoxideerd wordt;

4° Er komen geen regionale verlaagde grondwaterpeilen ("depressietrechter") voor die grondwaterkwaliteitsveranderingen veroorzaken;

5° Er komen geen aanhoudende peildalingen voor (rekening houdend met klimatologische variaties);

6° De baseflow blijft voldoende groot zodat waterlopen in stand gehouden worden;

7° Een verlaging van de baseflow leidt niet tot het niet-behalen van de milieukwaliteitsnormen voor het ontvangende oppervlaktewater;

8° Een verandering van de stroming vanuit of naar aangrenzende grondwaterlichamen leidt niet tot het niet-behalen van de goede kwantitatieve toestand en de milieukwaliteitsnormen voor een of meer grondwaterlichamen.

Appendix B

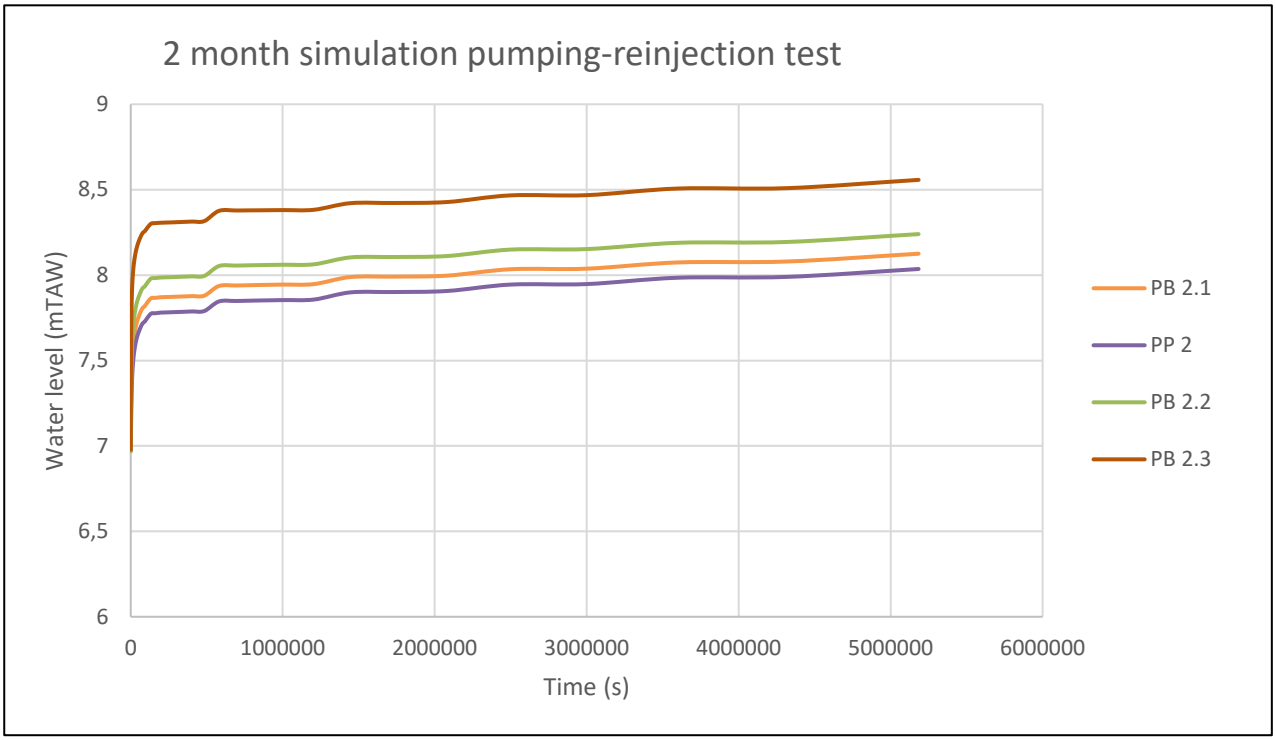

Additional 2-month simulation of pumping in PP 4 and reinjecting in PB JE to check whether a new equilibrium will be reached in Yd 2. This pumping-reinjection test was also carried out in the field but for a shorter period of time.